

Properties and Applications of Deep Eutectic Solvents and Low-Melting Mixtures

Dissertation

Zur Erlangung des Doktorgrades der Naturwissenschaften

(Dr. rer. nat.)

an der Fakultät für Chemie und Pharmazie

der Universität Regensburg



vorgelegt von

Veronika Fischer

aus Pfaffenhofen an der Ilm

2015

Promotionsgesuch eingereicht am: 20.3.2015

Die Arbeit wurde angeleitet von: Prof. Dr. Werner Kunz

Promotionskolloquium am: 24.4.2015

Prüfungsausschuss:

Prof. Dr. Jörg Daub	(Vorsitzender)
Prof. Dr. Werner Kunz	(1. Gutachter)
Prof. Dr. Hubert Motschmann	(2. Gutachter)
Prof. Dr. Frank-Michael Matysik	(3. Prüfer)

This work was carried out between October 2011 and April 2015 at the University of Regensburg, Institute of Physical and Theoretical Chemistry under the supervision of Prof. Dr. Werner Kunz.

Herzlich bedanken möchte ich mich...

... bei Prof. Dr. Werner Kunz für die Betreuung meiner Arbeit, das interessante Thema und ein allseits offenes Ohr für jedes Problem und jede Frage.

... bei Prof. Dr. Hubert Motschmann, der die Aufgabe als Zweitgutachter übernimmt. Des Weiteren danke ich Prof. Dr. Frank-Michael Matysik, dass er als Drittprüfer eintritt sowie Prof. Dr. Jörg Daub, dass er den Vorsitz meines Promotionskolloquiums übernimmt.

... bei Prof. Dr. Richard Buchner und PD Dr. Rainer Müller vom Institut für Physikalische und Theoretische Chemie der Universität Regensburg für die Bereitstellung des Viskosimeters, Dichtemessgeräts, TGA, DSC, Handschuhkastens und vor allem für die ein oder andere Hilfestellung.

... bei Andreas Nazet, Dr. Andreas Eiberweiser und Dr. Thomas Sonnleitner für die Unterstützung bei Viskosiäts- und Dichtemessung und dem Umgang mit dem Handschuhkasten. Weiter möchte ich mich gerne bei Dr. Didier Touraud bedanken, der mir vor allem bei Formulierungsfragen hilfreich zur Seite gestanden ist.

... bei dem COSMOlogic Team für die geduldige Beantwortung all meiner Fragen.

... bei Rosi und Sonja dafür, dass sie sich jeden Problem angenommen haben und mir immer mit Rat und Tat zur Seite gestanden sind.

... bei Julien Marcus und Dr. Olivier Diat für die SAXS Messungen und die hervorragende Zusammenarbeit im Bereich Mikroemulsionen.

... bei Dr. Christian Ehrenreich für die vielen Tipps und Tricks in organischer und präparativer Chemie.

... bei Julien Marcus, Andreas Nazet und Christian Ehrenreich für das Korrekturlesen dieser Arbeit.

... bei Martina Müller, Tobias Lopian, Patrick Geyer, Eddie Zwicker, Ulrich Lennert, Corinna Lorenz, Christian Luigs und Claudia Endert für die Unterstützung im Labor.

... bei Sabine, Julien, Auriane, Tatjana und Manu dafür, dass sie die wohl besten Labor- und Büronachbarn sind, die man sich vorstellen kann. Danke für Kaffee, Tee, Kekse, gute

Gespräche und dafür, dass ihr meine Freunde geworden seid. Mit euch kann man es aushalten.

... bei der Kaffeerunde für die kulinarische und kulturelle Weiterbildung. Ihr habt mich wirklich jeden Tag aufs Neue erheitert.

... natürlich bei all meinen Kollegen. Danke, dass ihr die Zeit hier für mich so angenehm gemacht habt. Ich werde das gemeinsame Arbeiten, aber auch die Feiern, Grillabende, Feierabendbiere, Wanderungen oder Spieleabende ziemlich vermissen. Ich möchte mich auch besonders bei Susanne, Michi, Theresa und natürlich dem Team Kondi bedanken. Danke, dass ihr meine Laune immer nur verbessert habt.

... bei all meinen Freunden.

... im Besonderen bei meinen Eltern Eleonore und Werner und meinem Bruder Bernhard. Danke für die großartige Unterstützung und Fürsorge. Was ihr alles für mich macht ist unglaublich und ich kann mir keine bessere Familie vorstellen.

... vor allem bei Christian, der mich in allen Lebenslagen immer unterstützt und so ein wunderbarer Mensch ist. Danke für die tollen Jahre, viel Liebe und das schönste Koala Face der Welt.

Table of Contents

I	Introduction	1
1.1	References	5
II	Fundamentals	7
1.	Deep Eutectic Solvents.....	8
1.1	History of Deep Eutectic Solvents	8
1.2	Sugar-Based Low-Melting Mixtures.....	10
1.3	Properties of Deep Eutectic Solvent and Low-Melting Mixtures	12
1.3.1	<i>Freezing Point</i>	12
1.3.2	<i>Density</i>	13
1.3.3	<i>Viscosity</i>	14
1.3.4	<i>Conductivity</i>	15
1.4	Applications of Deep Eutectic Solvents and Low-Melting Mixtures	16
1.4.1	<i>Organic Synthesis</i>	16
1.4.2	<i>Biocatalysis</i>	17
1.4.3	<i>Electrochemistry</i>	18
1.4.4	<i>Other Applications</i>	19
1.5	Environmental Aspects	20
1.6	References	22
2.	Conductor-Like Screening Model for Realistic Solvation.....	27
2.1	σ -Profiles.....	27
2.2	Solid-Liquid Equilibrium	29
2.3	References	30
3.	Microemulsions	31
3.1	General Information	31
3.2	Classification.....	31
3.3	Waterless Microemulsions	34

3.4	Surfactantless Microemulsions	35
3.5	Scattering Techniques	36
3.5.1	<i>Dynamic Light Scattering</i>	36
3.5.2	<i>Small-Angle X-Ray Scattering</i>	38
3.6	References	40
4.	Caffeic Acid Phenethyl Ester	44
4.1	Properties.....	44
4.2	Caffeic Acid Phenethyl Ester in Honey Bee Propolis	45
4.3	Synthesis of Caffeic Acid Phenethyl Ester.....	45
4.4	References	48
III	<i>Experimental</i>	53
1.	Chemicals.....	54
2.	Experimental Methods	55
2.1	NMR spectroscopy.....	55
2.2	Karl-Fischer Titration.....	55
2.3	Refractive Index	55
2.4	UV-Vis Spectroscopy.....	55
2.5	High Performance Liquid Chromatography	55
2.6	Thermal Analysis	57
2.7	Density	58
2.8	Viscosity.....	58
2.9	Ternary Phase Diagrams	59
2.10	Dynamic Light Scattering	59
2.11	Small Angle X-Ray Scattering.....	59
2.12	References	60
3.	Synthesis.....	61
3.1	Synthesis of Caffeic Acid Phenethyl Ester.....	61
IV	<i>Results and Discussion</i>	63
1.	New Low-Melting Mixtures	64
1.1	Abstract	64
1.2	Introduction	64

1.3	Results and Discussion.....	67
1.3.1	<i>Alternative Ammonium Compounds to Choline Chloride</i>	67
1.3.2	<i>Sugar-Based Low-Melting Mixtures</i>	70
1.4	Concluding Remarks.....	76
1.5	References.....	77
2.	COSMO-RS Calculations of Deep Eutectic Solvents.....	80
2.1	Abstract.....	80
2.2	Introduction.....	80
2.3	Results and Discussion.....	82
2.3.1	<i>σ-Profiles</i>	82
2.3.2	<i>Phase Diagrams</i>	83
2.4	Concluding Remarks.....	85
2.5	References.....	86
3.	Eco-Friendly Synthesis of Caffeic Acid Phenethyl Ester Using Deep Eutectic Solvents.....	87
3.1	Abstract.....	87
3.2	Introduction.....	87
3.3	Preparation of the Deep Eutectic Solvents and Reaction Mixtures.....	88
3.4	Results and Discussion.....	89
3.4.1	<i>Rheological Behaviour of the Reaction Mixtures</i>	89
3.4.2	<i>Lipase-Catalysed Reactions</i>	91
3.4.3	<i>Acid-Catalysed Esterification</i>	93
3.4.4	<i>Isolation of Caffeic Acid Phenethyl Ester</i>	97
3.5	Concluding Remarks.....	97
3.6	References.....	98
4.	Towards Surfactantless and Waterless Microemulsions.....	101
4.1	Abstract.....	101
4.2	Introduction.....	101
4.3	Results and Discussion.....	105
4.3.1	<i>Ternary Phase Diagrams</i>	105
4.3.2	<i>Dynamic Light Scattering</i>	106
4.3.3	<i>Small Angle X-Ray Scattering</i>	107
4.4	Concluding Remarks.....	108

4.5	References	109
V	Summary	113
1.1	References	117
VI	Appendix	119
1.	New low melting mixtures	120
1.1	Density	120
1.2	Viscosity.....	120
1.3	Thermogravimetric Analysis.....	121
1.4	Differential Scanning Calorimetry	122
2.	COSMO-RS Calculations of Deep Eutectic Solvents.....	124
2.1	Differential Scanning Calorimetry	124
3.	Eco-Friendly Synthesis of Caffeic Acid Phenethyl Ester Using Deep Eutectic Solvents	126
3.1	Viscosity.....	126
3.2	Composition, Reaction Time and Molar Conversion.....	127
3.3	NMR.....	131
4.	Towards Surfactantless and Waterless Microemulsions.....	132
4.1	Composition of the Samples	132
4.2	Density, Viscosity and Refractive Index	132
5.	List of Figures.....	133
6.	List of Schemes	136
7.	List of Tables	137
8.	List of Publications	139
9.	List of Abbreviations	140
10.	Eidesstattliche Erklärung.....	145

I Introduction

In chemistry, the choice of the right solvent is essential, since it constitutes around 80% of the total volume of chemicals used in a process.¹ Solvents present numerous environmental, health and safety challenges including human and eco-toxicity issues, process safety hazards and waste management issues.² Following the principles of green chemistry, most of the organic solvents do not fulfil the requirements for their use in green technology, since they have an inherent toxicity and a high volatility.¹ Figure I-1 illustrates graphically that the use of solvents must be minimised and optimised to enhance the reactions with the minimum environmental and operational concerns.

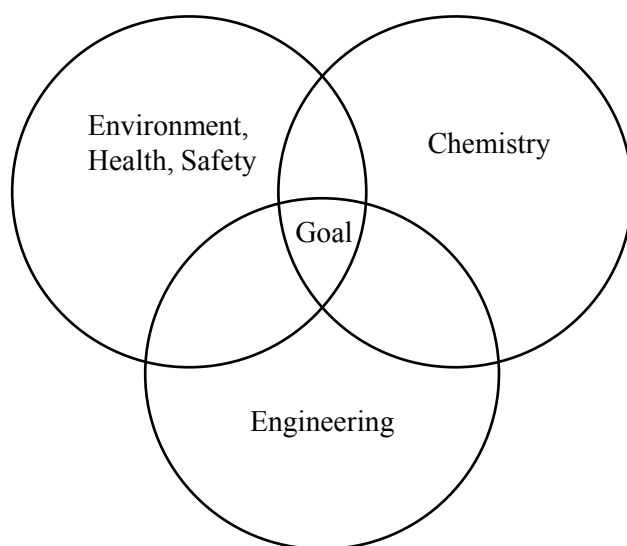


Figure I-1. The goal a solvent should attain is the agreement of its performance in the chemical and engineering process, the minimisation of energy use as well as the avoidance of adverse influence on environment, health and safety.²

In the last decades, efforts have been made to replace organic solvents. These approaches comprise the utilisation of easy recyclable systems such as supercritical CO₂ (scCO₂) or fluorous solvents, using no solvent at all, or the application of involatile systems such as ionic liquids (ILs), deep eutectic solvents (DESS) and low-melting mixtures (LMMs).³

ILs are salts, which are generally liquid below 100 °C.⁴ The first IL, ethylammonium nitrate, ([EtNH₃][NO₃]; melting point: 13-14 °C) was reported in 1914.⁵ Since then and especially over the last two decades, the number of published articles concerning ILs has grown exponentially.⁶ The great advantage of ILs is that they can be tuned by combining different cations and anions. However, their big drawback is the controversial environmental acceptability concerning their application and synthesis.^{6,7} To overcome these disadvantages,

DESs were discovered as a new class of IL analogues. Although they share many characteristics and properties with ILs, they represent a different type of solvent.⁸

The first paper on DESs was only published in 2001,⁹ so it is clear that the subject, compared to ILs, is in its infancy. In contrast to ILs, which are composed of one type of discrete anion and cation, DESs systems are formed from a eutectic mixture of Lewis and Brønsted acids and bases. They can comprise a variety of anionic and/or cationic species and have a large depression in melting point compared to the pure substances.⁸ The main application of DESs are metal processing and reaction media. DESs have been employed as alternative media for metals that are traditionally difficult to plate or process, or involve environmentally hazardous processes. In organic synthesis, DESs serve as environmentally benign alternative to organic solvents.^{8, 10} Further, DESs are used as sustainable media for the creation of well-defined nanoscale and functional materials involving shape-controlled nanoparticles, metal-organic frameworks, colloidal assemblies, hierarchally porous carbons, and DNA/RNA architectures.¹¹ Also the solubility of biomaterials such as chitin or cellulose in DESs was recently studied intensely as well as the use in extraction processes.¹²⁻¹⁶

The properties of a DES regarding its biodegradability and biocompatibility are solely dependent on the substances used. Therefore, natural-based DESs can be constituted by using primary metabolites, namely, amino acids, organic acids, sugars, or choline derivatives.¹⁷ These DESs fully fulfil the green chemistry principles. It is difficult to imagine the whole range of possibilities, since the amount of compounds suitable for the preparation of DESs is tremendous. Although there is a large pool of substances and lots of DESs have been presented, the mechanism of their formation is not well understood. The depression of the melting point is considered to arise from a combination of hydrogen bond interactions, lattice energy, and entropy change.¹⁸ Since at least three parameters contribute, it is difficult to make predictions about building principles, feasible mechanisms of formation, and intermolecular interactions.

The motivation and concept of this work is to find new natural-based DESs, to investigate formation mechanisms and examine the structure within DES as well as the quest for new applications.

At the beginning of this thesis, the main task was the development of new natural-based DESs to establish more alternatives to ILs and already existing DESs. Betaine and carnitine derivatives were tested as possible constituents. Both substance classes occur in the human

body and nature and are, therefore, not harmful to the environment.¹⁹ They serve as an alternative to choline chloride which is mainly used in DESs. Further, sugar-based mixtures were investigated. With a percentage of 75%, carbohydrates represent the largest part of all biomass and, hence, they are the most important and widespread renewable feedstock on earth.²⁰ The applicability of a DESs is dependent on the melting point which should be as low as possible. Therefore, the newly created mixtures were tested with regard to their melting points. Further, main properties such as density, viscosity or thermal stability were investigated.

As mentioned before, the prediction of the phase diagram of a DES is difficult, since diverse effects interact. The calculation of possible mixtures and their properties before preparing them, is an elegant way to save time and energy. Moreover, conclusions about building principles und intermolecular interactions can be made. This was the motivation for a study about the prediction of DESs. Compositions and melting points of DESs comprising choline halides and urea were predicted with the conductor-like screening model for realistic solution (COSMO-RS). By investigating the influence of the halide anion on the depression of the melting point, further insight into the formation mechanism of DESs could be gained. From the calculation results, it is revealed that hydrogen bonds are an important factor. Nevertheless, by comparing the prediction to experimental data, only a trend can be drawn for the melting points, whereas the composition is predicted accurately.

DESs have the potential to offer a viable alternative to existing technologies. As mentioned before, eutectic systems are already used in many fields. One area of interest focuses on their use in organic synthesis. Since a main part of this work is the quest for new applications, a natural-based DES, comprising caffeic acid and choline chloride, was used as reaction medium. It was first planned to perform an enzyme catalysed reaction. However, the incorporation of enzymes into this medium turned out to be difficult. The acidic and salty surrounding of the enzyme favours the denaturation of proteins. Therefore, an esterification was considered as a more suitable approach. A reaction of caffeic acid and phenethyl alcohol was studied. This reaction has the advantage that caffeic acid serves in the DES as part of the solvent as well as reaction partner. Further, the immiscible starting materials, namely caffeic acid and phenethyl alcohol, mix after a DES with choline chloride was generated. The product could be isolated by the use of water which makes the process more eco-friendly. Further, in comparison to the starting materials, the synthesised product is very expensive, which makes the process also economically profitable.

Another project was the formulation of microemulsions with DESs as polar phase. It is well-known that waterless microemulsions exist.²¹⁻²³ Microemulsions comprising ILs instead of water were already presented.^{24, 25} In a second step, surfactantless and waterless microemulsions were formulated. The existence of nanodomains were proofed using DLS and SAXS measurements. These results corroborate the hypothesis that surfactants are not mandatory for the formation of structures.²⁶⁻²⁹ Non-aqueous microemulsions may find their application as template materials or in nanoparticle synthesis. Also their use in separation chemistry, encapsulation, or nanocontainers is of growing interest.

All in all, this thesis sheds light on various sides of DESs. One focus lies on the environmental aspect with regard to the principles of green chemistry. Moreover, the intermolecular interactions in DESs as well as the formation of nanostructures in waterless and surfactantless DES-based microemulsions were elucidated. Finally, a DES was applied in organic synthesis as solvent and reactant which shows their great potential.

1.1 References

- 1 P. T. Anastas and M. M. Kirchhoff, *Acc. Chem. Res.*, 2002, **35**, 686-694.
- 2 R. Gani, C. Jiménez-González and D. J. C. Constable, *Comput. Chem. Eng.*, 2005, **29**, 1661-1676.
- 3 J. H. Clark and S. J. Tavener, *Org. Process Res. Dev.*, 2006, **11**, 149-155.
- 4 P. Wasserscheid and T. Welton, *Ionic liquids in synthesis*, Wiley Online Library, 2008.
- 5 P. Walden, *Bull. Acad. Imp. Sci. St.-Petersbourg*, 1914, 405-422.
- 6 M. Petkovic, K. R. Seddon, L. P. N. Rebelo and C. Silva Pereira, *Chem. Soc. Rev.*, 2011, **40**, 1383-1403.
- 7 M. Deetlefs and K. R. Seddon, *Green Chem.*, 2010, **12**, 17-30.
- 8 E. L. Smith, A. P. Abbott and K. S. Ryder, *Chem. Rev.*, 2014.
- 9 A. P. Abbott, G. Capper, D. L. Davies, H. L. Munro, R. K. Rasheed and V. Tambyrajah, *Chem. Commun.*, 2001, 2010-2011.
- 10 C. Russ and B. König, *Green Chem.*, 2012, **14**, 2969-2982.
- 11 D. V. Wagle, H. Zhao and G. A. Baker, *Acc. Chem. Res.*, 2014, **47**, 2299-2308.
- 12 M. Sharma, C. Mukesh, D. Mondal and K. Prasad, *RSC Advances*, 2013, **3**, 18149-18155.

- 13 C. Mukesh, D. Mondal, M. Sharma and K. Prasad, *Carbohydr. Polym.*, 2014, **103**, 466-471.
- 14 A. P. Abbott, P. M. Cullis, M. J. Gibson, R. C. Harris and E. Raven, *Green Chem.*, 2007, **9**, 868-872.
- 15 Y. Dai, J. van Spronsen, G.-J. Witkamp, R. Verpoorte and Y. H. Choi, *J. Nat. Prod.*, 2013, **76**, 2162-2173.
- 16 F. S. Oliveira, A. B. Pereira, L. P. N. Rebelo and I. M. Marrucho, *Green Chem.*, 2013, **15**, 1326-1330.
- 17 A. Paiva, R. Craveiro, I. Aroso, M. Martins, R. L. Reis and A. R. C. Duarte, *ACS Sustainable Chem. Eng.*, 2014, **2**, 1063-1071.
- 18 A. P. Abbott, D. Boothby, G. Capper, D. L. Davies and R. K. Rasheed, *JACS*, 2004, **126**, 9142-9147.
- 19 B. Caballero, *Guide to nutritional supplements*, Academic Press, 2009.
- 20 D. Peters, *Chem. Ing. Tech.*, 2006, **78**, 229-238.
- 21 I. Rico and A. Lattes, *J. Colloid Interface Sci.*, 1984, **102**, 285-287.
- 22 M. Gautier, I. Rico, A. Ahmad-Zadeh Samii, A. de Savignac and A. Lattes, *J Colloid Interface Sci*, 1986, **112**, 484-487.
- 23 J. Peyrelasse, C. Boned and Z. Saidi, *Phys. Rev. E: Stat. Phys., Plasmas, Fluids, Relat. Interdiscip. Top.*, 1993, **47**, 3412-3417.
- 24 A. Harrar, O. Zech, R. Hartl, P. Bauduin, T. Zemb and W. Kunz, *Langmuir*, 2011, **27**, 1635-1642.
- 25 O. Zech, S. Thomaier, A. Kolodziejski, D. Touraud, I. Grillo and W. Kunz, *Chem. Eur. J.*, 2010, **16**, 783-786.
- 26 M. L. Klossek, D. Touraud, T. Zemb and W. Kunz, *ChemPhysChem*, 2012, **13**, 4116-4119.
- 27 M. L. Klossek, D. Touraud and W. Kunz, *PCCP*, 2013, **15**, 10971-10977.
- 28 O. Diat, M. L. Klossek, D. Touraud, B. Deme, I. Grillo, W. Kunz and T. Zemb, *J. Appl. Crystallogr.*, 2013, **46**, 1665-1669.
- 29 S. Schöttl, J. Marcus, O. Diat, D. Touraud, W. Kunz, T. Zemb and D. Horinek, *Chem. Sci.*, 2014.

II Fundamentals

1. Deep Eutectic Solvents

1.1 History of Deep Eutectic Solvents

A eutectic system is a mixture of chemical compounds or elements that exhibits a single chemical composition that solidifies at a lower temperature than any other composition. As depicted in Figure II-1, the eutectic point is given by the intersection of the eutectic temperature and the eutectic composition.^{1,2}

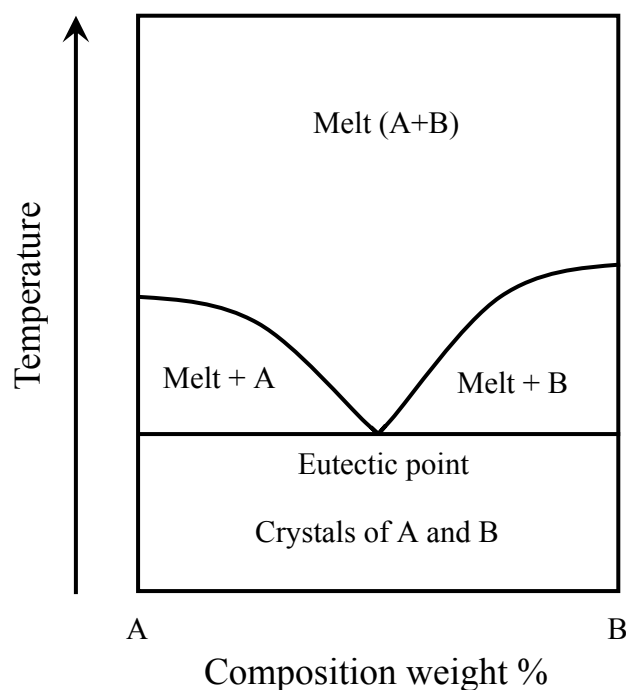


Figure II-1. Exemplary phase diagram of a binary mixture.

Eutectic systems with a very large depression of the melting point in the region of 200 °C are called deep eutectic solvents (DESs).³ In comparison to ionic liquids (ILs), which consist of a cation and a complex anion or the other way round, DESs comprise a cation, an anion and a complexing agent.⁴ In general, three types of DESs are defined.⁵

Type 1: Metal salt + organic salt (e.g. ZnCl_2 + choline chloride)

Type 2: Metal salt hydrate + organic salt (e.g. $\text{CoCl}_2 \cdot 6\text{H}_2\text{O}$ + choline chloride)

Type 3: Hydrogen bond donor + organic salt (e.g. urea + choline chloride)

This work concentrates on the third type of DESs. The first DES of this type was published by Andrew Abbott in 2003.⁶ A phase diagram was realised by mixing urea and choline chloride in various compositions.

Table II-1. Typical structures of organic salts and HBD used for DESs.³

Organic salt			Hydrogen bond donors		

Urea and choline chloride (ChCl) melt at 134 °C and 302 °C, respectively. The eutectic point was determined to be at a molar ratio of ChCl-urea 1-2. Since this mixture has a freezing point of 12 °C, it is liquid at room temperature. Abbott *et al.* stated that the depression of the freezing point must arise from an interaction between urea molecules and the chloride ion. Further, homogeneous liquids are only formed with compounds capable of forming hydrogen bonds with chloride ions.⁶ The principle of DESs is not limited to ureas. It can be also applied to a variety of other hydrogen bond donors (HBDs) such as acids, amines and alcohols. Over the years, an enormous number of DESs was created. In Table II-1 some typical structures of salts and HBDs used for DESs are depicted. In Table II-2 freezing points of various ChCl-HBD DESs are presented.³

Choline chloride is a commonly used organic salt for DESs, since it is biocompatible and known as former vitamin B₄.⁷ Further, most of the HBDs are cheap and environmentally benign such as urea, glycerol or carboxylic acids. DESs are easy to produce by just mixing

the components and heating them up under stirring. The purity of the resulting mixture is only dependent on the purity of the individual components. Other advantages of DESs are their non-volatility, non-inflammability and their inertness towards reactions with water.³

Table II-2. Freezing points (T_f) of various ChCl-HBD DESs with corresponding melting temperatures of the pure HBD (T_m^*).

HBD	T_f in °C	T_m^* in °C	Ref.
Urea	12	134	6
1-Methyl urea	29	93	6
Acetamide	51	80	6
Malonic acid	10	135	8
Oxalic acid	34	190	9
Phenylacetic acid	25	77	8
Ethylene glycol	-66	-13	10

1.2 Sugar-Based Low-Melting Mixtures

Carbohydrates were discovered as suitable mixing partners for low-melting systems.¹¹⁻¹⁶ The largest part of all biomass is carbohydrates with a percentage of 75 and, hence, they are the most important and widespread renewable feedstock on earth.¹⁷

Table II-3. Compositions and melting points (T_m) of different sugar-based LMMs.

Carbohydrate	Urea	Salt	Ratio (weight %)	T_m in °C	Ref.
Sorbitol	DMU ^a	NH ₄ Cl	70-20-10	67	14
Maltose	DMU ^a	NH ₄ Cl	50-40-10	84	14
Mannitol	DMU ^a	NH ₄ Cl	50-40-10	89	14
Lactose	DMU ^a	NH ₄ Cl	50-40-10	88	14
Mannose	DMU ^a	-	30-70	75	14
Fructose	DMU ^a	-	40-60	80	14
Fructose	Urea	NaCl	70-20-10	73	14
Fructose	Urea	-	40-60	65	11
Glucose	Urea	NaCl	60-30-10	78	14
Glucose	Urea	CaCl ₂	50-40-10	75	11
Galactose	Urea	NH ₄ Cl	30-70-10	80	15
L-Rhamnose	Urea	NH ₄ Cl	30-70-10	80	15
2-Deoxy-D-glucose	Urea	NH ₄ Cl	30-70-10	80	15

^a DMU: 1,3-dimethylurea

Carbohydrates are poorly soluble in almost all solvents except water, which is a major drawback concerning their use.¹⁸ A few years ago, it has been reported that carbohydrates can be incorporated in ILs.^{9, 18, 19} However, from an environmental point of view, creating fluids by combining carbohydrates and ILs is not a good idea, since ILs tend to be toxic and only show moderate biodegradability.^{16, 20, 21}

Therefore, it is tempting to combine carbohydrates and DESs. First approaches were made by Imperato *et al.* and Russ *et al.* They generated low-melting mixtures (LMMs) comprising carbohydrates, a HBD and a salt in order to create reaction media for organic transformations.^{11, 14, 15} The melting points and compositions of some exemplary LMMs are presented in Table II-3. However, these sugar-based LMMs suffer from high melting points in the range of 65 to 85 °C, which limits their application.

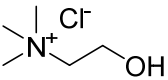
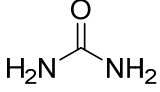
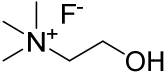
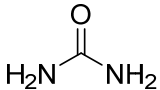
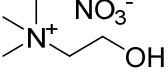
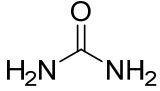
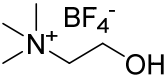
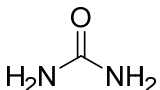
1.3 Properties of Deep Eutectic Solvent and Low-Melting Mixtures

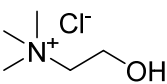
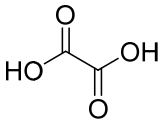
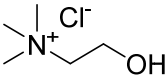
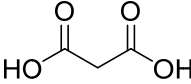
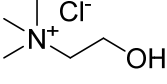
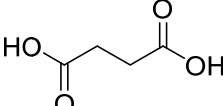
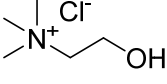
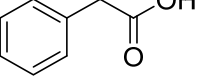
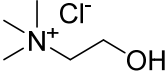
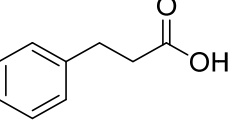
Although only a small selection of molecules is presented in section 1.1 and section 1.2, an enormous number of DESs and LMMs exists. Therefore, specific DESs and LMMs can be tailored with the desired physico-chemical properties such as freezing point, density, viscosity or conductivity. These main characteristics are discussed in this section.

1.3.1 Freezing Point

The freezing point of a DES or LMM is dependent on the choice of the HBD, the composition and the organic salt. Thereby, the strength of interaction between the HBD and the anion plays an important role. For instance, the freezing point of a choline salt-derived DES combined with urea decreases in the order $F^- > NO_3^- > Cl^- > BF_4^-$ (Table II-4) indicating a correlation with the hydrogen bond strength. NMR spectroscopy showed the existence of a hydrogen bond network within the eutectic mixtures. Further, an intense cross-correlation between the fluoride anion of choline fluoride and the NH_2 groups of the urea molecule in a DES was observed by HOESY measurements.⁶

Table II-4. Structures, compositions and freezing points (T_f) of different DES with corresponding melting points (T_m^*) of the pure HBD. The temperatures are given in °C.

Organic salt	HBD	Molar ratio	T_f	$T_m^*(HBD)$	Ref.
	 Urea	1-2	12	134	6
	 Urea	1-2	1	134	6
	 Urea	1-2	4	134	6
	 Urea	1-2	67	134	6

Organic salt	HBD	Molar ratio	T _f	T _m [*] (HBD)	Ref.
	 Oxalic acid	1-1	34	190	8
	 Malonic acid	1-1	10	135	8
	 Succinic acid	1-1	71	185	8
	 Phenylacetic acid	1-2	25	77	8
	 Phenylpropionic acid	1-2	20	48	8

As mentioned before, the nature of the HBD and the composition have a significant impact on the freezing point of a DES. For instance, similar to a mixture of ChCl-urea, which has a eutectic molar composition of 1-2, phenylpropionic acid and phenylacetic acid-based DESs show the lowest freezing point at a composition of 67 mol% of acid. Hence, two molecules of carboxylic acid are required to complex one chloride anion. In contrast, for dicarboxylic acids such as oxalic, malonic or succinic acid, the eutectic is formed at a molar ratio of 1-1 (Table II-4). It can be assumed that the anion interacts with two carboxylic groups. However, no clear correlation between the freezing point and the pure melting points of the components could be drawn.³ Abbott *et al.* suggested that the depression of the freezing point is dependent on the lattice energies of the DESs and LMMs, the interaction of the anion and HBD, and the entropy changes arising from forming a liquid.⁸

1.3.2 Density

In general, the densities of DESs and LMMs exhibit higher values than water. They are comparable to those of ILs which vary between 1.1 g cm⁻³ and 2.4 g cm⁻³.²² The density is dependent on the packing and molecular organisation of the DES.⁵ Similar to ILs, it is

suggested that DESs and LMMs are composed of holes and empty vacancies which govern the density behaviour. Mostly, the densities decrease with increasing temperature. The decline in density may be caused by the faster movement and creation of space of the high temperature molecule.¹⁰ Further, the density is dependent on the water content as it decreases with increasing percentage of water.^{23,24}

Moreover, the ratio of organic salt and HBDs has also an effect on the density. For instance, the addition of ChCl to glycerol results in a decrease in density (Table II-5), which can also be explained in terms of free volume and hole theory.^{10,25}

Table II-5. Densities of different DESs and glycerol systems at 25 °C.

Organic salt	HBD	Molar ratio	Density in g cm ⁻³	Ref.
ChCl	Urea	1-2	1.25	26
ChCl	Malonic acid	1-1	1.25	26
ChCl	Ethylene glycol	1-2	1.12	26
ChCl	Glycerol	1-2	1.18	25
ChCl	Glycerol	1-3	1.20	25
ChCl	Glycerol	1-4	1.21	25

1.3.3 Viscosity

The viscosity of a substance or a mixture is of importance for practical application. Most of the DESs and LMMs exhibit a relatively high viscosity at room temperature (> 100 cP) compared to molecular solvents.^{3,27} Similar to the density behaviour, the viscosity is related to the free volume and the probability of finding holes of suitable dimensions for the solvent molecules or ions to move into.^{27,28} Therefore, the viscosity is also dependent on the size of the ions.

Table II-6. Viscosities of different DESs and glycerol systems at 25 °C.

Organic salt	HBD	Molar ratio	Viscosity in cP	Ref.
ChCl	Urea	1-2	750	26
ChCl	Malonic acid	1-1	1124	26
ChCl	Ethylene glycol	1-2	37	26
ChCl	Glycerol	1-2	259	25
ChCl	Glycerol	1-3	320	25
ChCl	Glycerol	1-4	350	25

Less viscous liquids can be obtained using small quaternary ammonium cations such as ethylammonium and fluorinated HBD such as trifluoroacetamide.²⁷ Furthermore, the existence of an extensive hydrogen bond network, which results in a lower mobility of free species within the mixture, contributes to the high viscosity of DESs. Moreover, other forces such as electrostatic or van der Waals interactions may lead to high viscosities.³ The temperature, composition and water content have also an important impact.²⁵

The viscosity of a DESs or LMMs follows an Arrhenius-like behaviour as it decreases with increasing temperature.^{3, 25, 26} Consistent with the observed density behaviour of different ChCl-glycerol mixtures, the viscosity decreases with increasing ChCl amount whereas mixtures with ethylene glycol have the opposite effect.⁴ These examples show that the viscosity is dependent on the composition and resulting interactions. Since water has a lower viscosity than DESs and LMMs, the value decreases with increasing water content.^{23, 24, 29} Table II-6 presents viscosities of different DESs and LMMs.

1.3.4 Conductivity

There is a strong correlation between conductivity and viscosity. DESs and LMMs show poor conductivity (lower than 2 mS cm^{-1} at room temperature) due to their high viscosity.³ An Arrhenius like behaviour was observed for DESs and LMMs.^{8, 30} Since the composition has an impact on the viscosity, the conductivity is also dependent thereon. As mentioned before, the successive addition of ChCl to glycerol lowers the viscosity and increases the conductivity (from 0.74 mS cm^{-1} for a molar ratio of 1-4 ChCl-glycerol to 1.30 mS cm^{-1} for a molar ratio of 1-2 ChCl-glycerol) due to more available charge carriers in an increasingly less viscous solvent.²⁵

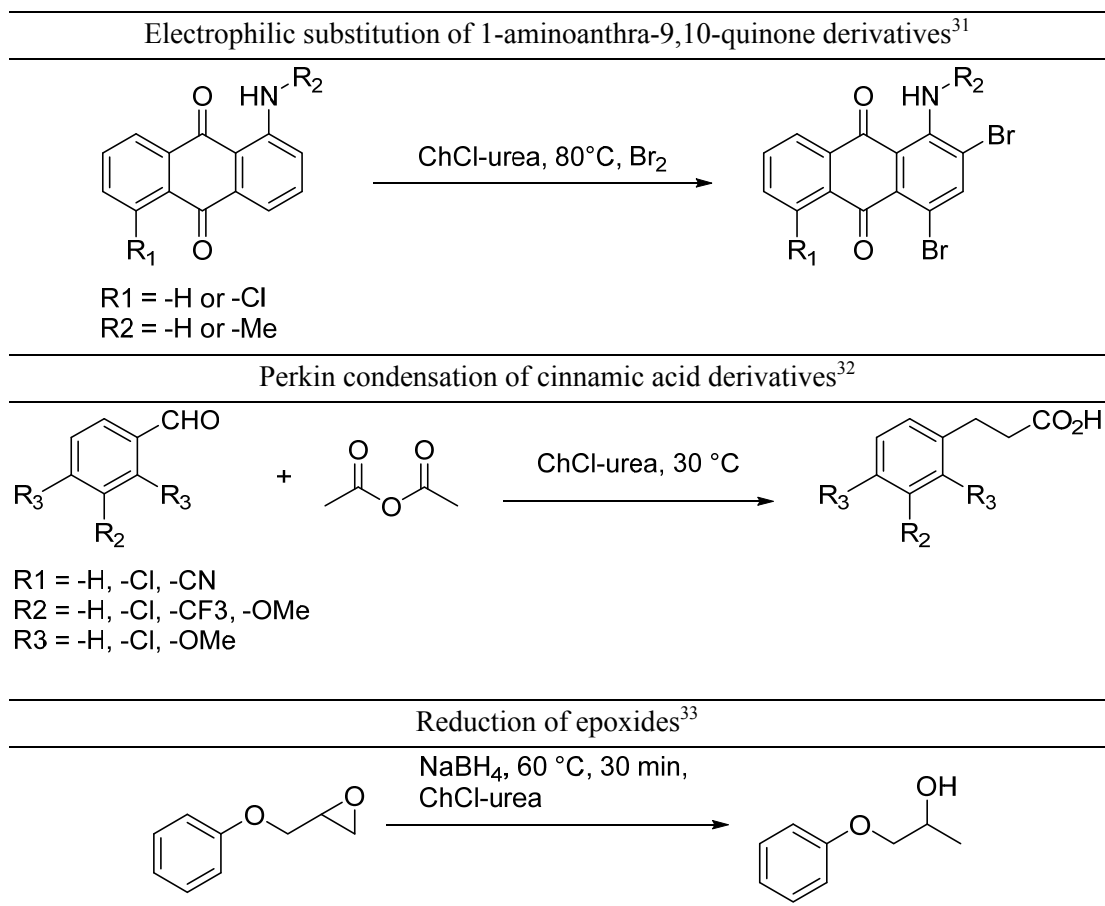
1.4 Applications of Deep Eutectic Solvents and Low-Melting Mixtures

Since DESs and LMMs are liquid at ambient temperature and have other advantages, they have been proposed for many applications. Some of them will be presented in this section.

1.4.1 Organic Synthesis

In organic synthesis the choice of solvent is crucial. They are often the largest source of waste, therefore, it is of great importance to look for non-toxic alternatives like DESs and LMMs. They are not only used as solvents, but also as catalysts and reactants.

Table II-7. Examples of organic reactions in ChCl-urea (1-2).

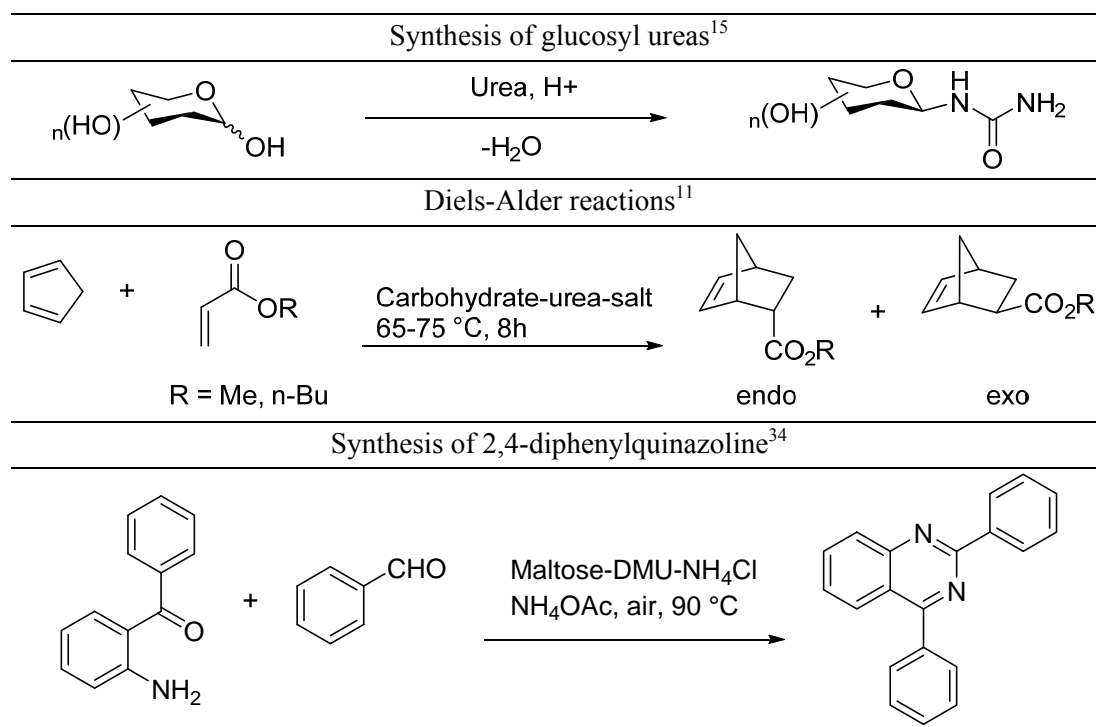


A mixture of ChCl-urea, for example, was used as solvent for bromination, Perkin reaction, or the reduction of epoxides and carbonyl compounds.³¹⁻³³ The reaction procedures are outlined in Table II-7. The synthesis of the shown products usually requires drastic conditions involving strong acids, high temperatures and environmentally toxic solvents.

However, by using a DES as solvent the reaction can be performed at lower temperatures with decreased reaction time and increased eco-friendliness.³¹⁻³³

Sugar-based LMMs can also be used as reaction media. Some examples are summarised in Table II-8. Russ *et al.* performed the condensation of β -D-glucose and urea in a carbohydrate-urea-salt melt.¹⁵ Thereby, the sugar and the urea were used as solvent and reactants without the need of an additional solvent. However, the use of sugar-based LMMs is still limited due to their high viscosities and high melting points.¹⁶

Table II-8. Examples of organic reactions in sugar-based LMMs.

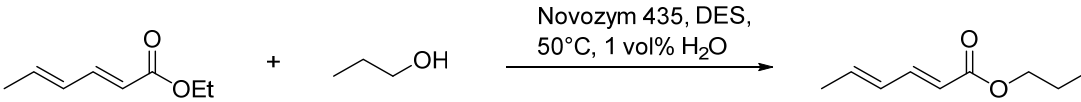


1.4.2 Biocatalysis

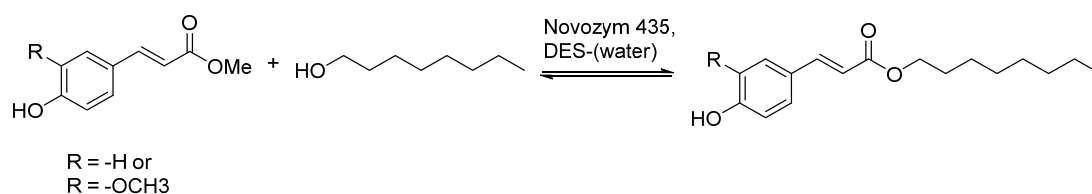
It is well known that biotransformations can be accomplished in ILs.³⁵ However, a lot of ILs are toxic and harmful to the environment. Further, their synthesis and purification is often expensive and time-consuming.^{20, 36} The utilization of DESs and LMMs has not been extensively investigated in this domain, since strong hydrogen bond donors such as urea are known to denature proteins.^{37, 38} Nevertheless, Gorke *et al.* tested the catalytic activity of hydrolases in DESs.³⁹ As a test reaction, the lipase-catalyzed transesterification of ethyl valerate with 1-butanol was carried out. In some of the DESs such as ChCl-urea, ChCl-glycol, or ethylammonium chloride-glycol the conversion rate was comparable to

toluene. Moreover, Zhao *et al.* tested the activity and selectivity of Novozym 435, an immobilized *Candida antarctica* lipase B (CALB), in different DESs.⁴⁰ The investigated reaction, presented in Table II-9, was an enzymatic transesterification of ethyl sorbate with 1-propanol. A mixture of choline acetate-glycerol (1-1.5) exhibited the best activity.

Table II-9. Reaction scheme, activity and selectivity of the transesterification of ethyl sorbate with 1-propanol.⁴⁰

		
Solvent	Initial activity ($\mu\text{mol min}^{-1} \text{g}^{-1}$)	Selectivity
<i>t</i> -Butanol	0.57	>99%
Glycerol	0.71	38%
ChCl-urea (1-2)	1.00	>99%
ChCl-glycerol (1-2)	1.12	45%
Choline acetate-urea (1-2)	0.21	40%
Choline acetate-glycerol (1-1.5)	1.02	99%

Other approaches were made by Durand *et al.* They performed lipase-catalysed reactions in DESs, for instance the alcoholysis of phenolic esters with 1-octanol (Scheme II-1).⁴¹⁻⁴⁴ Further, the effect of water content was studied. The results showed that it is extremely difficult to perform lipase-catalysed reactions without the addition of water. The improved catalytic activity may be attributed to reduced viscosity and improved mass transfer, a significant increase in lipase's initial activity and final conversion rate and a maintenance of the enzyme's catalytic activity.⁴¹



Scheme II-1. Reaction of lipase-catalysed alcoholysis of phenolic esters with 1-octanol in a DES.⁴¹

1.4.3 Electrochemistry

In electrochemistry, DESs have become an area of interest in the last few years. A major application for DESs is the incorporation of metal ions in solution for metal deposition,

metal dissolution or metal processing. Eutectic mixtures have the advantage that metal salts are highly soluble, no water is involved, and the conductivity is high compared to non-aqueous solvents.⁴⁵

Electrodeposition of metals is widely used to functionalize surfaces by plating. This process leads to the formation of solid materials by an electrochemical reaction in a liquid phase. In aqueous solution, electrodeposition is limited to the metals which exhibit a redox potential higher than that of water. Electrodeposition has already been performed in ILs. However, in contrast to ILs, DESs have the advantage of being water tolerant, biodegradable and cheap.^{3, 46, 47} In DESs the plating of chrome⁴⁸, aluminium⁴⁹, copper⁵⁰, nickel^{51, 52}, zinc⁵³ and other metals was reported.⁴⁵

Another application in electrochemistry is electropolishing, which is the controlled dissolution of a metal surface to reduce roughness and, therefore, increase the optical reflectivity. For electropolishing of stainless steel, a mixture of ChCl-ethylene glycol has been used.⁵⁴ In the field of metal extraction, metal oxides were solubilized in a eutectic mixture of ChCl-urea. Metal oxides are usually insoluble in molecular solvents. Only aqueous acid or basic solutions allow their solubilisation. However, ChCl-urea is able to dissolve several metal oxides such as Cu₂O, NiO or ZnO.⁵⁵ Further, ligands like urea, thiourea and oxalate are well-known to complex a variety of metals and can be used as a component of a DES. Nevertheless, these mixtures are totally miscible with water and cannot be used for biphasic extraction.^{55, 56}

1.4.4 Other Applications

In the last few years DESs and LMMs have become more and more popular and, therefore, the range of application has increased as well.⁴⁵ An interesting field, which has received attention, is the solvation of biomass like lignocellulose, cellulose or chitin.⁵⁷⁻⁵⁹ Further, DESs are used as sustainable media for nanoscale and functional materials as well as the creation of well-defined nanomaterials involving shape-controlled nanoparticles, metal-organic frameworks, colloidal assemblies, hierarchally porous carbons, and DNA/RNA architectures.⁶⁰ Also the adsorption of gas, for example CO₂, was discussed in various publications.⁶¹⁻⁶⁴ Moreover, eutectic mixtures were used for extraction, e.g. of glycerol from biodiesel into eutectic based ILs or DESs as extraction media for azeotropic mixtures.^{65, 66} In inorganic synthesis, DESs are used as organic templates for the synthesis of ionothermal

materials and zeolite analogues.^{67, 68} Also the potential as drug solubilisation vehicles was investigated.⁶⁹

1.5 Environmental Aspects

Over two decades ago, the green chemistry movement has begun and, therefore, the quest towards alternative solvents. Most organic solvents jeopardise the environment and are toxic, and hazardous in handling. Especially chlorofluorocarbons (CFCs) and volatile organic compounds (VOCs) were banned, since CFCs cause ozone depletion and VOCs were implicated in the production of photochemical smog.^{36, 70} Different alternatives to substitute and create more environmentally benign chemical processes have been proposed such as supercritical fluids, water, ILs or solvent-free processes.³⁶ However, it is still difficult to define a solvent as green. Inspired by the twelve principles of green chemistry by P. Anastas and J. Warner⁷⁰, Y. Gu and F. Jérôme created a list with twelve criteria a green solvent needs to meet:⁷¹

- 1) Availability: Solvents must be available on a large scale. Further, the production capacity should not fluctuate to ensure a constant availability.
- 2) Price: Solvents have to be competitive in terms of price and the costs should not be volatile during time to ensure sustainability of the chemical process.
- 3) Recyclability: The solvent has to be fully recycled in a chemical process using eco-efficient procedures.
- 4) Grade: In order to avoid energy-consuming purification, technical grade solvents are preferred.
- 5) Synthesis: Preparation of the solvents should be through an energy-saving process and the synthetic reaction should be highly atom-efficient.
- 6) Toxicity: In order to reduce the risk for humans or nature, solvents have to exhibit a negligible toxicity when used for personal and home care products, paints, etc.

- 7) Biodegradability: Green solvents should not produce toxic metabolites and should be biodegradable.
- 8) Performance: Compared to currently employed solvents, green solvents should show similar and even superior performances to be eligible.
- 9) Stability: During a chemical process, the solvent has to be thermally and (electro)chemically stable.
- 10) Flammability: Green solvents should be non-flammable to ensure a safe manipulation.
- 11) Storage: The storage of the solvent should be easy and should fulfil all legislation to be transported by road, train, boat or plane easily.
- 12) Renewability: Concerning the carbon footprint, renewable raw materials should be used for the production of green solvents.

Certainly, a solvent that fulfils all these requirements is hard to find if non-existent. Nevertheless, good approaches have been made, one of them being DESs and LMMs.⁷¹ Since DESs and LMMs have lower vapour pressures than many organic solvents, their emission to the atmosphere is decreased. However, most of them are miscible with water which has the disadvantage that they could end up in the aqueous environment. DESs and LMMs are mainly composed of non-toxic, natural-based and environmentally benign substances.⁴⁵ For instance, ChCl, which is often used in DESs and LMMs, is biocompatible and known as former vitamin B₄. It has some important key functions in the human body, e.g. as a precursor for phospholipids and acetylcholine.⁷ Further, urea, another important molecule in the development of DESs and LMMs, is not toxic to the human body. It is produced during the mammalian metabolism and even salvaged due to the metabolized activity of the colonic microflora. It is further used in the body and can be easily excreted in the urine.⁷² Also eco-friendly and biodegradable organic compounds like carboxylic acids (e.g. oxalic acid, malonic acid, succinic acid, etc.), amino acids or sugars (glucose, sorbitol, fructose, etc.) can be parts of a DESs or LMMs.^{8, 11, 57, 73-76} Although the components of eutectic mixtures are biodegradable and non-toxic, this is not necessarily valid for the

mixture. Hayyan *et al.* investigated the toxicity and cytotoxicity of DESs comprising ChCl and HBDs such as glycerine, ethylene glycol, triethylene glycol and urea.^{77, 78} The DESs were compared to the aqueous solutions of the pure components. The results indicate that the cytotoxicity is higher for DESs than for the individual components. The results were dependent on the structure of the components. This study shows that more investigations have to be done on the toxicity of DESs and LMMs to further explore their impact on the environment.

1.6 References

- 1 W. F. Smith and J. Hashemi, *Foundations of materials science and engineering*, McGraw-Hill, 2004.
- 2 P. Atkins and J. de Paula, *Physical Chemistry*, W. H. Freeman, 2006.
- 3 Q. Zhang, K. De Oliveira Vigier, S. Royer and F. Jerome, *Chem. Soc. Rev.*, 2012, **41**, 7108-7146.
- 4 A. P. Abbott, R. C. Harris and K. S. Ryder, *J. Phys. Chem. B*, 2007, **111**, 4910-4913.
- 5 A. P. Abbott, J. C. Barron, K. S. Ryder and D. Wilson, *Chem. Eur. J.*, 2007, **13**, 6495-6501.
- 6 A. P. Abbott, G. Capper, D. L. Davies, R. K. Rasheed and V. Tambyrajah, *Chem. Commun.*, 2003, 70-71.
- 7 J. K. Blusztajn, *Science*, 1998, **281**, 794-795.
- 8 A. P. Abbott, D. Boothby, G. Capper, D. L. Davies and R. K. Rasheed, *JACS*, 2004, **126**, 9142-9147.
- 9 L. Poletti, C. Chiappe, L. Lay, D. Pieraccini, L. Polito and G. Russo, *Green Chem.*, 2007, **9**, 337-341.
- 10 K. Shahbaz, F. S. Mjalli, M. A. Hashim and I. M. AlNashef, *Thermochim. Acta*, 2011, **515**, 67-72.
- 11 G. Imperato, E. Eibler, J. Niedermaier and B. König, *Chem. Commun.*, 2005, **0**, 1170-1172.
- 12 F. Ilgen and B. König, *Green Chem.*, 2009, **11**, 848-854.
- 13 F. Ilgen, D. Ott, D. Kralisch, C. Reil, A. Palmberger and B. König, *Green Chem.*, 2009, **11**, 1948-1954.
- 14 G. Imperato, S. Hoger, D. Lenoir and B. König, *Green Chem.*, 2006, **8**, 1051-1055.
- 15 Russ, F. Ilgen, C. Reil, C. Luff, A. Haji Begli and B. König, *Green Chem.*, 2011, **13**, 156-161.

-
- 16 C. Russ and B. König, *Green Chem.*, 2012, **14**, 2969-2982.
- 17 D. Peters, *Chem. Ing. Tech.*, 2006, **78**, 229-238.
- 18 M. E. Zakrzewska, E. Bogel-Łukasik and R. Bogel-Łukasik, *Energy Fuels*, 2010, **24**, 737-745.
- 19 M. E. Zakrzewska, E. Bogel-Łukasik and R. Bogel-Łukasik, *Chem. Rev.*, 2010, **111**, 397-417.
- 20 M. Deetlefs and K. R. Seddon, *Green Chem.*, 2010, **12**, 17-30.
- 21 M. T. Garcia, N. Gathergood and P. J. Scammells, *Green Chem.*, 2005, **7**, 9-14.
- 22 P. Wasserscheid and T. Welton, *Ionic liquids in synthesis*, Wiley Online Library, 2008.
- 23 A. Yadav and S. Pandey, *J. Chem. Eng. Data*, 2014, **59**, 2221-2229.
- 24 A. Yadav, S. Trivedi, R. Rai and S. Pandey, *Fluid Phase Equilib.*, 2014, **367**, 135-142.
- 25 A. P. Abbott, R. C. Harris, K. S. Ryder, C. D'Agostino, L. F. Gladden and M. D. Mantle, *Green Chem.*, 2011, **13**, 82-90.
- 26 C. D'Agostino, R. C. Harris, A. P. Abbott, L. F. Gladden and M. D. Mantle, *PCCP*, 2011, **13**, 21383-21391.
- 27 A. P. Abbott, G. Capper and S. Gray, *ChemPhysChem*, 2006, **7**, 803-806.
- 28 A. P. Abbott, *ChemPhysChem*, 2004, **5**, 1242-1246.
- 29 M. Francisco, A. van den Bruinhorst and M. C. Kroon, *Angew. Chem. Int. Ed.*, 2013, **52**, 3074-3085.
- 30 D. Rengstl, V. Fischer and W. Kunz, *PCCP*, 2014, **16**, 22815-22822.
- 31 S. B. Phadtare and G. S. Shankarling, *Green Chem.*, 2010, **12**, 458-462.
- 32 P. M. Pawar, K. J. Jarag and G. S. Shankarling, *Green Chem.*, 2011, **13**, 2130-2134.
- 33 N. Azizi, E. Batebi, S. Bagherpour and H. Ghafuri, *RSC Advances*, 2012, **2**, 2289-2293.
- 34 Z.-H. Zhang, X.-N. Zhang, L.-P. Mo, Y.-X. Li and F.-P. Ma, *Green Chem.*, 2012, **14**, 1502-1506.
- 35 U. Kragl, M. Eckstein and N. Kaftzik, *Curr. Opin. Biotechnol.*, 2002, **13**, 565-571.
- 36 J. H. Clark and S. J. Tavener, *Org. Process Res. Dev.*, 2006, **11**, 149-155.
- 37 J. Gorke, F. Srienc and R. Kazlauskas, *Biotechnol. Bioprocess Eng.*, 2010, **15**, 40-53.
- 38 P. Domínguez de María and Z. Maugeri, *Curr. Opin. Chem. Biol.*, 2011, **15**, 220-225.

- 39 J. T. Gorke, F. Srienc and R. J. Kazlauskas, *Chem. Commun.*, 2008, 1235-1237.
- 40 H. Zhao, G. A. Baker and S. Holmes, *OBC*, 2011, **9**, 1908-1916.
- 41 E. Durand, J. Lecomte, B. Barea, E. Dubreucq, R. Lortie and P. Villeneuve, *Green Chem.*, 2013, **15**, 2275-2282.
- 42 E. Durand, J. Lecomte, B. Baréa, G. Piombo, E. Dubreucq and P. Villeneuve, *Process Biochem.*, 2012, **47**, 2081-2089.
- 43 E. Durand, J. Lecomte and P. Villeneuve, *Eur. J. Lipid Sci. Technol.*, 2013, **115**, 379-385.
- 44 E. Durand, J. Lecomte, B. Baréa and P. Villeneuve, *Eur. J. Lipid Sci. Technol.*, 2014, **116**, 16-23.
- 45 E. L. Smith, A. P. Abbott and K. S. Ryder, *Chem. Rev.*, 2014.
- 46 K. Izutsu, in *Electrochemistry in Nonaqueous Solutions*, Wiley-VCH Verlag GmbH & Co. KGaA, 2009, pp. 111-170.
- 47 K. Izutsu, in *Electrochemistry in Nonaqueous Solutions*, Wiley-VCH Verlag GmbH & Co. KGaA, 2009, pp. 355-384.
- 48 E. S. C. Ferreira, C. M. Pereira and A. F. Silva, *J. Electroanal. Chem.*, 2013, **707**, 52-58.
- 49 H. M. A. Abood, A. P. Abbott, A. D. Ballantyne and K. S. Ryder, *Chem. Commun.*, 2011, **47**, 3523-3525.
- 50 D. Lloyd, T. Vainikka, L. Murtomäki, K. Kontturi and E. Ahlberg, *Electrochim. Acta*, 2011, **56**, 4942-4948.
- 51 C. Gu and J. Tu, *Langmuir*, 2011, **27**, 10132-10140.
- 52 A. P. Abbott, K. El Ttaib, K. S. Ryder and E. L. Smith, *Transactions of the IMF*, 2008, **86**, 234-240.
- 53 A. P. Abbott, J. C. Barron, G. Frisch, K. S. Ryder and A. F. Silva, *Electrochim. Acta*, 2011, **56**, 5272-5279.
- 54 A. P. Abbott, G. Capper, K. J. McKenzie and K. S. Ryder, *Electrochim. Acta*, 2006, **51**, 4420-4425.
- 55 A. P. Abbott, G. Capper, D. L. Davies, R. K. Rasheed and P. Shikotra, *Inorg. Chem.*, 2005, **44**, 6497-6499.
- 56 A. P. Abbott, G. Frisch, J. Hartley and K. S. Ryder, *Green Chem.*, 2011, **13**, 471-481.
- 57 M. Francisco, A. van den Bruinhorst and M. C. Kroon, *Green Chem.*, 2012, **14**, 2153-2157.

- 58 M. Sharma, C. Mukesh, D. Mondal and K. Prasad, *RSC Advances*, 2013, **3**, 18149-18155.
- 59 C. Mukesh, D. Mondal, M. Sharma and K. Prasad, *Carbohydr. Polym.*, 2014, **103**, 466-471.
- 60 D. V. Wagle, H. Zhao and G. A. Baker, *Acc. Chem. Res.*, 2014, **47**, 2299-2308.
- 61 S. Chen, J. Zhang, T. Wu, P. Feng and X. Bu, *JACS*, 2009, **131**, 16027-16029.
- 62 G.-P. Hao, Z.-Y. Jin, Q. Sun, X.-Q. Zhang, J.-T. Zhang and A.-H. Lu, *Energy Environ. Sci.*, 2013, **6**, 3740-3747.
- 63 M. C. Gutierrez, D. Carriazo, C. O. Ania, J. B. Parra, M. L. Ferrer and F. del Monte, *Energy Environ. Sci.*, 2011, **4**, 3535-3544.
- 64 J. Zhang, T. Wu, S. Chen, P. Feng and X. Bu, *Angew. Chem. Int. Ed.*, 2009, **48**, 3486-3490.
- 65 A. P. Abbott, P. M. Cullis, M. J. Gibson, R. C. Harris and E. Raven, *Green Chem.*, 2007, **9**, 868-872.
- 66 F. S. Oliveira, A. B. Pereiro, L. P. N. Rebelo and I. M. Marrucho, *Green Chem.*, 2013, **15**, 1326-1330.
- 67 E. R. Parnham, E. A. Drylie, P. S. Wheatley, A. M. Z. Slawin and R. E. Morris, *Angew. Chem.*, 2006, **118**, 5084-5088.
- 68 E. R. Cooper, C. D. Andrews, P. S. Wheatley, P. B. Webb, P. Wormald and R. E. Morris, *Nature*, 2004, **430**, 1012-1016.
- 69 H. G. Morrison, C. C. Sun and S. Neervannan, *Int. J. Pharm.*, 2009, **378**, 136-139.
- 70 P. T. Anastas and M. M. Kirchhoff, *Acc. Chem. Res.*, 2002, **35**, 686-694.
- 71 Y. Gu and F. Jerome, *Chem. Soc. Rev.*, 2013, **42**, 9550-9570.
- 72 A. Jackson, *Arch. Dis. Child.*, 1994, **70**, 3.
- 73 Y. H. Choi, J. van Spronsen, Y. Dai, M. Verberne, F. Hollmann, I. W. C. E. Arends, G.-J. Witkamp and R. Verpoorte, *Plant Physiol.*, 2011, **156**, 1701-1705.
- 74 Y. Dai, J. van Spronsen, G.-J. Witkamp, R. Verpoorte and Y. H. Choi, *Anal. Chim. Acta*, 2013, **766**, 61-68.
- 75 F. M. Kerton and R. Marriott, *Alternative solvents for green chemistry*, Royal Society of chemistry, 2013.
- 76 V. Fischer and W. Kunz, *Mol. Phys.*, 2014, **112**, 1241-1245.
- 77 M. Hayyan, M. A. Hashim, A. Hayyan, M. A. Al-Saadi, I. M. AlNashef, M. E. S. Mirghani and O. K. Saheed, *Chemosphere*, 2013, **90**, 2193-2195.

- 78 M. Hayyan, M. A. Hashim, M. A. Al-Saadi, A. Hayyan, I. M. AlNashef and M. E. S. Mirghani, *Chemosphere*, 2013, **93**, 455-459.

2. Conductor-Like Screening Model for Realistic Solvation

2.1 σ -Profiles

In 1993, Klamt and Schüürmann developed the **conductor-like screening model** (COSMO). It is a quantum chemical model, which works on scaled-conductor boundary conditions.¹ In 1995, a novel combination of the COSMO model with statistical thermodynamics was introduced, the **conductor-like screening model for realistic solvation** (COSMO-RS).^{2, 3} Interaction energies of the surface depend only on the local polarization charge densities. Each molecule has a screening charge σ , which can be used to identify qualitatively molecular properties like polarity or hydrogen bonding donor (HBD) and acceptor (HBA) abilities. This polarization charge-density σ on the molecular COSMO surface is called σ -surface. On this basis, COSMO-RS describes the interactions between molecules. It is assumed that all surfaces are in contact and, therefore, the liquid is incompressible. Further, only pair wise surface interactions are possible and the 3D geometry is neglected. The relevant interaction in liquids, which COSMO-RS takes into consideration, are Coulomb interactions, hydrogen bond interactions, Van der Waals interactions and a combinatorial term. The latter takes the size and shape differences of the molecules in the system into account. The term is dependent on the area and volume of all compounds in the mixture.

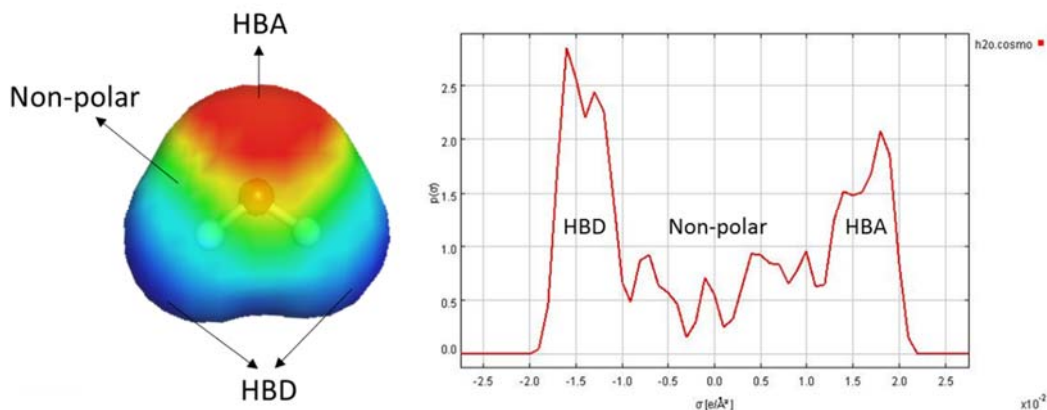


Figure II-2. σ -surface (left) and σ -profile (right) of water. The blue areas mark a HBD, the red areas a HBA, and the green areas a non-polar region.

The 3D information about σ on the molecular surface is reduced to a histogram $p^x(\sigma)$ which indicates how much surface can be found in a polarity interval. This histogram is called σ -

profile. The σ -regions beyond $\pm 1 \text{ e/nm}^2$ can be considered as strongly polar and potentially hydrogen bonding and the regions around 0 e/nm^2 as weakly polar or non-polar.^{3, 4} The σ -surface and corresponding σ -profile of water are depicted in Figure II-2.

Regarding the colour coding, HBD regions are labelled as deep blue and HBA regions as deep red on the σ -surface. Non-polar regions are marked in green. The σ -profile of water is dominated by two major peaks arising from the strongly negative polar regions of the electron lone-pairs of the oxygen atom (HBA) and from the strongly positively polar hydrogen atoms (HBD), respectively. The remarkable symmetry of the profile is an important feature. There is almost an equal amount of strongly negative and strongly positive surface areas. This enables strong hydrogen bonding between the molecules in the liquid, since energetically favourable pairings of positive and negative surfaces can be formed. This phenomenon is almost unique and leads to the relatively high boiling point for such a small molecule.³

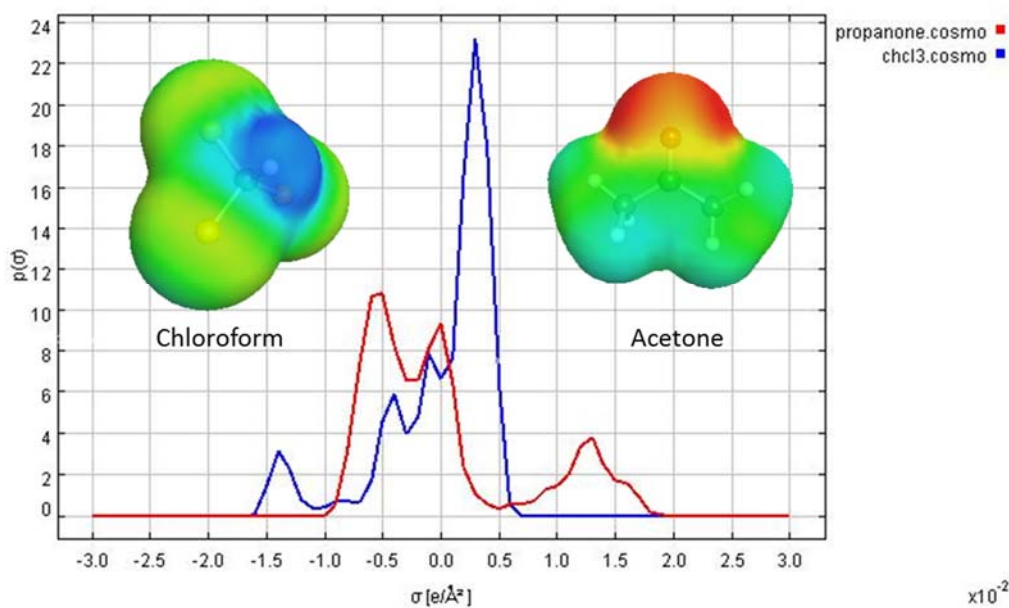


Figure II-3. σ -Profile for a mixture of chloroform and acetone.

The σ -surfaces and σ -profiles give valuable information about a molecule's polarity. On the basis of the σ -profiles, qualitative predictions can also be made for binary mixtures. One of the most striking examples is a mixture of acetone and chloroform. In Figure II-3, the σ -profiles for a mixture of both substances are presented. The σ -profiles of acetone is marked in red and the one of chloroform in blue.

The σ -profiles of the neat substances are very asymmetric. A reason for that is the oxygen atom in acetone, which does not find appropriate counterparts, and the polar hydrogen atom in chloroform which does not find a partner with a reasonably positive σ -profile. Consequently, in each pure substance there is a considerable amount of electrostatic misfit. However, by mixing both liquids, the σ -profiles complement each other. The polar oxygen surface polarity of acetone matches the polar hydrogen of chloroform. As a consequence, the misfit energy is strongly reduced in the mixture, causing a negative heat of mixing. Therefore, when the liquids are poured together, the mixture becomes warm.³

σ -Profiles and σ -surfaces give valuable information about HBD and HBA abilities of a molecule. Therefore, they are a useful tool for the prediction of the mixing behaviour of substances. However, only qualitative assumptions can be made.

2.2 Solid-Liquid Equilibrium

COSMO-RS is a theory for substances in the liquid state. However, to calculate, for instance, solubilities of crystalline compounds involving a solid-liquid equilibrium (SLE), COSMO-RS requires methods to estimate free energy differences. Usually, one can use an extrapolation of the free energy of fusion, ΔG_{fus} , for SLE calculations. In general, the prediction of chemical potential of crystalline substances is a rather unsolved task, because it requires the prediction of the crystal structure and the free energy of the potential polymorphs as an initial step.^{3, 4} Currently, it is impossible to predict the free energy differences between the liquid and solid state from first principles. The SLE calculations performed by COSMO-RS use an experimental estimate for the fusion free energy ΔG_{fus}^X based on the melting point and the heat of melting according to:

$$\Delta G_{fus}^X = -\Delta H_{fus}^X \left(1 - \frac{T}{T_{melt}^X}\right) + \Delta Cp_{fus}^X (T_m^X - T) - \Delta Cp_{fus}^X T \ln \frac{T_{melt}^X}{T} \quad 1$$

ΔH_{fus}^X represents the enthalpy of fusion, T_{melt}^X the melting temperature, T the temperature and ΔCp_{fus}^X the heat capacity change of fusion. The use of the melting temperatures, the enthalpy of fusion and optionally the heat capacity change of fusion allows the automatic calculation of the compounds' solid-liquid equilibrium at different temperatures. High melting compounds, such as drugs or fine chemicals, should be calculated using the extended formula containing ΔCp_{fus}^X . Unfortunately, this value is rarely available from experiment.

The implementation of COSMO-RS is the software *COSMOtherm*. For eutectic systems, the SLE option of *COSMOtherm* will compute a range of mixtures and search for possible concentrations of solidification. The SLE search assumes that there is a simple eutectic point in binary mixtures. Consequently, complex systems with several phase transitions in the solid state cannot be predicted.⁵

The SLE option was already used to predict phase equilibria properties for ionic liquid (IL) mixtures.⁶ Verma *et al.* used the SLE for binary systems consisting of IL and thiophene. They compared the predicted solubility values to the experimental results. Further, solubility values of binary mixtures consisting of IL and alcohol mixtures as well as IL and hydrocarbons were predicted. It turned out that the deviations between calculated and experimental results were within satisfactory limits. For the IL/thiophene systems, the deviation increases with decreasing concentration of solute. Similar to the experimental data, in the IL/alcohol system, the predicted solubility decreases with increasing length of carbon chain of the alcohol at a particular temperature. For a system comprising IL and hydrocarbon, it was discovered that an increase in the alkyl chain length of the substituent of the hydrocarbon decreases the solubility of the IL. This phenomenon can be explained by a hindrance effect.⁶

2.3 References

- 1 A. Klamt and G. Schuurmann, *J. Chem. Soc., Perkin Trans. 2*, 1993, 799-805.
- 2 A. Klamt, *J. Phys. Chem.*, 1995, **99**, 2224-2235.
- 3 A. Klamt, *COSMO-RS: From Quantum Chemistry to Fluid Phase Thermodynamics and Drug Design*, Elsevier Science, 2005.
- 4 A. Klamt, F. Eckert and W. Arlt, *Annu. Rev. Chem. Biomol. Eng.*, 2010, **1**, 101-122.
- 5 F. Eckert, *COSMOtherm Users Manuel*, 2012.
- 6 N. R. Verma, G. Gopal, R. Anantharaj and T. Banerjee, *J. Chem. Thermodyn.*, 2012, **48**, 246-253.

3. Microemulsions

3.1 General Information

Microemulsions were observed the first time in 1943 by Hoar and Schulman.¹ Also Winsor was a pioneer in this field and suggested a first classification of microemulsions.² Nevertheless, the term microemulsion was coined by Schulman *et al.* They studied the mechanism of formation and structures of mixtures consisting of oil, alcohol, soap, and water.³ In general, microemulsions are isotropic, optically transparent, and thermodynamically stable solutions.^{4,5}

However, the word micro is misleading, since the systems exhibit a nanostructure. Therefore, the expressions “micellar emulsion” or “swollen micelle” were also established.^{6,7} Danielsson and Lindman also defined microemulsions as systems consisting of water, oil and an amphiphile. This system is thereby a single optically isotropic and thermodynamically stable liquid solution.⁸ The term amphiphile describes substances with an affinity to polar and non-polar phases and was introduced by Winsor.⁹ In the late 1970’s and early 1980’s, as the oil prices reached high levels, there was a growing interest in microemulsions when it was discovered that these systems improve oil recovery.¹⁰ Since then, research in the field of microemulsions has become more and more important. Not only the range of application has increased, but also the understanding of the nanostructure by using NMR¹¹, transmission electron microscopy^{11,12}, X-ray or neutron scattering¹³⁻¹⁵, etc.

3.2 Classification

A microemulsion consists of a strongly polar component (usually water) and a strongly non-polar component (usually oil) that are stabilized by an amphiphile. Microemulsions exhibit a substantial structural diversity. Two examples are oil-in-water (O/W) and water-in-oil (W/O) microemulsions in which the dispersed medium forms typically, but not exclusively, spherical droplets with a small size polydispersity. O/W systems are also abbreviated as L1-phases and W/O as L2-phases. Microemulsion droplets mostly have radii in the range of 5 – 20 nm.¹⁶

The third type of structures are bicontinuous or sponge phases also called L3-phase. A scheme of the three phases is depicted in Figure II-4. The L3-phase consists of a network of oil and water nanodomains and is separated and stabilised by a surfactant interfacial film. This phenomenon can mostly be found at almost equal amounts of water and oil.^{17, 18} To

stabilise these nanostructures, additives such as cosurfactants or salts are often introduced in the systems. Especially when anionic surfactants are used, a cosurfactant is necessary. However, they are not always essential for the formation of a microemulsion. Exceptions are microemulsions comprising sodium di-(2-ethylhexyl) sulfsuccinate (AOT).¹⁹

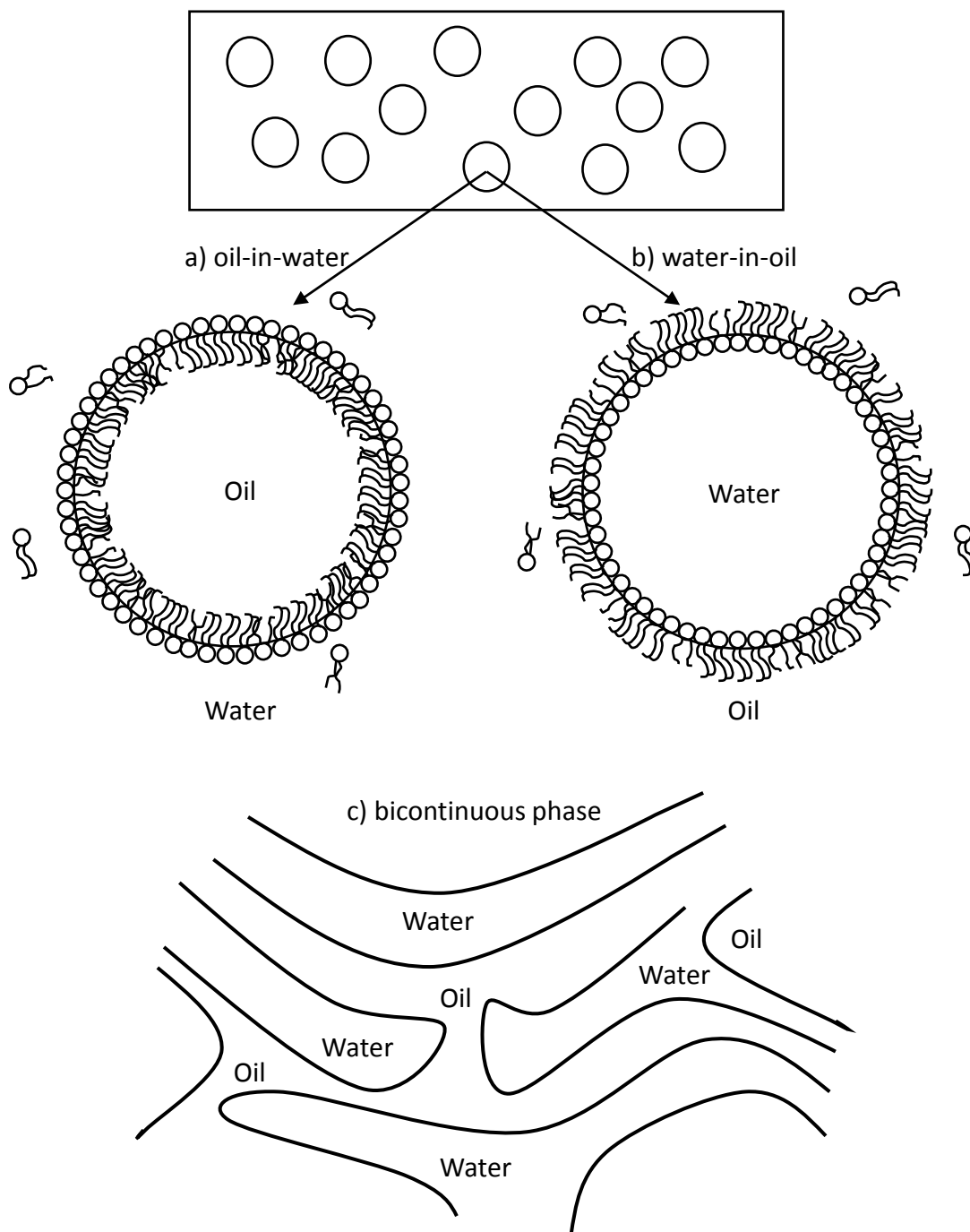


Figure II-4. Three different types of microemulsion a) oil-in-water, b) water-in-oil or c) bicontinuous.

Another classification was introduced by Winsor. He discovered four types of equilibrium systems:²

- Type I: Two phases are in equilibrium. The system consists of an O/W phase and nearly pure oil phase.
- Type II: Two phases are in equilibrium. The system consists of a W/O phase and a surfactant-poor aqueous phase.
- Type III: The system consists of three phases. A surfactant-poor aqueous phase, a bicontinuous phase and a nearly pure oil phase.
- Type IV: A single phase microemulsion of type L1, L2 or L3 is formed. No free aqueous or oil phase exists.

A three-component system can be illustrated by a triangular representation, also known as *Gibbs triangle*. An exemplary ternary phase diagram of a system with a nonionic surfactant can be seen in Figure II-5.

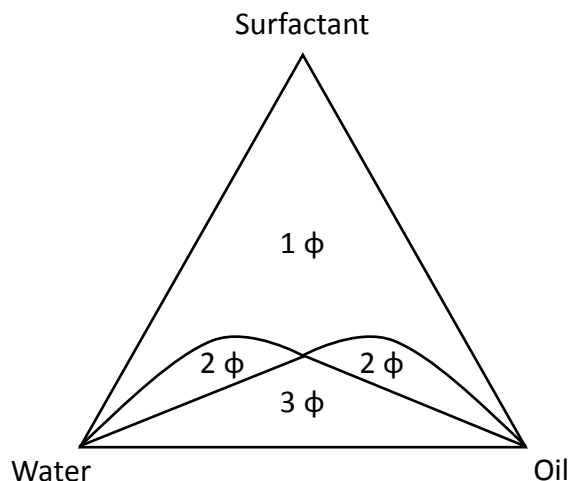


Figure II-5. Scheme of a phase diagram of water, oil and surfactant showing 1, 2, and 3 phase domains. The phase diagram is typical for a system with a nonionic surfactant

In these types of diagrams, the domains of microemulsion, macroemulsion, or liquid crystals can be seen at a glance. The mass, volume, or mole fractions are plotted along the axes and every corner represents one species (polar, non-polar or amphiphilic). The phase diagrams are determined at a constant temperature and pressure.

To investigate the temperature dependant behaviour, other depictions have to be chosen. Two examples are the fish cut and the χ cut. Both diagrams are binary. In the fish cut the oil-to-water ratio and in the χ cut the water-to-surfactant ratio is kept constant.¹⁶ The fish cut shows the temperature as a function of the surfactant concentration. The χ cut, however, shows the temperature as a function of α , which is the oil/(oil+water) w/w ratio.¹⁶

3.3 Waterless Microemulsions

In microemulsions, usually water serves as polar phase. However, it is also possible to replace the aqueous phase by another polar constituent. Lattes *et al.* used formamide in a system composed of cyclohexane as oil, butanol as cosurfactant, and two different surfactants.²⁰ They created these microemulsions to use them as media for reactions involving compounds which react with water. Other approaches towards waterless microemulsions exhibit ethylene glycol²¹, glycerol, and propylene glycol as polar phase.²² Also the formation of micelles in ethylammonium nitrate, one of the first known room-temperature ionic liquids, was already discovered in 1982.²³ Over the last years, ILs were used more frequently in microemulsions.²⁴⁻²⁷ Especially as a substitute for water, ILs have several advantages. They are stable above 100 °C and below 0 °C which offers new ways of applications, for example for the synthesis of new nanoparticles or high temperature surface cleaning.²⁷⁻³⁰ An example for a “cold” waterless microemulsion is a system containing the IL [Emim][EtSO₄], limonene as oil phase, and Triton X-114 as surfactant which was investigated by Harrar *et al.*²⁸ A large temperature stability of the system down to -35 °C was achieved by using high amounts of IL. As mentioned before, a second advantage is the use of water-free microemulsions as reaction medium for water sensitive reactions. For instance, non-aqueous reverse micelles work as nanoreactors.³¹ One of the first examples was a Diels-Alder reaction of cyclopentadiene with methyl acrylate.³² Further, biocompatible, structured solvents can be created by combining a low-toxic polar liquid with a low-toxic organic phase and a low-toxic surfactant.³³ However, the use of DESs or LMMs in microemulsions is still limited. Recently, Rengstl *et al.* reported the aggregation of choline dodecylsulfate in a LMM consisting of choline glutarate, ChCl, and urea.³⁴ Further, the self-aggregation of

sodium dodecyl sulphate in a DES was studied. In this work, also a SDS-assisted cyclohexane in DES microemulsion was introduced.³⁵

3.4 Surfactantless Microemulsions

In 1976, Smith *et al.* discovered that ternary systems of hexane, water, and 2-propanol have typical properties of microemulsions.^{36,37} At special compositions, the mixture appeared as a transparent, stable microemulsion even though soap or detergent were not present. The addition of hexadecyltrimethylammonium salts as surfactant had only a small effect on the phase diagram. This led to the assumption that the alcohol is the dominant structure-inducing component.³⁶ Another study was conducted by Keiser *et al.* who investigated the influence of NaCl on surfactantless microemulsions via ¹H NMR.³⁸ Their results show that the phase boundaries are dependent on the salt content and can be detected by NMR measurements.

Surfactantless microemulsions have the advantage that they dissolve hydrophilic and hydrophobic reagents, possess a large interphase area, can be prepared from inexpensive solvents, and no surfactant has to be removed in the purification step of the product.³⁹ At first, surfactantless microemulsions were tested for the incorporation of copper(II) into meso-tetraphenylporphine.³⁹ Later, the microemulsions served as reaction media. For instance, enzymatic reactions were carried out. The organic solvent enables the enzymatic conversion of water-insoluble compounds or the shift of the equilibrium towards the products.⁴⁰⁻⁴² It was discovered that proteins can be dissolved in the surfactantless microemulsion. In contrast to surfactant-based systems, the enzymes can be recovered easily without losing their catalytic activity.⁴²

Recently, surfactantless microemulsions were investigated in depth by Klossek *et al.*^{43, 44} While studying the so-called Ouzo-effect, they discovered a “pre-ouzo” region. In general, the Ouzo-effect appears when water, or any other solvent, is added rapidly to a highly or entirely miscible second solvent (e.g. ethanol) and a third component that is highly soluble in the second solvent, but not in the first one (e.g. anethole or octanol). The result is a fine and time-stable emulsion.⁴⁵ However, Klossek *et al.* found defined structures, observed by dynamic and static light scattering, in the system water/ethanol/*n*-octanol close to the phase-separation line. This phenomenon was named “pre-Ouzo” effect.⁴⁴ The work was extended to surfactantless microemulsion containing eco-solvents such as ethyl lactate or γ -valerolactone (Figure II-6).⁴³

Further proof for the existence of micelle-like structures was given by X-ray and neutron scattering, where two distinct nanoscopic pseudo-phases, one octanol rich and one water-rich, were detected.⁴⁶ To gain further insight about the molecular level shape and structures of these aggregates, molecular dynamic simulations were carried out for the system water/ethanol/*n*-octanol. The study showed the formation of octanol aggregates in the “pre-ouzo” region that are swollen by ethanol. The concentration of the latter is enhanced at the interface. The octanol aggregation is driven by the partial hydrophobic nature of octanol. These results suggest a common mechanism for structure formation.⁴⁷

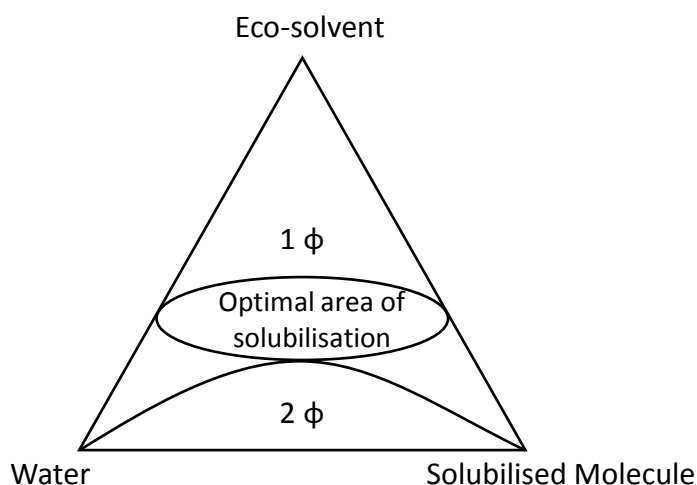


Figure II-6. Ternary phase diagram which shows the optimal region to solubilise a hydrophobic molecule with the minimum of eco-solvent.⁴³

This nano-clustering is present in several applications. For instance, in insect repellent formulations the nano-structuring may have an impact on the behaviour of the active components on the skin and their diffusion in the upper skin layers.^{48, 49} Nano-droplets have also a significant influence on the vapour pressures of the different components in perfumes or tinctures.^{50, 51} Also water/acetone/CO₂ systems were used as surfactant-free pressurised microemulsions to solubilise hydrophobic compounds such as ibuprofen.⁵²

3.5 Scattering Techniques

3.5.1 *Dynamic Light Scattering*

Dynamic light scattering (DLS) is a powerful tool for the measurement of particle sizes. Usually, the measurements are performed by a dynamic light scattering goniometer. A scattering medium, such as a suspension of colloid particles, is illuminated by a coherent

light. The light is scattered by the individual particles. The individual fields interfere largely constructively to give a large intensity. However, destructive interference leads to a small intensity at other points. Furthermore, since the scattering medium evolves in time, i.e. the position of the particles changes due to Brownian motion, the phase change and pattern fluctuate from one random configuration to another.⁵³

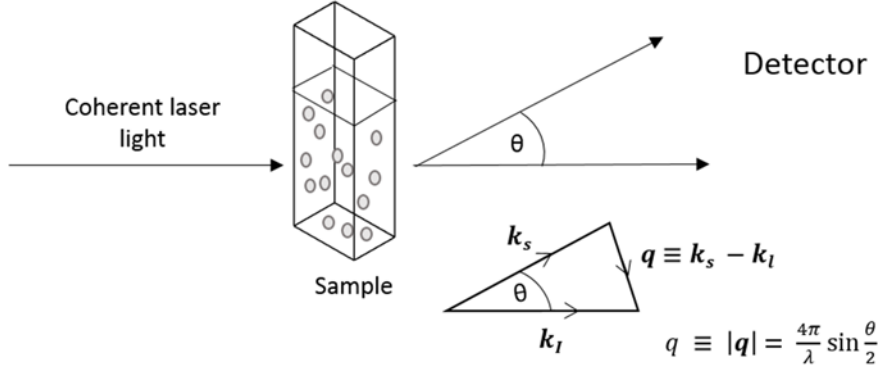


Figure II-7. Scheme of coherent laser light hitting a particle resulting in scattered light and definition of the scattering vector q .

Normally, useable information are extracted from the fluctuating intensity $I(\mathbf{q}, t)$ by constructing its time correlation function:

$$\langle I(\mathbf{q}, 0)I(\mathbf{q}, \tau) \rangle \equiv \lim_{T \rightarrow \infty} \frac{1}{T} \int_0^T dt I(\mathbf{q}, t)I(\mathbf{q}, t + \tau) \quad 2$$

\mathbf{q} , the scattering vector, is defined as the difference between the propagation vectors of the scattered and incident light (Figure II-7). From equation 2 it can be seen that the time correlation function compares the signal $I(\mathbf{q}, t)$ with a delayed version $I(\mathbf{q}, t + \tau)$ of itself for all starting times t and for a range of delayed times τ .

DLS measurements are performed in the time domain. Information about the dynamic properties of the studied scatterers can be obtained from the autocorrelation function $g_2(\tau)$ of the scattered intensity $I(t)$. The autocorrelation function correlates the current arrangement of the particles with the initial state. It is an average value of the product of the intensity at a time t , $I(t)$, and a delayed intensity $I(t + \tau)$:

$$g_2(\tau) = \langle I(t) \cdot I(t + \tau) \rangle \quad 3$$

The brackets represent an average which is performed by forming the product in equation (3) for a large number of times t . For short time delays τ , the positions and, hence, the scattered intensities of the particle are highly correlated so that $g_2(\tau)$ is, on average, large. However,

for delay times much greater than the typical fluctuation times, the positions of the particles are no longer correlated and $g_2(\tau)$ is just the square of the average scattered intensity.

One of the main applications of DLS is determination of particle size. This is done by measuring the diffusion constants of particles which undergo Brownian motion in dilute suspension. The ‘free-particle’ diffusion constant is given by the Stokes-Einstein equation:

$$D_0 = \frac{k_B T}{6 \pi \eta R_H} \quad 4$$

k_B is the Boltzmann constant, T the temperature, η the viscosity. The size of the objects can be deduced from DLS measurements using these equations. Since the diffusion coefficient is determined, the hydrodynamic radius, R_H , of the particle can be calculated as well.^{53, 54}

The simplest case is a system with monodisperse spherical particles. The autocorrelation function, $g_1(q; \tau)$, is then given by a single exponential decay:^{53, 55}

$$g_1(q; \tau) = \exp(-\Gamma\tau) \quad 5$$

$g_1(q; \tau)$ is obtained by the DLS measurement and fitted to an exponential in delay time τ giving the decay rate Γ . The latter is linked to the diffusion coefficient D_0 and the scattering vector q (Figure II-7):

$$\Gamma = D_0 q^2 \quad 6$$

For polydisperse systems, a decay rate has to be introduced for every particle size. The autocorrelation function is described as the sum of diverse exponential functions. However, only one decaying autocorrelation function is measured. It is composed of different, fastly decaying exponential functions. Therefore, it is very challenging to calculate the actual particle size distribution.⁵⁵

In general, DLS is used for the characterisation of dispersions of pigments and polymers, macromolecular solvents, macroemulsions, erythrocyte, liposomes, micelles, and microemulsions. The latter were investigated in this thesis. DLS is used to determine the particle size in the range of 10 to 1000 nm. Further advantages are the short measuring time (2-3 min), no calibration, the uncomplicated sample preparation and a small sample volume.⁵⁵

3.5.2 *Small-Angle X-Ray Scattering*

Small-angle scattering occurs in all kinds of materials such as (partially) crystalline or amorphous solids, liquids, or even gases. As a probe, electrons, gamma rays, light, X-rays,

and even neutrons can be used for small-angle scattering.⁵⁶ Scattering experiments are governed by the reciprocity principle. The incident wavelength λ has to fall within the size range of the structures to be detected.⁵⁵ A scheme of scattered radiation by a sample to small angles is depicted in Figure II-8.

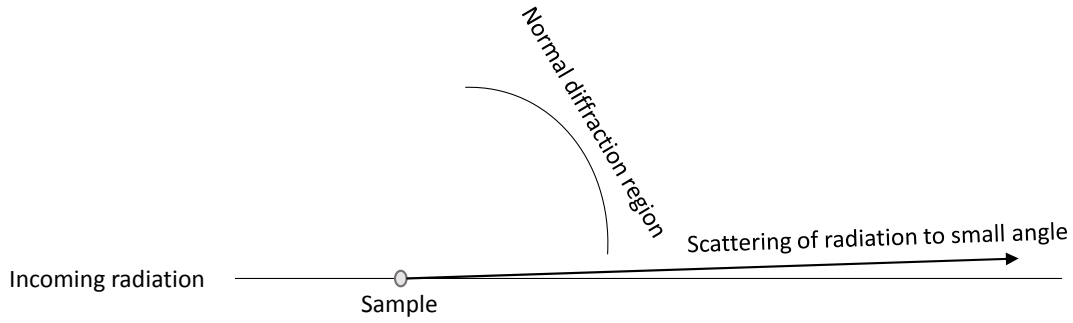


Figure II-8. Small angle scattering of radiation by a sample. Angles normally used are shown.⁵⁶

If X-rays are used for small angle scattering (SAXS), the distance between two particles is much larger than the irradiated wavelength. This leads to an increased interference of the reemitted spherical waves which is only possible with small angles. Using coherent radiation, the amplitude is only dependent on the optical retardation. The scattering vector \vec{q} describes the change of momentum of the scattered wave (Figure II-7). The X-rays interact with the electron density $\rho(r)$, since the local physical properties are identical. $\rho(r)$ is the number of electrons per unit volume (cm^3). A volume element dV at a position r then contains $\rho(r) dV$ electrons.⁵⁷ The scattering amplitude is then given by

$$F(q) = \int_V \rho(\vec{r}) e^{-i\vec{q}\cdot\vec{r}} dV \quad 7$$

Mathematically, the scattering amplitude $F(q)$ is the Fourier transform of the electron density within the scattering volume. By using the conjugate complex F^* , the intensity $I(q)$ can be derived.^{55, 57}

$$I(q) = F(q)F^*(q) = \int_{V_1} \int_{V_2} \rho(\vec{r}_1)\rho(\vec{r}_2) e^{-i\vec{q}\cdot(\vec{r}_1-\vec{r}_2)} dV_1 dV_2 \quad 8$$

Predictions about the structure can only be made if the electron density of the particle, ρ_p , and the solvent, ρ_s , is different. Therefore, only the contrast $\Delta\rho = \rho_p - \rho_s$ will be relevant for diffraction.⁵⁷ Consequently, if ρ_p and ρ_s are equal, the continuum is homogeneous and no scattering effect can be observed.

SAXS measurements can be employed for the investigation of microemulsions and micellar solutions. Detailed and quantitative knowledge of the local structure can be obtained.^{57, 58} In this thesis, SAXS was used for the investigation of surfactantless and waterless microemulsions. SAXS probes pertinent colloidal length of 1-100 nm and delivers information about the size and shape of the particles via the intensity.⁵⁸

Further, SAXS is applied to study the precipitation in metal alloys^{59, 60}, structural defects in diamonds⁶¹, pore structures in fibres^{62, 63}, particle growth in solution⁶⁴, structures in glasses⁶⁵, and the characterisation of structural correlations in liquids^{28, 34, 66, 67}, to name but a few. However, when the number of phases is increased, the complexity increases dramatically. Moreover, in SAXS measurements, only the scattered intensity is collected. Therefore, critical information are lost which prevents the full retrieval of the original structure.⁵⁶

3.6 References

- 1 T. P. Hoar and J. H. Schulman, *Nature*, 1943, **152**, 102-103.
- 2 P. A. Winsor, *Trans. Faraday Soc.*, 1948, **44**, 376-398.
- 3 J. H. Schulman, W. Stoeckenius and L. M. Prince, *J. Phys. Chem.*, 1959, **63**, 1677-1680.
- 4 H.-F. Eicke, in *Micelles*, Springer Berlin Heidelberg, 1980, vol. 87, ch. 2, pp. 85-145.
- 5 B. Lindman and H. Wennerström, in *Micelles*, Springer Berlin Heidelberg, 1980, vol. 87, ch. 1, pp. 1-83.
- 6 A. W. Adamson, *J. Colloid Interface Sci.*, 1969, **29**, 261-267.
- 7 S. Friberg, L. Mandell and M. Larsson, *J. Colloid Interface Sci.*, 1969, **29**, 155-156.
- 8 I. Danielsson and B. Lindman, *Colloids Surf.*, 1981, **3**, 391-392.
- 9 P. A. Winsor, *Solvent properties of amphiphilic compounds*, Butterworths, London, 1954.
- 10 D. O. Shah, *Surface phenomena in enhanced oil recovery*, Plenum Publishing Company Limited, 1981.
- 11 J. F. Bodet, J. R. Bellare, H. T. Davis, L. E. Scriven and W. G. Miller, *J. Phys. Chem.*, 1988, **92**, 1898-1902.
- 12 W. Jahn and R. Strey, *J. Phys. Chem.*, 1988, **92**, 2294-2301.
- 13 F. Lichterfeld, T. Schmeling and R. Strey, *J. Phys. Chem.*, 1986, **90**, 5762-5766.
- 14 L. Magid, P. Butler, K. Payne and R. Strey, *J. Appl. Crystallogr.*, 1988, **21**, 832-834.

-
- 15 S. H. Chen, *Annu. Rev. Phys. Chem.*, 1986, **37**, 351-399.
- 16 D. F. Evans and H. Wennerström, *The Colloidal Domain: Where Physics, Chemistry, Biology, and Technology Meet*, Wiley, 1999.
- 17 D. Langevin, *Annu. Rev. Phys. Chem.*, 1992, **43**, 341-369.
- 18 L. E. Scriven, *Nature*, 1976, **263**, 123-125.
- 19 B. K. Paul and S. P. Moulik, *J. Dispersion Sci. Technol.*, 1997, **18**, 301-367.
- 20 I. Rico and A. Lattes, *J. Colloid Interface Sci.*, 1984, **102**, 285-287.
- 21 S. E. Friberg and W. M. Sun, *Colloid. Polym. Sci.*, 1990, **268**, 755-759.
- 22 A. Martino and E. W. Kaler, *Langmuir*, 1995, **11**, 779-784.
- 23 D. F. Evans, A. Yamauchi, R. Roman and E. Z. Casassa, *J. Colloid Interface Sci.*, 1982, **88**, 89-96.
- 24 T. L. Greaves and C. J. Drummond, *Chem. Soc. Rev.*, 2008, **37**, 1709-1726.
- 25 J. Hao and T. Zemb, *Curr. Opin. Colloid Interface Sci.*, 2007, **12**, 129-137.
- 26 Z. Qiu and J. Texter, *Curr. Opin. Colloid Interface Sci.*, 2008, **13**, 252-262.
- 27 W. Kunz, E. Maurer, R. Klein, D. Touraud, D. Rengstl, A. Harrar, S. Dengler and O. Zech, *J. Dispersion Sci. Technol.*, 2011, **32**, 1694-1699.
- 28 A. Harrar, O. Zech, R. Hartl, P. Bauduin, T. Zemb and W. Kunz, *Langmuir*, 2011, **27**, 1635-1642.
- 29 O. Zech, S. Thomaier, A. Kolodziejcki, D. Touraud, I. Grillo and W. Kunz, *Chem. Eur. J.*, 2010, **16**, 783-786.
- 30 O. Zech, S. Thomaier, A. Kolodziejcki, D. Touraud, I. Grillo and W. Kunz, *J. Colloid Interface Sci.*, 2010, **347**, 227-232.
- 31 N. M. Correa, J. J. Silber, R. E. Riter and N. E. Levinger, *Chem. Rev.*, 2012, **112**, 4569-4602.
- 32 A. A.-Z. Samii, A. de Savignac, I. Rico and A. Lattes, *Tetrahedron*, 1985, **41**, 3683-3688.
- 33 O. Zech, P. Bauduin, P. Palatzky, D. Touraud and W. Kunz, *Energy Environ. Sci.*, 2010, **3**, 846-851.
- 34 D. Rengstl, V. Fischer and W. Kunz, *PCCP*, 2014, **16**, 22815-22822.
- 35 M. Pal, R. Rai, A. Yadav, R. Khanna, G. A. Baker and S. Pandey, *Langmuir*, 2014.
- 36 G. D. Smith, C. E. Donelan and R. E. Barden, *J. Colloid Interface Sci.*, 1977, **60**, 488-496.
- 37 G. D. Smith, B. B. Garrett, S. L. Holt and R. E. Barden, *J. Phys. Chem.*, 1976, **80**, 1708-1713.

-
- 38 B. A. Keiser, D. Varie, R. E. Barden and S. L. Holt, *J. Phys. Chem.*, 1979, **83**, 1276-1280.
- 39 B. A. Keiser and S. L. Holt, *Inorg. Chem.*, 1982, **21**, 2323-2327.
- 40 Y. L. Khmelnsky, A. Van Hoek, C. Veeger and A. J. W. G. Visser, *J. Phys. Chem.*, 1989, **93**, 872-878.
- 41 C. J. O'Connor, A. Aggett, D. R. Williams and R. A. Stanley, *Aust. J. Chem.*, 1991, **44**, 53-60.
- 42 Y. L. Khmelnsky, A. K. Gladilin, I. N. Neverova, A. V. Levashov and K. Martinek, *Collect. Czech. Chem. Commun.*, 1990, **55**, 555-563.
- 43 M. L. Klossek, D. Touraud and W. Kunz, *PCCP*, 2013, **15**, 10971-10977.
- 44 M. L. Klossek, D. Touraud, T. Zemb and W. Kunz, *ChemPhysChem*, 2012, **13**, 4116-4119.
- 45 R. Botet, *J. Phys. Conf. Ser.*, 2012, **352**, 1-10.
- 46 O. Diat, M. L. Klossek, D. Touraud, B. Deme, I. Grillo, W. Kunz and T. Zemb, *J. Appl. Crystallogr.*, 2013, **46**, 1665-1669.
- 47 S. Schöttl, J. Marcus, O. Diat, D. Touraud, W. Kunz, T. Zemb and D. Horinek, *Chem. Sci.*, 2014.
- 48 J. Drapeau, M. Verdier, D. Touraud, U. Kröckel, M. Geier, A. Rose and W. Kunz, *Chem. Biodivers.*, 2009, **6**, 934-947.
- 49 J. Marcus, M. Mueller, J. Nistler, D. Touraud and W. Kunz, *Colloids Surf., A*, 2014, **458**, 3-9.
- 50 J. Marcus, M. L. Klossek, D. Touraud and W. Kunz, *Flavour Fragrance J.*, 2013, **28**, 294-299.
- 51 V. Tchakalova, F. Testard, K. Wong, A. Parker, D. Benczedi and T. Zemb, *Colloids Surf., A*, 2008, **331**, 40-47.
- 52 R. F. Hankel, P. E. Rojas, M. Cano-Sarabia, S. Sala, J. Veciana, A. Braeuer and N. Ventosa, *Chem. Commun. (Cambridge, U. K.)*, 2014, **50**, 8215-8218.
- 53 T. Zemb and P. Lindner, *Neutrons, X-rays and Light: Scattering Methods Applied to Soft Condensed Matter*, Elsevier, 2002.
- 54 R. Finsy, *Adv. Colloid Interface Sci.*, 1994, **52**, 79-143.
- 55 H.-D. Dörfler, *Grenzflächen und kolloid-disperse Systeme: Physik und Chemie*, Springer, 2002.
- 56 P. Brian Richard, *J. Phys.: Condens. Matter*, 2013, **25**, 383201.
- 57 O. Glatter and O. Kratky, *Small Angle X-ray Scattering*, Academic Press, 1982.

-
- 58 C. Press, *Microemulsions: Properties and Applications*, Taylor & Francis Group, 2009.
- 59 P. Fratzl, *J. Appl. Crystallogr.*, 2003, **36**, 397-404.
- 60 A. Deschamps and F. de Geuser, *Metall. Mater. Trans. A*, 2013, **44**, 77-86.
- 61 A. Shiryaev, K. Dembo, Y. Klyuev, A. Naletov and B. Feigelson, *J. Appl. Crystallogr.*, 2003, **36**, 420-424.
- 62 A. F. Thünemann and W. Ruland, *Macromolecules*, 2000, **33**, 1848-1852.
- 63 B. Chu and B. S. Hsiao, *Chem. Rev.*, 2001, **101**, 1727-1762.
- 64 R. Viswanatha, H. Amenitsch and D. D. Sarma, *JACS*, 2007, **129**, 4470-4475.
- 65 G. Walter, R. Kranold and U. Lembke, *J. Appl. Crystallogr.*, 1997, **30**, 1048-1055.
- 66 R. Rai and S. Pandey, *Langmuir*, 2014, **30**, 10156-10160.
- 67 L. Temleitner and L. Pusztai, *J. Phys.: Condens. Matter*, 2007, **19**, 335203.

4. Caffeic Acid Phenethyl Ester

4.1 Properties

Phenolic acids and their derivatives widely occur in nature, especially in plants such as vegetables, fruits, grains, and spices. Since they act as antioxidants, they may have a favourable effect on human health.¹⁻⁶ Caffeic acid (CA) is a main representative of the hydroxycinnamic and phenolic acids and its derivatives such as glycosides, amides, esters, and sugar esters can be found in many plants.⁷ An ester of the CA is the caffeic acid phenethyl ester also known as CAPE. The molecular structures of CA and CAPE are depicted in Figure II-9.

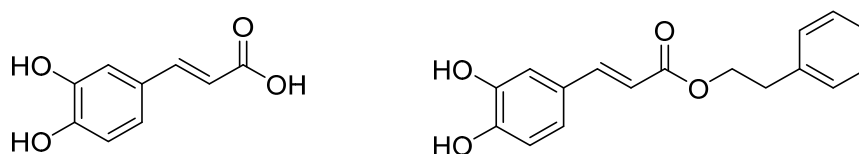


Figure II-9. Molecular structures of caffeic acid (CA) and caffeic acid phenethyl ester (CAPE).

CAPE is one of the most active compounds in honey bee propolis and exhibits some interesting pharmacological and biological properties.⁸ For example, CAPE has an antimicrobial activity. Studies demonstrated the destruction of the bacteria *Enterococcus faecalis*, *Listeria monocytogenes* and *Staphylococcus aureus* by CAPE.⁹⁻¹¹ The antimicrobial activity against *Haemophilus influenza* showed that RNA, DNA and cellular proteins are possible targets of CAPE.^{9, 12} Further, CAPE has been proposed as a HIV-1 integrase inhibitor and, therefore, can be used potentially in anti-HIV therapy.¹³⁻¹⁶ CAPE showed also a cytotoxicity on tumour cells, which makes it a feasible active compound in cancer treatment.¹⁷⁻¹⁹ Other properties of CAPE are its anti-inflammatory and antioxidant activity.⁷ The antioxidant effect can result from the transcriptional inhibition of NF- κ B and a reduced expression of pro-inflammatory genes.²⁰ The antioxidant activity of CAPE has also diverse mechanisms such as free radical scavenging, metal ion chelation, and inhibition of specific enzymes that induce free radical or lipid peroxidation.^{21, 22} Structural factors as well as the medium used to assay these activities are the basis for the antioxidant activities of CA and CAPE.^{23, 24}

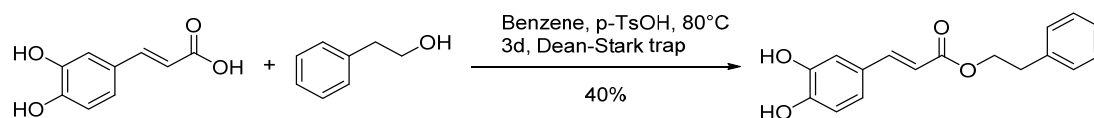
4.2 Caffeic Acid Phenethyl Ester in Honey Bee Propolis

In nature, CAPE occurs in honeybee propolis which is a natural resinous substance collected by bees from plants, buds and exudates.²⁵ Bees use it as sealer for their hives and to prevent the decomposition of invaders killed by the bees.^{26, 27} Depending on their composition, propolis is a lipophilic, yellow-brown to dark brown and sometimes greenish material. Upon cooling it is hard and wax-like. However, it softens and turns resinous and sticky upon warming, hence it is also named bee-glue.²⁸ The chemical composition and biological activities are ascribed to geographical settings, plant sources and collecting season.²⁹ The major components are flavonoids, aromatic acids, diterpenoid acids, triterpenoids and phenolic compounds.³⁰⁻³⁸ Since honey bee propolis has a complex composition, it is difficult to separate the different constituents by simple fractionation. Mostly, propolis is divided into the alcohol soluble fraction, also called propolis balsam, and in the alcohol-insoluble or wax fraction.³⁹ However, it is very difficult to extract active compounds, especially CAPE, since i) honey bee propolis contains over 180 constituents and ii) the CAPE content is dependent on the type of propolis.⁴⁰ Although ethanol extract of propolis is the most common extraction method, new approaches such as microwave-assisted extraction, extraction with supercritical CO₂ or hot-pressurized fluid extraction were performed to leach phenolic compounds.⁴¹⁻⁴⁴ However, the isolation of CAPE is often challenging since it is tedious and suffers from impurities.³⁰

4.3 Synthesis of Caffeic Acid Phenethyl Ester

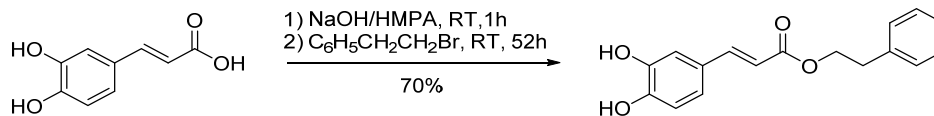
As described in section 4.2, the extraction of CAPE from honey bee propolis has some drawbacks. Therefore, it is important to find alternatives to obtain CAPE. An overview of diverse synthetic routes towards CAPE is presented in this section.

In 1988, Grunberger *et al.* synthesised CAPE via an acid-catalyzed (*p*-toluenesulfonic acid) esterification of CA and phenethyl alcohol (molar ratios 1:15) in benzene yielding CAPE in 40%.¹⁷ Water was removed by a Dean-Stark trap. The reaction scheme can be seen in Scheme II-2.



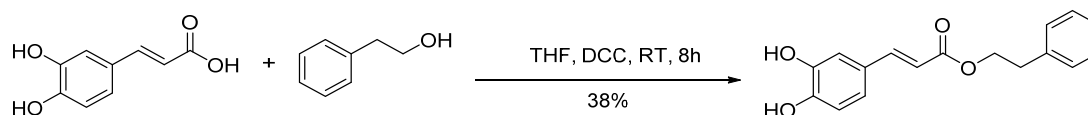
Scheme II-2. Scheme of acid-catalyzed reaction of CA and phenethyl alcohol to CAPE.¹⁷

Another route was suggested by Hashimoto *et al.* (Scheme II-3).^{45, 46} CAPE was prepared via a base-catalysed alkylation of CA with β -bromoethylbenzene in a dipolar aprotic solvent such as hexamethylphosphoramide (HMPA) in 70% yield.



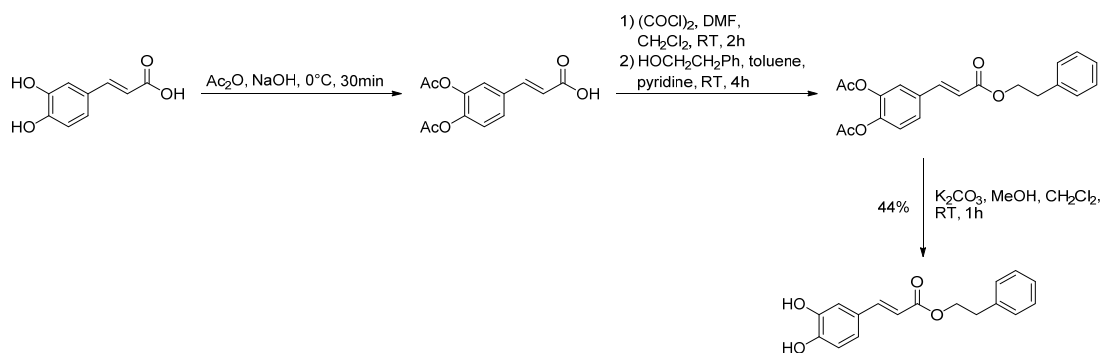
Scheme II-3. Reaction scheme of the base-catalyzed alkylation of CA and β -bromoethylbenzene.⁴⁵

In 1996, Chen *et al.* introduced the synthesis of CAPE using dicyclohexyl carbodiimide (DCC) as a condensing agent in 38% yield.¹⁸ DCC is used as peptide coupling reagent.⁴⁷ Despite the rather low yield, the advantage of this method is a relative short reaction time and mild conditions. The reaction is depicted in Scheme II-4. However, the major drawback of the last two synthesis is the carcinogenicity of HMPA and also the toxicity of DCC.^{47, 48}



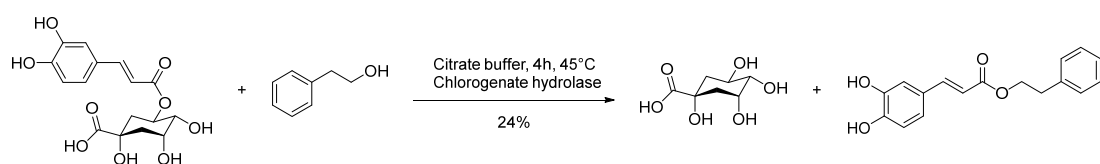
Scheme II-4. Reaction scheme of the esterification of CA and phenethyl alcohol using DCC as condensing agent.¹⁸

Further, a three-step synthesis of CAPE was conducted by Touaibia and Guay.⁴⁹ In the first step, CA is treated with sodium hydroxide and acetic anhydride at 0 °C affording diacetylcaffeic acid. The subsequent step is the esterification of phenethyl alcohol with the acetylated caffeic acid chloride. The latter was prepared from the Vilsmeier-Haack adduct derived from oxalyl chloride and *N,N*-dimethylformamide (DMF) as catalyst. Oxalyl chloride can also be replaced by thionyl chloride (SOCl₂). In the last step, a base-induced de-O-acetylation was accomplished using potassium carbonate in methanol/dichloromethane to obtain CAPE in 44% overall yield. The three-step synthesis is summarized in Scheme II-5.



Scheme II-5. Three-step synthesis to CAPE according to Touaibia and Guay.⁴⁹

In order to avoid environmental pollution and harm to the human body, other approaches towards CAPE were made by using enzymes. In 2005, Kishimoto *et al.* described the enzymatic synthesis of CAPE from 5-chlorogenic acid (5-CQA) and phenethyl alcohol, 5-CQA and phenethyl bromide, and CA and phenethyl alcohol or phenethyl bromide using chlorogenate hydrolase (CQA hydrolase) with a maximum yield of 24%.^{50, 51} An example of this type of reaction is shown in Scheme II-6.

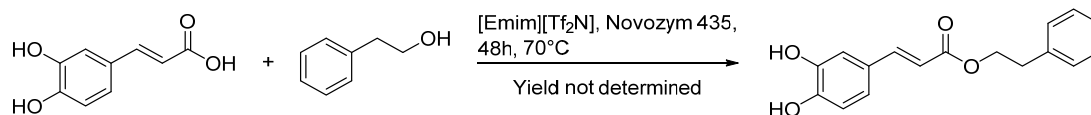


Scheme II-6. Reaction scheme of the hydrolysis of 5-chlorogenic acid and the synthesis of CAPE catalysed by chlorogenate hydrolase.⁵⁰

Specificity, milder conditions, and minimization of side products are advantages offered by enzyme catalysed synthesis. Therefore, Chen *et al.* used an immobilized lipase (Novozym 435) from *Candidia Antarctica* supported on acrylic beads to synthesize CAPE from CA and phenethyl alcohol in isooctane.⁵² They achieved a molar conversion of 79% after two days.

It is well known that ionic liquids (ILs) serve as reaction media for all kinds of reactions.⁵³ ILs are able to dissolve many compounds, have a wide temperature range for the liquid phase, and possess no vapour pressure. They have already been studied extensively as reaction media for enzymatic synthesis.^{54, 55} Kurata *et al.* reported the enzymatic synthesis of CAPE analogues in diverse ILs.⁵⁶ Further work was done by Ho Ha *et al.* who investigated the effect of ILs on the enzymatic synthesis of CAPE.^{57, 58} They used Novozym 435 for the lipase-catalyzed esterification of CA with phenethyl alcohol and discovered that 1-ethyl-3-methylimidazolium bis[(trifluoromethyl)sulfonyl]imide ($[\text{Emim}][\text{Tf}_2\text{N}]$) leads to the highest

conversion rate among nine tested hydrophobic ILs. Further, the effect of temperature, enzyme amount, and substrate ratio was investigated. After 48h, a conversion of 92% was achieved.⁵⁷ The reaction scheme is depicted in Scheme II-7. However, despite the high conversion rate, the reaction suffers from the toxicity of the ILs.^{59, 60}



Scheme II-7. Reaction scheme of the lipase-catalysed esterification of CA and phenethyl alcohol in an IL.⁵⁷

4.4 References

- 1 J. A. Maga and I. Katz, *Crit. Rev. Food Sci. Nutr.*, 1978, **10**, 323-372.
- 2 M. Nsangou, Z. Dhaouadi, N. Jaidane and Z. Ben Lakhdar, *J. Mol. Struct.: THEOCHEM*, 2008, **850**, 135-143.
- 3 A. Russo, R. Longo and A. Vanella, *Fitoterapia*, 2002, **73**, Supplement 1, 21-29.
- 4 P. Stratil, B. Klejdus and V. Kubáň, *Talanta*, 2007, **71**, 1741-1751.
- 5 H. S. Lee and S. Nagy, *J. Food Sci.*, 1990, **55**, 162-163.
- 6 O. Holtomo, M. Nsangou, J. J. Fifen and O. Motapon, *J. Chem. Chem. Eng.*, 2013, **7**, 910-923.
- 7 L. LeBlanc, A. Paré, J. Jean-François, M. Hébert, M. Surette and M. Touaibia, *Molecules*, 2012, **17**, 14637-14650.
- 8 G. Murtaza, S. Karim, M. R. Akram, S. A. Khan, S. Azhar, A. Mumtaz and M. H. H. Bin Asad, *Biomed Res. Int.*, 2014, **2014**, 9.
- 9 N. Kishimoto, Y. Kakino, K. Iwai, K. Y. O. Mochida and T. Fujita, *Biocontrol Sci.*, 2005, **10**, 155-161.
- 10 C. Velazquez, M. Navarro, A. Acosta, A. Angulo, Z. Dominguez, R. Robles, R. Robles-Zepeda, E. Lugo, F. M. Goycoolea, E. F. Velazquez, H. Astiazaran and J. Hernandez, *J. Appl. Microbiol.*, 2007, **103**, 1747-1756.
- 11 A. Kujumgiev, V. Bankova, A. Ignatova and S. Popov, *Pharmazie*, 1993, **48**, 785-786.
- 12 J. Serkedjieva, N. Manolova and V. Bankova, *J. Nat. Prod.*, 1992, **55**, 294-297.
- 13 T. R. Burke, Jr., M. Fesen, A. Mazumder, J. Yung, J. Wang, A. M. Carothers, D. Grunberger, J. Driscoll, Y. Pommier and K. Kohn, *J. Med. Chem.*, 1995, **38**, 4171-4178.

-
- 14 M. C. Nicklaus, N. Neamati, H. Hong, A. Mazumder, S. Sunder, J. Chen, G. W. A. Milne and Y. Pommier, *J. Med. Chem.*, 1997, **40**, 920-929.
- 15 A. A. Johnson, C. Marchand and Y. Pommier, *Curr. Top. Med. Chem. (Sharjah, United Arab Emirates)*, 2004, **4**, 1059-1077.
- 16 Y. Pommier, A. A. Johnson and C. Marchand, *Nat. Rev. Drug Discovery*, 2005, **4**, 236-248.
- 17 D. Grunberger, R. Banerjee, K. Eisinger, E. Oltz, L. Efros, M. Caldwell, V. Estevez and K. Nakanishi, *Experientia*, 1988, **44**, 230-232.
- 18 J.-H. Chen, Y. Shao, M.-T. Huang, C.-K. Chin and C.-T. Ho, *Cancer Lett.*, 1996, **108**, 211-214.
- 19 H.-F. Liao, Y.-Y. Chen, J.-J. Liu, M.-L. Hsu, H.-J. Shieh, H.-J. Liao, C.-J. Shieh, M.-S. Shiao and Y.-J. Chen, *J. Agric. Food Chem.*, 2003, **51**, 7907-7912.
- 20 K. Natarajan, S. Singh, T. R. Burke, D. Grunberger and B. B. Aggarwal, *Proc. Natl. Acad. Sci. USA*, 1996, **93**, 9090-9095.
- 21 M. Sugiura, Y. Naito, Y. Yamaura, C. Fukaya and K. Yokoyama, *Chem. Pharm. Bull. (Tokyo)*, 1989, **37**, 1039-1043.
- 22 T. Toyoda, T. Tsukamoto, S. Takasu, L. Shi, N. Hirano, H. Ban, T. Kumagai and M. Tatematsu, *Int. J. Cancer*, 2009, **125**, 1786-1795.
- 23 S. Son and B. A. Lewis, *J. Agric. Food Chem.*, 2001, **50**, 468-472.
- 24 H. Göçer and İ. Gülçin, *Int. J. Food Sci. Nutr.*, 2011, **62**, 821-825.
- 25 E. L. Ghisalberti, *Bee World*, 1979, **60**, 59-84.
- 26 W. Brumfitt, J. M. Hamilton-Miller and I. Franklin, *Microbios*, 1990, **62**, 19-22.
- 27 C. Garcia-Viguera, W. Greenaway and F. R. Whatley, *Z. Naturforsch., C: Biosci.*, 1992, **47**, 634-637.
- 28 B. M. Hausen, E. Wollenweber, H. Senff and B. Post, *Contact Dermatitis*, 1987, **17**, 163-170.
- 29 J. Sforcin and V. Bankova, *J. Ethnopharmacol.*, 2011, **133**, 253 - 260.
- 30 M. Marcucci, C., *Apidologie*, 1995, **26**, 83-99.
- 31 V. Bankova, S. De Castro and M. Marcucci, *Apidologie*, 2000, **31**, 3 - 15.
- 32 Y. Chen, S. Wu, K. Ho, S. Lin, C. Huang and C. Chen, *J. Sci. Food Agric.*, 2008, **88**, 412 - 419.
- 33 O. Cursta-Rubio, A. Piccineli, M. Campo Fernandez, I. Hernandez, A. Rosado and L. Rastrelli, *J. Agric. Food Chem.*, 2007, **55**, 7502 - 7509.

- 34 A. Dausgch, C. Moraes, P. Fort and Y. Park, *Evid Based Complement Alternat Med*, 2008, **5**, 435 - 441.
- 35 S. Kumazawa, J. Nakamura, M. Murase, M. Miyagawa, A. MR and S. Fukumoto, *Naturwissenschaften*, 2008, **95**, 781 - 786.
- 36 K. Markham, K. Mitchell, A. Wilkins, J. Daldy and Y. Lu, *Phytochemistry*, 1996, **42**, 205 - 211.
- 37 F. Pellati, G. Orlandini, D. Pinetti and S. Benvenuti, *J. Pharm. Biomed. Anal.*, 2011, **55**, 934-948.
- 38 M. Popova, C. Chen, P. Chen, C. Huang and V. Bankova, *Phytochem Anal*, 2010, **21**, 186 - 191.
- 39 E. Ghisalberti, *Bee World*, 1979, **60**, 59 - 84.
- 40 V. Bankova, *J. Ethnopharmacol.*, 2005, **100**, 114 - 117.
- 41 C.-R. Chen, Y.-N. Lee, C.-M. J. Chang, M.-R. Lee and I. C. Wei, *J. Chin. Inst. Chem. Eng.*, 2007, **38**, 191-196.
- 42 L. C. Paviani, E. Saito, C. Dariva, M. C. Marcucci, A. P. Sánchez-Camargo and F. A. Cabral, *Braz. J. Chem. Eng.*, 2012, **29**, 243-251.
- 43 G.-S. You, S.-C. Lin, C.-R. Chen, W.-C. Tsai, C. J. Chang and W.-W. Huang, *J. Chin. Inst. Chem. Eng.*, 2002, **33**, 233-241.
- 44 F. Pellati, F. P. Prencipe, D. Bertelli and S. Benvenuti, *J. Pharm. Biomed. Anal.*, 2013, **81–82**, 126-132.
- 45 T. Hashimoto, M. Tori, Y. Asakawa and E. Wollenweber, *Z. Naturforsch., C: Biosci.*, 1987, **43**, 470-472.
- 46 S. Son, E. B. Lobkowsky and B. A. Lewis, *Chem. Pharm. Bull.*, 2001, **49**, 236-238.
- 47 J. Otera and J. Nishikido, *Esterification: Methods, Reactions, and Applications*, Wiley, 2009.
- 48 International Programme on Chemical Safety's INCHEM service, <http://www.inchem.org/>, Accessed 30.10.2013.
- 49 M. Touaibia and M. Guay, *J. Chem. Educ.*, 2011, **88**, 473-475.
- 50 N. Kishimoto, Y. Kakino, K. Iwai and T. Fujita, *Appl. Microbiol. Biotechnol.*, 2005, **68**, 198-202.
- 51 N. Kishimoto, Y. Kakino, K. Iwai and T. Fujita, *Colloq. Sci. Int. Cafe*, 2005, **20th**, 249-253.
- 52 H.-C. Chen, H.-Y. Ju, Y.-K. Twu, J.-H. Chen, C.-m. J. Chang, Y.-C. Liu, C. Chang and C.-J. Shieh, *New Biotechnology*, 2010, **27**, 89-93.

-
- 53 T. Welton, *Chem. Rev.*, 1999, **99**, 2071-2084.
- 54 A. S. Roger, F. v. Rantwijk and R. M. Lau, in *Ionic Liquids as Green Solvents*, American Chemical Society, 2003, vol. 856, ch. 16, pp. 192-205.
- 55 P. Wasserscheid and T. Welton, *Ionic liquids in synthesis*, Wiley Online Library, 2008.
- 56 A. Kurata, Y. Kitamura, S. Irie, S. Takemoto, Y. Akai, Y. Hirota, T. Fujita, K. Iwai, M. Furusawa and N. Kishimoto, *J. Biotechnol.*, 2010, **148**, 133-138.
- 57 S. Ha, T. Anh and Y.-M. Koo, *Bioprocess Biosystems Eng.*, 2013, **36**, 799-807.
- 58 S. Ha, T. Anh, S. Lee and Y.-M. Koo, *Bioprocess Biosystems Eng.*, 2012, **35**, 235-240.
- 59 M. Deetlefs and K. R. Seddon, *Green Chem.*, 2010, **12**, 17-30.
- 60 S. Stolte, J. Arning, U. Bottin-Weber, M. Matzke, F. Stock, K. Thiele, M. Uerdingen, U. Welz-Biermann, B. Jastorff and J. Ranke, *Green Chem.*, 2006, **8**, 621-629.

III Experimental

1. Chemicals

Prior to use, choline chloride (Alfa Aesar > 98%), choline bromide (TCI Europe n.v.), urea (Merck, p.A.), D(-)-sorbitol (Merck, extra pure for microbiology) and D(+)-glucose (Merck, anhydrous for biochemistry), caffeic acid (Sigma Aldrich, $\geq 98\%$), ethylammonium chloride (Merck, $\geq 98\%$), glycolic acid (Merck, for synthesis), betaine (Sigma Aldrich, $\geq 99\%$), L-carnitine (Sigma Aldrich, >99%) and, malonic acid (Merck, for synthesis), were dried under vacuum for several days. L-Carnitine, L-Carnitine- α -tartrate and acetyl- α -carnitine hydrochloride was provided by Lonza. Ammonium persulfate (extra pure), caffeic acid phenethyl ester ($\geq 97\%$), phenethyl alcohol ($\geq 99\%$), benzyl alcohol (for synthesis) and sulphuric acid (95-97%) were purchased from Merck and used without further purification. Betaine hydrochloride ($\geq 99\%$), oxalic acid (anhydrous, p.a. $\geq 99\%$), Amberlyst 15 (hydrogen form), molecular sieve (3 Å), ethylene glycol (anhydrous, $\geq 99.8\%$), diethyl adipate ($\geq 99\%$), *p*-toluenesulfonic acid monohydrate as well as the lipases from *hog pancreas*, *Mucor miehei*, *Pseudomonas cepacia*, *Rhizopus arrhizus*, *Rhizopus niveus*, *Aspergillus niger*, *Candida cylindracea* and immobilised *Candida antarctica* lipase B (Novozym 435, acrylic resin) were obtained from Sigma Aldrich and used as received. Further, Amberlite IR-120 was purchased from Roth, DL- carnitine hydrochloride ($\geq 98\%$) and choline iodide from Alfa Aesar (98%) and tetrahydrofurfuryl alcohol ($\geq 99.5\%$) from Pennakem. Methanol, formic acid, acetic acid (100% waterfree) and acetonitrile were of analytical grade and obtained from Merck. Purified water was produced by a millipore system. Deuterated solvents, dimethyl sulfoxide- d_6 (99.9%), chloroform- d (99.8%) and methanol- d_4 (99.8%) were purchased from Deutero.

2. Experimental Methods

2.1 NMR spectroscopy

NMR spectra were recorded on a Bruker Avance 300 (¹300 MHz) at the University of Regensburg. All spectra were recorded at room temperature. Chemical shifts are reported in [ppm] relative to an internal standard (solvent residual peak).¹ Coupling constants J are reported in Hertz [Hz]. Resonance multiplicity of the signals is as follows: s = singlet, d = doublet, t = triplet, q = quartet, m = multiplet, bs = broad singlet, dd = doublet of doublets.

2.2 Karl-Fischer Titration

The water contents were determined with an Abimed MCI analyser (Model CA-02), a coulometric Karl-Fischer titration.

2.3 Refractive Index

The refractive indices were measured with a Krüss Abbe refractometer at 25 °C with a wavelength of 589 nm at 25 °C.

2.4 UV-Vis Spectroscopy

UV-Vis spectra of caffeic acid (CA) ($c = 6 \times 10^{-5}$ M), caffeic acid phenethyl ester (CAPE) ($c = 4 \times 10^{-5}$ M), ChCl ($c = 7 \times 10^{-4}$ M), each in methanol, and a 1:1 (v:v) mixture of phenethyl alcohol:methanol were recorded using a Varian Cary E3 UV-Vis spectrophotometer and a Varian Cary Win UV Scan Application Vers. 2.0 software.

2.5 High Performance Liquid Chromatography

High performance liquid chromatography (HPLC) was performed on a Waters HPLC system comprising two Waters 515 HPLC pumps, a Waters 717 plus autosampler, a Waters 2487 UV/VIS-Detector, and the Waters Empower 3 software. The column used was a Knauer Eurosphere C18-column (100 Å, 250 × 4.6 mm). The samples (6.5 - 70 mg) were diluted with MeOH (5 mL), filtered, and subsequently submitted to HPLC separation using gradient elution. The HPLC conditions are summarized in Table III-1. The temperature of the column was set to 30 °C. The injection volume was 10 µL. The detection wavelength of CAPE was determined with UV-Vis spectroscopy and was set to 289 nm. The measurements for each sample were repeated at least three times.

III Experimental

Table III-1. Gradient table for HPLC analysis.

Time in min.	Flow in mL min ⁻¹	vol% solvent A	vol% solvent B
0	0.7	50	50
20	0.7	0	100
30	0.7	50	50

In general, the separation of a mixture containing CA and CAPE using the aforementioned chromatographic method was possible. CA appeared in the chromatogram at a retention time around 6.5 min and CAPE at 18.3 min. It was not possible to detect ChCl with the applied settings.

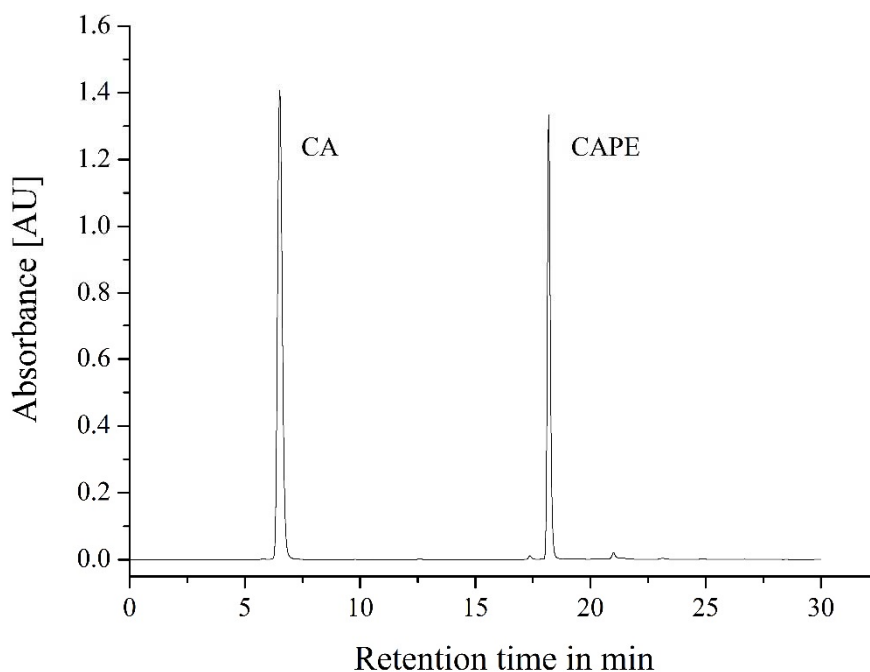


Figure III-1. Chromatogram of a mixture of CA and CAPE.

In order to determine a standard curve, solutions of pure CAPE in methanol with varying concentrations c in mg/mL were analysed by HPLC. As the peak area is proportional to the concentration, a standard curve could be plotted. The relative standard deviations for the peak areas were 1.6, 0.5 and 0.2% for concentrations of 0.20, 0.10 and 0.025 mg/mL, respectively.

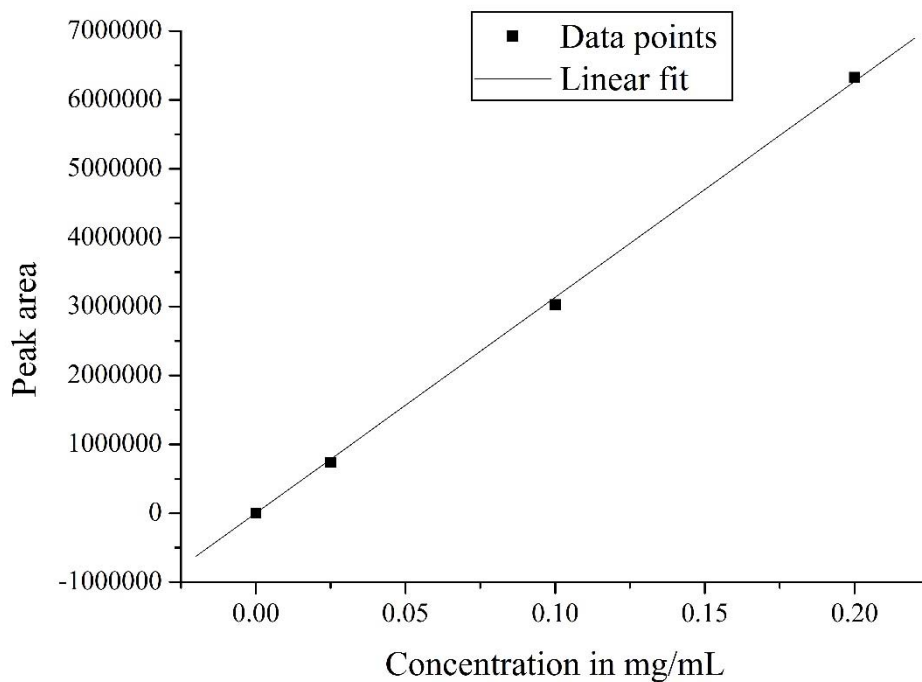


Figure III-2. Standard curve for CAPE in methanol.

The R^2 value, the slope and the standard error of the linear fit are presented in Table III-2. All concentrations c of CAPE were calculated using the standard curve equation via the peak area A measured by HPLC. The standard curve is defined as follows:

$$A = 3.13338 \cdot 10^7 \cdot c \quad 9$$

Table III-2. Results of the linear fit of the standard curve.

Equation	$y = b \cdot x$
R^2	0.99974
Slope	$3.1334 \cdot 10^7$
Standard error	$0.03335 \cdot 10^7$

2.6 Thermal Analysis

Thermogravimetric analysis (TGA) was carried out using a Perkin Elmer TGA 7 under oxygen atmosphere. The measurements were performed in a temperature range from 30 to 900 °C, with a heating rate of 10 °C min⁻¹. The decomposition temperatures were determined

from the onset of mass loss, derived from the intersection of the baseline before the thermal decomposition with the tangent during mass loss.

Differential scanning calorimetry (DSC) measurements were performed with a Perkin Elmer DSC 8000 under nitrogen atmosphere. The measurements of the glass transition temperatures of the sugar based low-melting mixtures were carried out with a heating rate of $15\text{ }^{\circ}\text{C min}^{-1}$, from -80 to $50\text{ }^{\circ}\text{C}$. The cycles were repeated 3 times. Glass transition points and heat capacity changes were determined using the half-step temperature of the transition.

The onset of the melting points presented in chapter IV 2 were determined with DSC measurements from $-10\text{ }^{\circ}\text{C}$ to $85\text{ }^{\circ}\text{C}$. The heating rate was $5\text{ }^{\circ}\text{C min}^{-1}$ for all measurements and the cycles were repeated 3 times.

2.7 Density

The density, ρ , was determined as a function of temperature with an Anton Paar DMA 5000M vibrating tube densiometer. The samples were inserted in a U-shaped borosilicate glass tube. The tube was excited until the eigenfrequency of the tube was reached. This frequency is directly proportional to the density of the sample. The densities of the low-melting mixtures in section IV 1.3.2.1 were measured in a temperature range from 15 to $65\text{ }^{\circ}\text{C}$. The densities used for the calculations of the dynamic light scattering in section IV4.3.2 were determined at $25\text{ }^{\circ}\text{C}$.

2.8 Viscosity

Viscosities presented in section IV 1.3.2.2 were determined using a Bohlin CVO 120 rheometer. All samples were measured with a CP4^o/4 mm cone under an argon atmosphere. The viscosity measurements were carried out in a temperature range between 15 and $75\text{ }^{\circ}\text{C}$, with shear rates from 0.076 to 10 s^{-1} .

Viscosities used for dynamic light scattering in section IV 4.3.2 were determined with a rolling-ball viscometer (AMVn, Anton Paar). The sample was inserted in a glass capillary equipped with a steel ball. The ball rolls a fixed distance at a given angle. The rolling time of the steel ball correlates with the dynamic viscosity of the fluid according to

$$\eta = K \times (\rho_{\text{sb}} - \rho_{\text{sample}}) \times t \quad 10$$

K represents a temperature and angle dependent calibration constant, ρ_{sb} the density of the steel ball, ρ_{sample} the density of the sample and t the rolling time of the steel ball. Except for

samples E6, for which a capillary with an inner diameter of 1.6 mm was necessary, a distinct glass capillary with a diameter of 1.8 mm was employed. The capillaries were calibrated with mineral oils purchased from Cannon (N44 for the 1.8 mm capillary and S3 for the 1.6 capillary).

2.9 Ternary Phase Diagrams

The domains of existence of the single clear and homogeneous phase were determined using a static and dynamic process described by Clausee *et al.*² The alcohol, tetrahydro furfuryl alcohol (THFA), was mixed with the DESs or diethyl adipate (DEA) at determined weight ratios to obtain a starting weight of 3 g. Then DEA and DESs, respectively, were added dropwise to the solutions until a phase transformation occurred. The amount of added constituent was recorded and the weight percentages for each mixture were calculated. The temperature was kept constant at 25 ± 1 °C with a thermostatically controlled test tube rack.

2.10 Dynamic Light Scattering

Dynamic light scattering (DLS) experiments were performed with CGS-3 goniometer from ALV (Langen, Germany). The system was equipped with an ALV-7004/FAST Multiple Tau digital correlator and a vertical-polarized 22-mW HeNe laser (wavelength $\lambda = 632.8$ nm). The measurements were carried out at 25 °C with a scattering angle of 90°. All samples were filtered with a 0.2 μm PTFE membrane filter to remove dust particles. The cylindrical light-scattering cells had an outer diameter of 10 mm. The measuring time was 300 s. The obtained correlation functions were fitted by a single exponential equation.

2.11 Small Angle X-Ray Scattering

Small angle X-ray scattering (SAXS) was performed and analysed by Julien Marcus at the Institut de Chimie Séparative de Marcoule, France. The measurements were carried out on a bench built by Xenocs. The X-ray radiation was generated by a sealed molybdenum tube with a wavelength λ of 0.71 Å. The scattered beam detection is maintained by a large online detector (MAR Research 345, diameter: 345 mm) located at 750 mm from the sample stage. The scattering vector q is described as following:

$$q = \frac{4\pi}{\lambda} \cdot \sin \frac{\theta}{2} \quad 11$$

The achievable q region was 0.2-30 nm^{-1} with an experimental resolution of $\Delta q/q = 0.05$. A 12: ∞ multilayer Xenocs mirror, coupled to two sets of Forvis scatterless slits providing a

$0.8 \times 0.8 \text{ mm}^2$ beam at the sample position, was used to apply collimation. As a calibration standard, a 2.36 mm thick high-density polyethylene sample (supplied by Goodfellow) was utilised to obtain absolute intensities. The acquisition time of the samples was 3600 s. The two-dimensional spectra were integrated with the FIT2D software. The electronic background of the detector, the transmission measurement and the empty cell subtraction were taken into account. The scattering intensity was then plotted against the magnitude of q and the curves were fitted with an Ornstein-Zernike function.

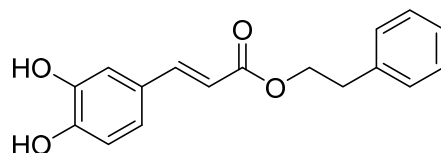
2.12 References

- 1 H. E. Gottlieb, V. Kotlyar and A. Nudelman, *J. Org. Chem.*, 1997, **62**, 7512-7515.
- 2 H. L. Rosano and M. Clause, *Microemulsion systems*, CRC Press, 1987.

3. Synthesis

3.1 Synthesis of Caffeic Acid Phenethyl Ester

Choline chloride (7.75 g, 55.5 mmol) and caffeic acid (5.00 g, 27.73 mmol) were combined in an inert atmosphere. The vial was sealed and the mixture stirred at 90 °C until a yellowish, homogeneous liquid was formed. Subsequently, the temperature was reduced to 80 °C, and phenethyl alcohol (50.45 g, 412.92 mmol) was added under vigorous stirring until the mixture was homogeneous. Amberlyst 15 (4.96 g) was added and the reaction mixture was stirred under exclusion of light to prevent degradation for 14 h at 80 °C. Amberlyst 15 was filtered off and the remaining liquid was poured slowly into hot water. Upon cooling to room temperature, caffeic acid phenethyl ester precipitated and was collected by filtration. The product was washed with water. Caffeic acid phenethyl ester was obtained as a slightly purple to off-white powder (56.4%).



^1H NMR (300.13 MHz, CDCl_3) δ [ppm] = 7.50 (d, J = 15.9 Hz, 1H), 7.33–7.18 (m, 5H), 7.01 (d, J = 2.0 Hz, 1H), 6.92 (dd, J = 8.2 and 2.1 Hz, 1H), 6.76 (d, J = 8.1 Hz, 1H), 6.22 (d, J = 15.9 Hz, 1H), 4.35 (t, J = 7.0 Hz, 2H), 3.98 (t, J = 7.0 Hz, 2H)

IV Results and Discussion

1. New Low-Melting Mixtures

1.1 Abstract

In the first part of this chapter, low-melting mixtures comprising carnitine and betaine derivatives as well as ammonium persulfate and ethylammonium chloride are introduced. The used ammonium compounds serve as alternative to choline chloride. In the second part, physico-chemical properties of ternary sugar-based low-melting mixtures were determined. Choline chloride, urea and as sugars glucose and sorbitol, respectively, were blended in various compositions. The refractive index, density, viscosity, decomposition temperatures and glass transition temperatures were measured. Further, the influence of temperature and water content was investigated. The results show that the mixtures are liquid below room temperature and the viscosity and density are dependent on the temperature and composition. Moreover, the viscosity decreases with increasing water content. These mixtures are biodegradable, low toxic, non-volatile, non-reactive with water and can be accomplished with low cost materials. In consideration of these advantages and a melting point below room temperature, these low-melting mixtures can be a good alternative to ionic liquids as well as environmentally unfriendly and toxic solvents.

1.2 Introduction

A eutectic system is the mixture of chemical compounds or elements which exhibits a single chemical composition at which it solidifies at a lower temperature than at any other composition.^{1,2} Eutectic systems with a very large depression of the melting point, which can be up to 200 °C, are called deep eutectic solvents (DESs). About ten years ago, Abbott *et al.* reported for the first time on such systems.³ The very significant melting temperature lowering at the eutectic point results mainly from the strong interaction of the anion with the hydrogen bond donor. Hence, the lattice energy is decreased which leads to a depression of the melting point.^{3,4} One type of DES is the blend of an organic salt and hydrogen bond donors (HBD),^{5,6} the most prominent being probably the mixture of choline chloride (ChCl) and urea.³

Not only the easy production, low costs, non-volatility and non-inflammability are considerable advantages of these new systems, but also their easy biodegradability.^{4,7}

Further, and also very important, typical DES derive from renewable resources, whereas most solvents used in industrial processes and chemistry still stem from petrol. For some

applications, for example in biocatalysis, the use of "green" DES can be a promising alternative.⁸⁻¹⁷

ChCl is the most dominant quaternary ammonium compound used in the field of DESs. A broad range of HBD in combination with ChCl has been established. However, the number of DES, liquid at room temperature, is still very limited.¹⁸ Instead of varying the HBD, the organic salt can also be altered. For instance, carnitine is a promising substance for the utilisation in DESs and low-melting mixtures (LMMs). L-Carnitine is produced naturally in the human body via trimethyllysine and γ -butyrobetaine hydrolases. It is needed for the mitochondrial oxidation of long-chain fatty acids.¹⁹ In industry, carnitine and also acetyl-carnitine are applied in cosmetics and in pharmacy.²⁰⁻²³ Further, L-carnitine is used as renewable building block for biomaterials like polycarnitine, polycrotonbetaine and polycarnitine allylester.²⁴ In the field of LMMs, a L-carnitine-urea (2-3 wt:wt) melt was used as a reaction medium for a Diels-Alder cycloaddition.²⁵ However, this mixture has a melting point of 74 °C which limits its range of application. Also, betaine, an oxidation product of choline, was already used for LMMs.^{10, 11} The first part of this chapter, concentrates on the screening of new LMMs comprising carnitine, betaine and some of their derivatives. Also ammonium persulfate and ethylammonium chloride were tested.

In order to create new systems, carbohydrates were discovered as mixing partners.²⁶ The largest part of all biomass is carbohydrates with a percentage of 75% and, hence, they are the most important and widespread renewable feedstocks on earth.⁸ Carbohydrates are poorly soluble in almost all solvents except water, which is a major drawback concerning their use.²⁷ For a few years, it has been reported that carbohydrates can be incorporated into ionic liquids (ILs).²⁷⁻²⁹ However, from an environmental point of view, creating 'green' fluids by combining carbohydrates and ILs is not advantageous, since ILs tend to be toxic and have only moderate biodegradability.³⁰⁻³²

Therefore, it is tempting to combine carbohydrates with DES. In this line, Imperator *et al.* reported the utilisation LMMs of sugars or sugar alcohols, urea and inorganic salts as solvents for Diels-Alder reactions.^{26, 30} In a carbohydrate-urea-salt melt, a [4+2] cycloaddition between cyclopentadiene and different acrylates yielded the respective products in good yields.²⁶ In a continuation of their work, the authors used these LMMs as a solvent medium for further reactions, in which both sugar and urea were used as reaction partners. For example, β -D-glucosyl urea was prepared from a D-glucose/urea/NH₄Cl melt (3:7:1 wt:wt:wt) in a condensation reaction using different catalysts.^{30, 33}

Table IV-1. Melting points of mixtures of carbohydrates, urea and inorganic salts in different compositions.

Carbohydrate	Urea	Salt	Mass ratio	Melting points in °C	Ref.
Glucose	Urea	NH ₄ Cl	5-2.5-2.5	84	13
Glucose	Urea	NH ₄ Cl	6-3-1	78	13
Glucose	Urea	NaCl	6-3-1	78	29
Glucose	Urea	CaCl ₂	5-4-1	75	13
Sorbitol	DMU ^a	NH ₄ Cl	7-2-1	67	29

^a DMU: 1,3-dimethylurea

The melting points of the used mixtures range from 65 to 85 °C, as summarised in Table IV-1.^{26, 34} Until now, such sugar-based LMMs, with melting points lower than 50 °C, are very rare.³⁵ Hence, in this chapter, ternary mixtures of urea and choline chloride as salt and glucose or sorbitol as sugar are introduced. The melting points of all mixtures were below room temperature. Some other basic properties are presented, such as temperature-dependent densities, viscosities, and degradation temperatures as well as glass transition temperatures.

1.3 Results and Discussion

1.3.1 *Alternative Ammonium Compounds to Choline Chloride*

Various LMMs comprising ammonium compounds and diverse HBDs were mixed. The used ammonium compounds and their abbreviation are listed in Table IV-2. Binary and ternary mixtures with different compositions comprising ammonium compounds and HBDs were produced. As HBD, urea, malonic acid (MA), glycolic acid (GA), glucose (Glu), sorbitol (Sor) and caffeic acid (CA) were used. The compounds were mixed under a nitrogen atmosphere and stirred at 80 °C until a homogeneous liquid was formed.

Table IV-2. Used ammonium compounds with their corresponding abbreviation and molecular structure.

Ammonium compound	Abbreviation	Molecular structure
Ammonium persulfate	APS	$\text{NH}_4^+ \left[\text{O}_3\text{S}-\text{O}-\text{SO}_3 \right]^{-2} \text{NH}_4^+$
L-Carnitine- α -tartrate	CT	
Acetyl- α -carnitine hydrochloride	ACH	
L-Carnitine	C	
DL-Carnitine hydrochloride	CCI	
Betaine	B	
Betaine hydrochloride	BCI	
Ethylammonium chloride	EAC	$\text{Cl}^- \text{NH}_3^+ \text{CH}_2\text{CH}_3$

IV Results and Discussion

The state of matter of various mixtures was investigated at 80 °C, room temperature (RT) and 0 °C. The results are presented in Table IV-3.

Table IV-3. List of performed LMMs comprising an ammonium compound and HBDs. The state of matter was determined at 80 °C, room temperature and 0 °C.

Ammonium Compound	HBD 1	HBD 2	Molar ratio	80 °C	RT	0 °C
APS	Urea	-	1-2	-	-	-
APS	Urea	-	1-1	-	-	-
APS	MA	-	1-1	-	-	-
APS	GA	-	1-3.3	+	~	-
CT	Urea	-	1-2	-	-	-
CT	Urea	-	1-1	-	-	-
CT	MA	-	1-1	-	-	-
CT	GA	-	1-3.14	+	+	+
ACH	Urea	-	1-2	~	~	-
ACH	Urea	-	1-1	~	~	-
ACH	MA	-	1-1	-	-	-
ACH	GA	-	1-3.5	+	+	+
ACH	Urea	GA	1-1.6-3.4	+	+	+
ACH	Urea	GA	1-1.9-3.6	+	+	+
ACH	Urea	GA	1-3.4-3.5	+	+	+
ACH	GA	-	1-1	~	~	~
ACH	GA	-	1-2	+	~	~
ACH	GA	-	2-1	-	-	-
ACH	GA	-	1-3	+	+	+
ACH	GA	-	1-3.5	+	+	+
ACH	GA	-	1-4	+	+	+
ACH	GA	-	1-5	+	+	+
ACH	GA	-	1-6	+	+	+
ACH	GA	-	1-7	+	+	+
ACH	GA	-	1-8	+	~	-
ACH	GA	-	1-9	+	~	-
ACH	GA	-	1-10	+	~	-
ACH	GA	-	1-12	+	~	-
C	Urea	-	1-1	-	-	-
C	Urea	-	1-2	+	+	+
C	Urea	-	1-3	+	+	+

1. New Low-Melting Mixtures

Ammonium Compound	HBD 1	HBD 2	Molar ratio	80 °C	RT	0 °C
C	MA	-	1-1	+	+	+
C	MA	-	1-2	+	+	+
C	MA	-	1-3	+	+	+
C	GA	-	1-1	~	-	-
C	GA	-	1-3	+	+	+
C	GA	-	1-4	+	+	+
C	GA	-	1-5	+	+	+
C	Glu	-	1-2	-	-	-
C	Sor	-	1-2	~	~	-
C	CA	-	1-2	-	-	-
C	CA	-	1-1	-	-	-
C	CA	-	2-1	-	-	-
CCl	U	-	1-1	-	-	-
CCl	U	-	1-2	-	-	-
CCl	MS	-	1-1	-	-	-
CCl	MS	-	1-2	+	-	-
CCl	GA	-	1-1	-	-	-
CCl	GA	-	1-2	-	-	-
CCl	GA	-	1-3	+	~	-
CCl	GA	-	1-4	+	~	-
CCl	GA	-	1-5	+	~	-
CCl	Sor	-	1-2	-	-	-
CCl	Sor	-	1-1	-	-	-
B	MA	-	1-1	+	~	-
B	GA	-	1-3.4	+	+	+
B	CA	-	1-2	-	-	-
B	CA	-	1-1	-	-	-
B	CA	-	2-1	-	-	-
BCl	MA	-	1-1	-	-	-
BCl	GA	-	1-4	~	~	~
EAC	U	-	1-1	+	-	-
EAC	U	-	1-2	+	-	-
EAC	MA	-	1-1	+	-	-
EAC	MA	-	1-2	~	-	-
EAC	GA	-	1-1	+	+	+
EAC	GA	-	1-2	+	+	+

Ammonium Compound	HBD 1	HBD 2	Molar ratio	80 °C	RT	0 °C
EAC	CA	-	1-2	+	-	-
EAC	CA	-	1-1	+	-	-
EAC	CA	-	2-1	+	-	-
	Urea	GA	1-3.5	+	-	-

+ \triangle homogeneous liquid, ~ \triangle liquid, not homogeneous, - \triangle solid

At first glance, GA seems a suitable HBD for the formation of LMMs. However, during the mixing process, bubbling was observed. This leads to the assumption that GA reacts with the ammonium compound. The determination of the water content as a function of time revealed that water is produced. The values of the time-dependent water contents are presented in Table IV-4. This might be a first hint that GA and the ammonium compounds esterified. A high water content also reduces the melting point. Therefore, many mixtures containing GA are liquid at RT and below.

Table IV-4. Time-dependent water contents of ACH-GA mixtures.

ACH-GA 1-7		ACH-GA 1-3	
Time in d	Water content in wt%	Time in d	Water content in wt%
0	0.29	0	0.15
1	1.57	1	0.20
2	2.00	2	0.61
3	2.35	3	1.41

A promising alternative to choline chloride is L-carnitine. Melts comprising L-carnitine, urea and malonic acid, respectively, form LMMs which are liquid at 0 °C. Since L-carnitine is a natural-derived and non-toxic compound, it is an auspicious candidate for the utilisation in DESs and LMMs.

1.3.2 Sugar-Based Low-Melting Mixtures

Sugar-based LMMs were formed by choline chloride, urea, glucose and sorbitol, respectively. The compounds were mixed under a nitrogen atmosphere and stirred at 75 °C until a homogenous colorless liquid was formed. The mixtures were stored in sealed flasks. The compositions, water content, their abbreviations and refractive indices of the four prepared mixtures are shown in Figure IV-5. Figure IV-1 shows a sample of Glu-U-ChCl1 at room temperature.

Table IV-5. Molar ratios and refractive indices as well as the water content of the four prepared low-melting mixtures

Mixture	Molar ratio	Refractive index	Water content (weight %)	Abbreviation
Glucose-Urea-ChCl	1-1-1	1.5166	0.39	Glu-U-ChCl1
Glucose-Urea-ChCl	1-2-1	1.5150	0.10	Glu-U-ChCl2
Sorbitol-Urea-ChCl	1-1-1	1.5108	0.19	Sor-U-ChCl1
Sorbitol-Urea-ChCl	1-2-1	1.5111	0.13	Sor-U-ChCl2



Figure IV-1. Mixture of Glucose-Urea-ChCl (1-1-1) at room temperature.

1.3.2.1 Density

The densities of the different mixtures were measured within a temperature range from 15 °C to 65 °C. The results are depicted in Figure IV-2. There is a linear dependence between density and temperature. The densities of the glucose systems vary between 1.315 g cm⁻³ at 15 °C and 1.290 g cm⁻³ at 65 °C and those of the sorbitol systems between 1.290 g cm⁻³ at 15 °C and 1.261 g cm⁻³ at 65 °C. The mixtures with higher urea content show a slightly higher density.

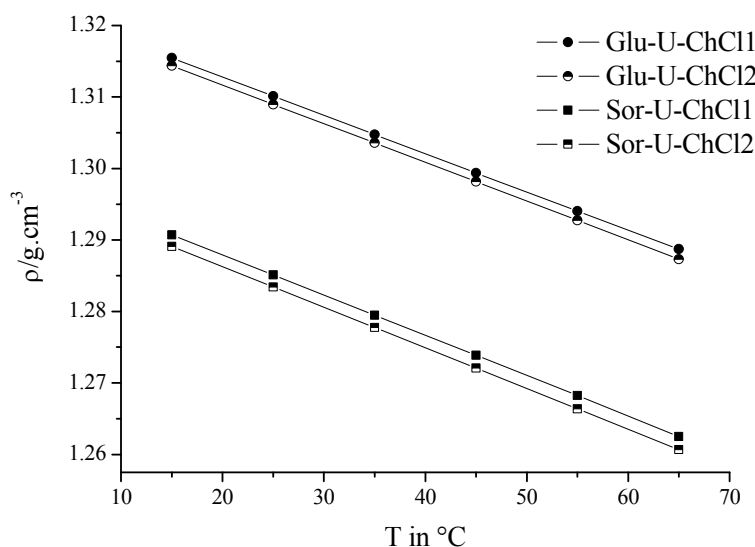


Figure IV-2. Densities of the mixtures as a function of temperature.

1.3.2.2 Viscosity

The viscosity of a LMM is an important characteristic, since high viscosities can decrease the reaction rate in case of diffusion-controlled chemical reactions. The measured values are presented in Figure IV-3. The viscosities vary significantly as a function of temperature with a more pronounced temperature dependence of the glucose systems. The viscosities were measured in a temperature range from 15 °C to 75 °C. Since the LMMs are very hygroscopic, moisture should be avoided. Note that for these glucose containing systems, the higher fraction of urea decreases the viscosity at all temperatures.

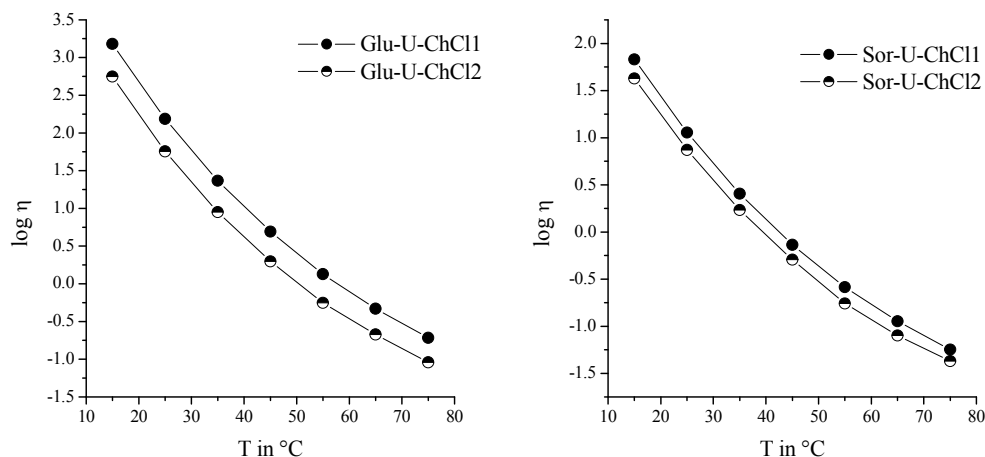


Figure IV-3. Logarithmic plots of the different viscosities of the low melting mixtures as a function of temperature. The viscosities are given in Pa·s.

Nevertheless and as expected,¹⁸ the viscosities are all very high around room temperature (up to 1520 Pa·s). They drop significantly at higher temperatures to values as low as 0.04 Pa·s. Presumably, the extensive hydrogen bond network between the components is responsible for both, the high viscosities at low temperatures and the strong temperature dependence.

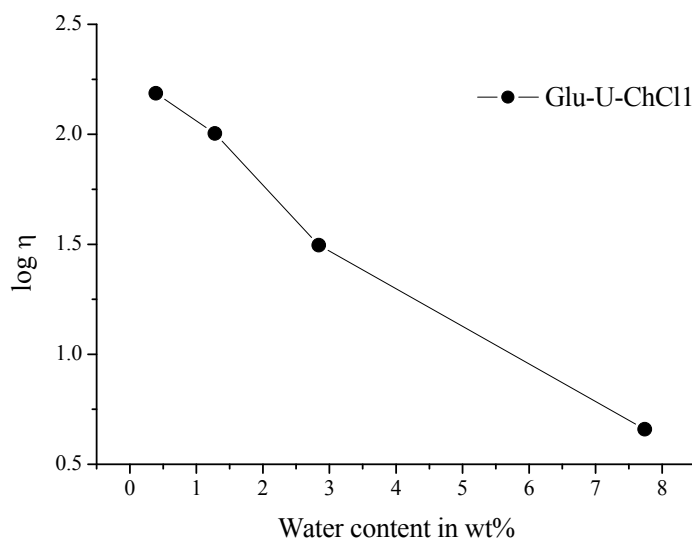


Figure IV-4. Logarithmic plot of the viscosity of a Glu-U-ChCl1 mixture as a function of water content. The viscosities are given in Pa·s.

Further, electrostatic and van der Waals interactions or the large sizes of the species, which cause a small void volume and, therefore, a lower mobility of these species may also contribute to the high viscosities.¹⁸ Note that all four mixtures show a Newtonian behaviour over the whole temperature range studied.³⁶

As the amount of water in such systems is an important parameter, we measured the viscosity as a function of the water content for one of the mixtures. Figure IV-4 shows the results for the system Glu-U-ChCl1. With a water content of 7.8 wt% the viscosity drops by a factor of 50 compared to the mixture with only 0.4 wt% of water.

1.3.2.3 Thermogravimetric Analysis

The thermal stability and decomposition temperatures were measured with a thermogravimetric analyser in a temperature range from 30 °C to 900 °C with a heating rate of 10 °C min⁻¹. The decomposition temperatures were determined from the onset of mass loss, derived from the intersection of the baseline before the thermal decomposition with the tangent during mass loss. Figure IV-5 depicts the mass loss in percent as a function of temperature for each mixture. The decomposition temperatures range around 175 °C. No appreciable difference in thermal stability between the different mixtures was detected. However, the further degradation of the LMMs containing glucose differs from the ones containing sorbitol. In the latter case, the mixtures degrade in one step, whereas the glucose mixtures decompose in several steps. The single step degradation of the sorbitol mixtures is consistent with previous studies and own measurements.^{9, 37}

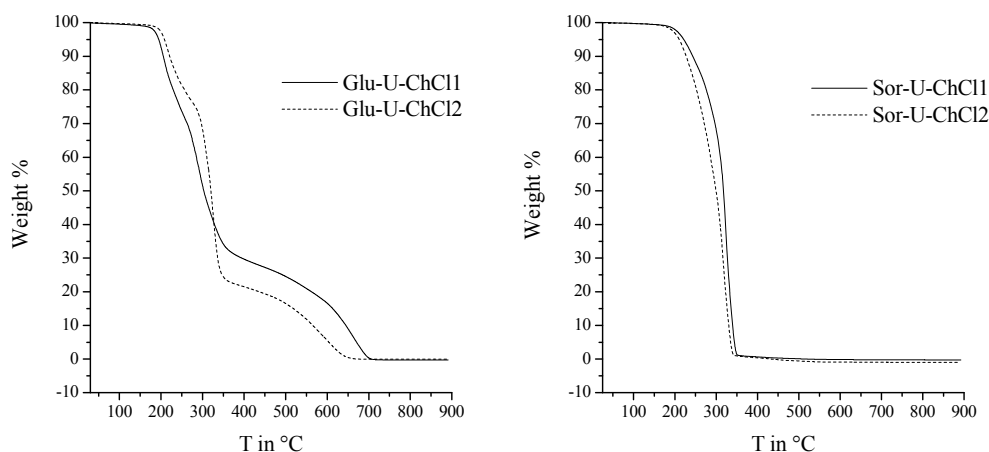


Figure IV-5. Weight losses of the mixtures in % as a function of temperature.

The thermograms of urea, choline chloride and the carbohydrates are presented in the appendix (VI 1.3). The first step in the thermogram of the Glu-U-ChCl mixtures results from the degradation of urea. The further steps arise from the degradation of glucose which decomposes in two steps.³⁸

1.3.2.4 Glass Transition Temperatures

A lot of ILs are good glass formers, i.e. they can be cooled from the equilibrium state down to low temperatures without crystallising.³⁹⁻⁴¹ They enter the metastable supercooled liquid state and undergo a glass transition which leads to an out-of-equilibrium glassy state.⁴⁰ The DSC signature of the glass transition is a sigmoidal change in heat flux reflecting a characteristic change in heat capacity, ΔC_p , when the sample is heated from the glassy state to the liquid state.⁴¹ For all four mixtures glass transition temperatures were found. The measurements were performed with a heating rate of $15\text{ }^\circ\text{C min}^{-1}$ from $-80\text{ }^\circ\text{C}$ to $50\text{ }^\circ\text{C}$. The glass transition temperatures of the mixtures vary from $-36.6\text{ }^\circ\text{C}$ to $-24.0\text{ }^\circ\text{C}$. The LMMs containing sorbitol exhibit a lower transition temperature than those containing glucose. Further, the compositions with higher carbohydrate content show a lower transition temperature.

ILs can exhibit a strong jump in their molar heat capacity, ΔC_{pm} , because each molecule unit is in fact composed of two sub-units (the cation and the anion). Therefore, they have an appreciable relative mobility in the supercooled liquid state.⁴⁰ For example, the values of a series of $[\text{C}_n\text{O}_m\text{mim}][\text{X}]$ of imidazolium cation-based room temperature ionic liquids (RTILs) are in the region of $92\text{ J mol}^{-1}\text{ K}^{-1}$ to $177\text{ J mol}^{-1}\text{ K}^{-1}$.⁴⁰ Compared to the RTILs, the measured LMMs have slightly lower ΔC_{pm} values, ranging from $60\text{ J mol}^{-1}\text{ K}^{-1}$ to $86\text{ J mol}^{-1}\text{ K}^{-1}$. However, these values are still very high compared to polymeric systems $\Delta C_{pm} = 10\text{ J mol}^{-1}\text{ K}^{-1}$ for polyethylene ($T_g = -133\text{ }^\circ\text{C}$) and $\Delta C_{pm} = 36\text{ J mol}^{-1}\text{ K}^{-1}$ for poly(vinyl acetate) ($T_g = -269\text{ }^\circ\text{C}$),^{40, 42} and typical solvents such as glycerol ($T_g = -88\text{ }^\circ\text{C}$) and toluene ($T_g = 116\text{ }^\circ\text{C}$) with values of $\Delta C_{pm} = 23\text{ J mol}^{-1}\text{ K}^{-1}$ and $53\text{ J mol}^{-1}\text{ K}^{-1}$, respectively.^{40, 43}

Compared to these substances, the higher values for ΔC_{pm} at T_g indicate that more degrees of freedom are released on heating above T_g , probably because the LMMs consist of three components. As shown in Table IV-6, the sorbitol systems exhibit higher ΔC_{pm} values than the corresponding glucose mixtures. Further, the melts with higher carbohydrate content have a larger change in heat capacity ΔC_{pm} .

Table IV-6. Glass transition temperature (T_g), heat capacity (ΔC_p) and molar heat capacity changes at T_g (ΔC_{pm}).

Mixture	T_g in $^{\circ}\text{C}$	ΔC_p in $\text{J g}^{-1} \text{K}^{-1}$	ΔC_{pm} in $\text{J mol}^{-1} \text{K}^{-1}$
Glu-U-ChCl1	-27.3	0.672	85
Glu-U-ChCl2	-24.0	0.545	60
Sor-U-ChCl1	-36.6	0.675	86
Sor-U-ChCl2	-34.4	0.635	70

1.4 Concluding Remarks

In the first part, various ammonium compounds as alternatives to choline chloride were introduced. These ammonium compounds were mixed with different HBDs. It was revealed that mixtures containing GA foam upon mixing. Further, the water content increased with time. This leads to the assumption that the ammonium compound and GA react. Possibly, an esterification took place since water is produced. Further, L-carnitine is a promising alternative to ChCl, since most of the mixtures are liquid at 0°C and L-carnitine is a natural-derived, non-toxic substance.

New very low-melting mixtures were obtained by mixing ChCl with urea and a carbohydrate (glucose or sorbitol). Their density measurements show a linear correlation between density and temperature. The densities of the LMMs containing glucose have higher values than those containing sorbitol. Further, the mixtures with a higher urea content show increased densities. The viscosities of the melts are relatively high at room temperature. Viscosities of the mixtures depending on the chemical nature of the LMM components (type of salt and molar ratios of the components), on the temperature, and on the water content were measured. Similar to other known DESs, the viscosity is governed by an extensive hydrogen bond network between the components, which results in lower mobility of the free species within the DES and, therefore, a higher viscosity.¹⁸ The LMMs were thermally stable up to 175°C .

Another typical feature of LMMs is the absence of a crystal structure. Upon cooling, the mixtures stay in a metastable supercooled liquid state down to at least -24.0°C . At lower temperatures they undergo a glass transition.

1.5 References

- 1 W. F. Smith and J. Hashemi, *Foundations of Materials Science and Engineering*, McGraw-Hill, 2003.
- 2 P. Atkins and J. de Paula, *Physical Chemistry*, W. H. Freeman, 2006.
- 3 A. P. Abbott, G. Capper, D. L. Davies, R. K. Rasheed and V. Tambyrajah, *Chem. Commun.*, 2003, 70-71.
- 4 A. P. Abbott, D. Boothby, G. Capper, D. L. Davies and R. K. Rasheed, *JACS*, 2004, **126**, 9142-9147.
- 5 A. P. Abbott, J. C. Barron, K. S. Ryder and D. Wilson, *Chem. Eur. J.*, 2007, **13**, 6495-6501.
- 6 D. Carriazo, M. C. Serrano, M. C. Gutierrez, M. L. Ferrer and F. del Monte, *Chem. Soc. Rev.*, 2012, **41**, 4996-5014.
- 7 International Programme on Chemical Safety's INCHEM service, <http://www.inchem.org/>, Accessed 30.10.2013.
- 8 D. Peters, *Chem. Ing. Tech.*, 2006, **78**, 229-238.
- 9 M. Sharma, C. Mukesh, D. Mondal and K. Prasad, *RSC Advances*, 2013, **3**, 18149-18155.
- 10 M. Francisco, A. van den Bruinhorst and M. C. Kroon, *Angew. Chem. Int. Ed.*, 2013, **52**, 3074-3085.
- 11 M. Francisco, A. van den Bruinhorst and M. C. Kroon, *Green Chem.*, 2012, **14**, 2153-2157.
- 12 B. Tang and K. Row, *Monatsh. Chem.*, 2013, **144**, 1427-1454.
- 13 M. C. Gutiérrez, M. L. Ferrer, L. Yuste, F. Rojo and F. del Monte, *Angew. Chem. Int. Ed.*, 2010, **49**, 2158-2162.
- 14 E. Durand, J. Lecomte, B. Baréa and P. Villeneuve, *Eur. J. Lipid Sci. Technol.*, 2013, n/a-n/a.
- 15 E. Durand, J. Lecomte, B. Barea, E. Dubreucq, R. Lortie and P. Villeneuve, *Green Chem.*, 2013, **15**, 2275-2282.
- 16 E. Durand, J. Lecomte and P. Villeneuve, *Eur. J. Lipid Sci. Technol.*, 2013, **115**, 379-385.
- 17 J. T. Gorke, F. Srienc and R. J. Kazlauskas, *Chem. Commun.*, 2008, 1235-1237.
- 18 Q. Zhang, K. De Oliveira Vigier, S. Royer and F. Jerome, *Chem. Soc. Rev.*, 2012, **41**, 7108-7146.

- 19 B. Caballero, *Guide to nutritional supplements*, Academic Press, 2009.
- 20 C. Cavazza, EP773020A2, 1997.
- 21 G. Gazzaniga, WO2006013082A1, 2006.
- 22 M. Giesen, K. R. Schroeder and D. Petersohn, WO2007003307A1, 2007.
- 23 W. F. Kohl and T. Scholl, EP434088A1, 1991.
- 24 B. Kamm, M. Kamm, A. Kiener and H. P. Meyer, *Appl. Microbiol. Biotechnol.*, 2005, **67**, 1-7.
- 25 F. Ilgen and B. König, *Green Chem.*, 2009, **11**, 848-854.
- 26 G. Imperato, E. Eibler, J. Niedermaier and B. König, *Chem. Commun.*, 2005, **0**, 1170-1172.
- 27 M. E. Zakrzewska, E. Bogel-Lukasik and R. Bogel-Lukasik, *Energy Fuels*, 2010, **24**, 737-745.
- 28 M. E. Zakrzewska, E. Bogel-Lukasik and R. Bogel-Lukasik, *Chem. Rev.*, 2010, **111**, 397-417.
- 29 L. Poletti, C. Chiappe, L. Lay, D. Pieraccini, L. Polito and G. Russo, *Green Chem.*, 2007, **9**, 337-341.
- 30 C. Russ and B. König, *Green Chem.*, 2012, **14**, 2969-2982.
- 31 M. Deetlefs and K. R. Seddon, *Green Chem.*, 2010, **12**, 17-30.
- 32 M. T. Garcia, N. Gathergood and P. J. Scammells, *Green Chem.*, 2005, **7**, 9-14.
- 33 Russ, F. Ilgen, C. Reil, C. Luff, A. Haji Begli and B. König, *Green Chem.*, 2011, **13**, 156-161.
- 34 G. Imperato, S. Hoger, D. Lenoir and B. König, *Green Chem.*, 2006, **8**, 1051-1055.
- 35 Y. Dai, J. van Spronsen, G.-J. Witkamp, R. Verpoorte and Y. H. Choi, *J. Nat. Prod.*, 2013, **76**, 2162-2173.
- 36 D. F. Evans and H. Wennerström, *The colloidal domain: where physics, chemistry, biology, and technology meet*, Wiley-VCH, 1999.
- 37 D. Rengstl, Ph. D. Thesis, University of Regensburg, 2013.
- 38 A. Magoń and M. Pyda, *Carbohydr. Res.*, 2011, **346**, 2558-2566.
- 39 J. D. Holbrey and K. R. Seddon, *J. Chem. Soc., Dalton Trans.*, 1999, **0**, 2133-2140.
- 40 L. C. Branco, J. N. Rosa, J. J. Moura Ramos and C. A. M. Afonso, *Chem. Eur. J.*, 2002, **8**, 3671-3677.
- 41 J. J. Moura Ramos, C. A. M. Afonso and L. C. Branco, *J. Therm. Anal. Calorim.*, 2003, **71**, 659-666.

- 42 P. G. DeBenedetti, *Metastable liquids: concepts and principles*, PRINCETON University Press, 1996.
- 43 L. H. Sperling, *Introduction to Physical Polymer Science*, Wiley, 2005.

2. COSMO-RS Calculations of Deep Eutectic Solvents

2.1 Abstract

In this chapter, the influence of the hydrogen bond acceptor (HBA) in deep eutectic solvents (DESs) is discussed. First, σ -profiles, generated by COSMO-RS, were created for DESs comprising urea and choline halides. From these σ -profiles, the strength of interaction between the hydrogen bond donor (HBD), urea, and hydrogen bond acceptor (HBA), the halide, can be deduced. The strength of interaction is an indicator for the decline of the melting point. In a second step, the melting points and eutectic compositions of choline fluoride (ChF)-urea, choline chloride (ChCl)-urea, choline bromide (ChBr)-urea and choline iodide (ChI)-urea were calculated. It was discovered that the strongest HBA causes the largest depression of the melting point. The predictions were confirmed by differential scanning calorimetry experiments.

2.2 Introduction

COSMO-RS is an abbreviation for **conductor-like screening model for realistic solvation**. This model describes interactions on the basis of surface pieces with the charge σ . The developed polarisation charge density of the molecule is reflected in the σ -surface. The 3D information about σ on the molecular surface can be converted to a histogram $p^x(\sigma)$ which indicates how much surface can be found in a polarity interval. This histogram is called σ -profile.

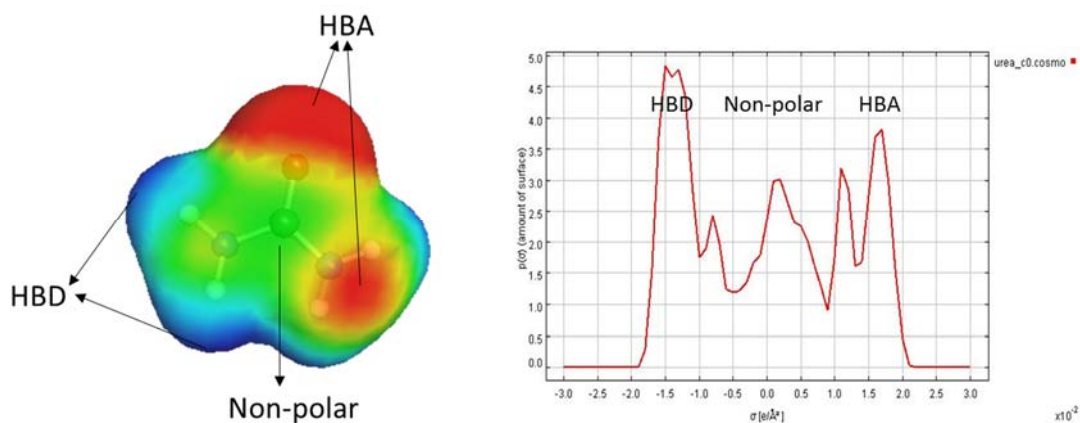


Figure IV-6. σ -surface (left) and σ -profile (right) of urea. The blue areas mark a HBD, the red areas a HBA and the green areas a non-polar region.

The σ -regions beyond $\pm 1 \text{ e/nm}^2$ are considered as strongly polar and potentially hydrogen bonding and the region around 0 e/nm^2 as weakly polar or non-polar (Figure IV-6).^{1,2} In the colour coding, HBD regions are labelled as deep blue and HBA regions as deep red on the surface. Non-polar regions are marked in green. The σ -profiles give valuable information about the behaviour of a substance in the liquid phase. Moreover, properties for binary mixtures can be deduced from these profiles. Therefore, σ -profiles of DESs can be provided by plotting the profile of a HBD, a cation and an anion serving as HBA i.e. urea, the choline cation, and the halide anions.

Abbott *et al.* suggested that the depression of the melting point arises from (i) the lattice energy of the DES, (ii) the entropy changes caused by the formation of a liquid phase and (iii) the interaction of the anion and HBD.³ Most of the time, the HBD or cation is varied to tune DESs with respect to their melting point. However, it is also possible to alter the anion, which serves as the HBA. The fact that the freezing points of DESs, consisting of urea, the choline cation and an anion, decline in the order $\text{F}^- > \text{NO}_3^- > \text{Cl}^- > \text{BF}_4^-$ leads to the assumption that the depression of the melting point is a matter of hydrogen bond strength.⁴

Table IV-7. Freezing temperatures T_f in $^\circ\text{C}$ of some choline-derived DESs with different anions and urea as HBD. All molar ratios of the salt and HBD are 1-2.

Cation	Anion	HBD	T_f in $^\circ\text{C}$	Ref.
Choline	F^-	Urea	1	4
Choline	NO_3^-	Urea	4	4
Choline	Cl^-	Urea	12	4
Choline	BF_4^-	Urea	67	4

To gain further insight into the behaviour of DESs, especially concerning hydrogen bond interactions, COSMO-RS is a useful tool. Since the σ -profiles give information about the hydrogen donor and acceptor abilities of a substance, the profiles of DES comprising urea, the choline cation and diverse halide anions were created. Further, the eutectic compositions and melting points of the mixtures were calculated. The results were compared to experimental data obtained by DSC measurements.

2.3 Results and Discussion

2.3.1 σ -Profiles

The histogram of urea and various choline halides is shown in Figure IV-7. The σ -profile of urea is plotted in red, the choline cation in blue, the fluorid anion in turquoise, the chloride anion in black, the bromide anion in yellow and the iodide anion in grey blue.

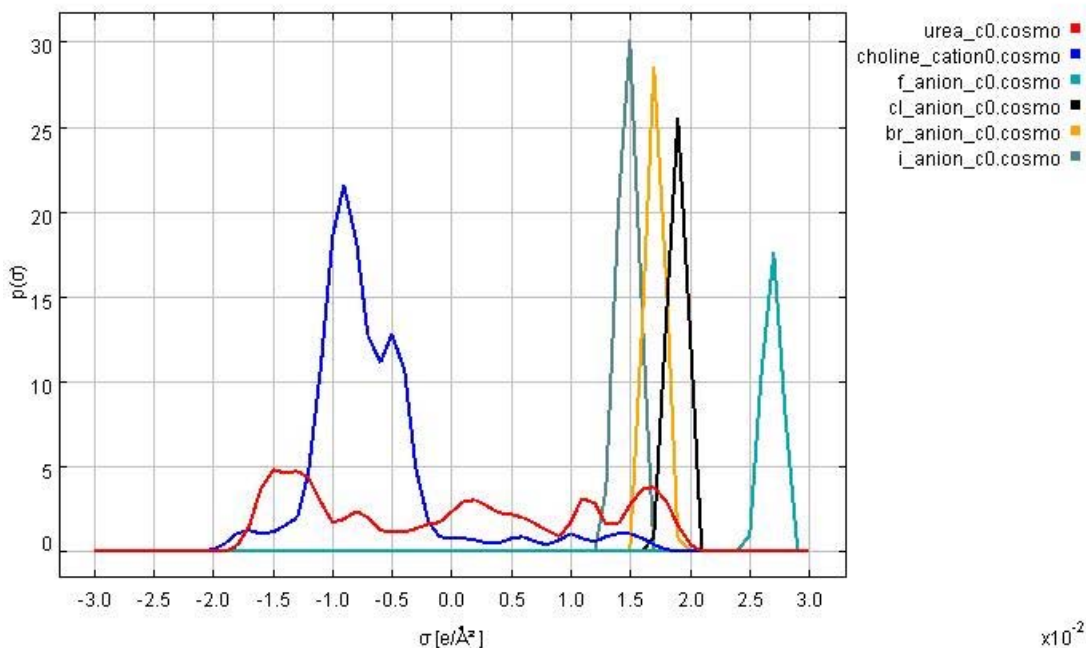


Figure IV-7. σ -profiles of urea, the choline cation and halide anions from fluoride to iodide.

From the histogram, it can be deduced that the strength of the hydrogen acceptor abilities of the halide ions increase in the order $\text{I}^- < \text{Br}^- < \text{Cl}^- < \text{F}^-$. The iodide anion is the weakest HBA. However, the σ -profiles presented in Figure IV-7 show that I^- is even a better HBA than the choline cation. With a peak around 1.5 e/nm^2 , urea is a good HBD. Consequently, urea is more likely to form hydrogen bonds with the halide anions than with the choline cation. Thus, the structure of the choline salt is destroyed and a DES can be formed. In theory, the melting points of the deep eutectics comprising urea and choline halides increases in the order $\text{F}^- < \text{Cl}^- < \text{Br}^- < \text{I}^-$. It can be assumed that the distance between the HBD and HBA is a measure for the strength of the hydrogen bond. To corroborate this theory, COSMO-RS calculations of the phase diagrams of urea and choline halides were performed with the solid-liquid equilibrium (SLE) option.

2.3.2 Phase Diagrams

Phase diagrams were computed with the SLE option. It calculates the composition at a certain temperature at which the mixture merges from the solid in the liquid state. The results are listed in Table IV-8 and depicted in Figure IV-8.

Table IV-8. SLE temperatures of mixtures comprising urea and a choline halide with corresponding molar fractions of urea.

ChF		ChCl		ChBr		ChI	
T _{SLE} in °C	x (Urea)	T _{SLE} in °C	x (Urea)	T _{SLE} in °C	x (Urea)	T _{SLE} in °C	x (Urea)
132.70	1	132.70	1.00	132.70	1.00	132.70	1.00
120.00	0.95	125.00	0.96	120.00	0.94	120.00	0.94
94.29	0.88	100.00	0.89	100.00	0.88	94.29	0.84
68.57	0.84	75.00	0.83	80.00	0.82	68.57	0.75
42.86	0.80	50.00	0.78	60.00	0.77	42.86	0.68
17.14	0.77	25.00	0.74	40.00	0.73	42.86	0.64
-8.57	0.75	0.00	0.71	20.00	0.69	68.57	0.61
-34.29	0.74	-25.00	0.69	20.00	0.67	94.29	0.57
-60.00	0.72	-50.00	0.67	40.00	0.65	120.00	0.52
-60.00	0.50	-50.00	0.66	60.00	0.63	145.71	0.46
-34.29	0.50	-25.00	0.65	80.00	0.61	171.43	0.39
-8.57	0.49	0.00	0.63	100.00	0.58	197.14	0.31
17.14	0.49	25.00	0.62	120.00	0.55	222.86	0.22
42.86	0.48	50.00	0.60	140.00	0.52	248.57	0.11
68.57	0.47	75.00	0.58	160.00	0.48	274.29	0.00
94.29	0.46	100.00	0.56	180.00	0.44		
120.00	0.44	125.00	0.52	200.00	0.38		
145.71	0.41	302.00	0.00	220.00	0.33		
171.43	0.38			240.00	0.26		
197.14	0.33			260.00	0.18		
222.86	0.28			280.00	0.09		
248.57	0.21			298.00	0.00		
274.29	0.11						
300.00	0.00						

All calculated mixtures show a eutectic composition around a molar ratio of 1-2 choline halide-urea confirming the theory that two molecules of urea interact with one halide

anion.^{4,5} Concerning the melting point, the calculations verify the trend deduced from the σ -profiles. The melting points of the deep eutectic mixtures decrease in the order $\text{ChI} > \text{ChBr} > \text{ChCl} > \text{ChF}$. However, a big gap appears in the phase diagram for the predicted eutectic composition of ChF -urea depicted in Figure IV-8. Ionic systems are described the more precisely by COSMO-RS the more charge is delocalized on the ion.² Therefore, properties of very small ions such as F^- or OH^- can be calculated with lower accuracy. This could be a reason why no clear result can be drawn from the calculation for ChF -urea. Nevertheless, more precise predictions were made for ChCl -urea, ChBr -urea and ChI -urea. The melting points of ChCl -urea, ChBr -urea and ChI -urea were calculated to be $-50.00\text{ }^\circ\text{C}$, $20.00\text{ }^\circ\text{C}$ and $42.86\text{ }^\circ\text{C}$, respectively.

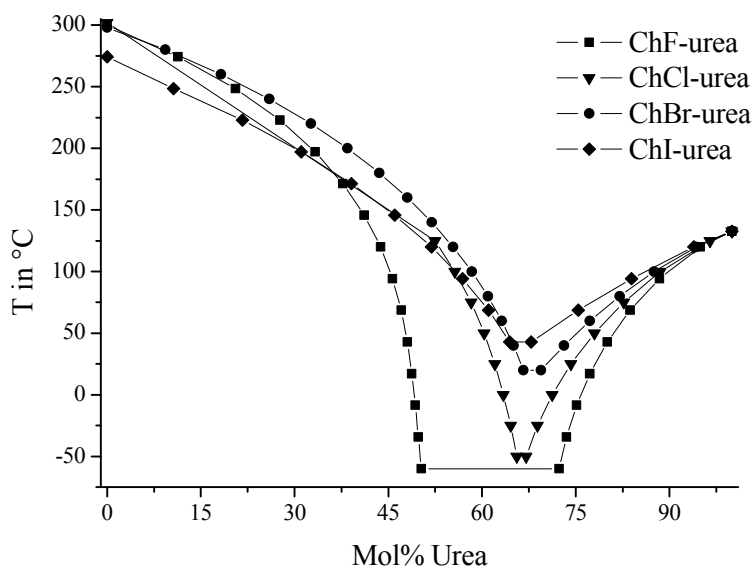


Figure IV-8. Calculated phase diagrams by COSMO-RS of diverse urea-choline halide mixtures.

To compare the predictions to experimental data, the melting points of the mixtures were determined by differential scanning calorimetry (DSC).

Table IV-9. Melting temperatures (T_m) of the different choline halide-urea mixtures (molar ratio 1-2) obtained from DSC with corresponding melting temperatures of the pure choline halide salts (T_m^*) and the calculated SLE temperatures (T_{SLE}).

Mixture	T_m in °C	T_m^* in °C	T_{SLE} in °C
ChCl-urea	22.53 ± 0.05	302	-50
ChBr-urea	41.77 ± 0.13	298	20
ChI-urea	67.28 ± 0.19	273	43

Since no reasonable result for ChF-urea could be obtained, the measurements were only carried out for ChCl-urea, ChBr-urea and ChI-urea. First, the mixtures were produced by mixing urea and the halide salt in a molar ratio of 2-1 at 75 °C. The samples were then measured in a temperature range from -10 °C to 85 °C with a heating rate of 5 °C min⁻¹. The results with corresponding melting points of the pure halide salts and the temperature calculated by COSMO-RS are presented in Table IV-9.

At first sight, the measured melting temperatures seem to differ significantly from the predicted ones. However, the trend that strong hydrogen bonds cause a great decrease of the melting point is confirmed. As discussed in the latter section, the hydrogen bond acceptor abilities of the anions increase in the order $I^- < Br^- < Cl^-$. Therefore, the predicted as well as the measured values show an increase in melting point in the order $I^- > Br^- > Cl^-$. This observation shows that the strength of interaction between the HBD and HBA is a significant factor for the formation of a DES and the depression of its melting point.

As mentioned before, the properties of small, highly charged ions can only be calculated with low accuracy.² The temperatures for the eutectic mixtures calculated by the SLE option show this effect. The precision decreases with decreasing ion size. Therefore, the predicted results for ChBr-urea and ChI-urea are closer to the experimental data than ChF-urea and ChCl-urea.

2.4 Concluding Remarks

In this chapter, it was shown that σ -profiles, generated by COSMO-RS, give valuable information about the formation and strength of hydrogen bonds between two species. This feature is very useful for the prediction of DESs, since, the depression of the melting point is derived from the interactions between the HBD and HBA. DESs, comprising urea and different choline halides, were compared by means of their σ -profiles. From these profiles it

can be deduced that the strength of interaction between urea and the anions increases from iodide to fluoride. Therefore, the melting points of the mixtures should decrease vice versa. To proof this hypothesis, the solid-liquid equilibrium (SLE) of the mixtures was computed. The results revealed that the eutectic composition emerges at a molar ratio of ChX-urea 1-2 which is consistent with the literature.^{4,5} Further, the calculated melting temperatures exhibit the same trend predicted from the σ -profiles. However, no reasonable results were obtained for the mixture ChF-urea. Since fluoride is a very small and highly charged anion, no accurate calculation could be made using COSMO-RS.² All other mixtures, namely ChCl-urea, ChBr-urea and ChI-urea, follow the trend suggested by the σ -profiles. To verify the accuracy of the calculations, DSC measurements were performed for the eutectic compositions. It was revealed that the experimental melting points are consistent with the trend predicted by the σ -profiles and SLE calculations. However, it was not possible to predict precisely the actual melting points and only a tendency can be drawn from the calculations. A reason for that could be the fact that DESs are not only dependent on hydrogen bonds but also on lattice energies and entropic effects.³ To conclude, COSMO-RS is a useful tool for the prediction of DESs via σ -profiles and the SLE option. Especially the σ -profiles provide further insight into the interactions between HBD and HBA.

2.5 References

- 1 A. Klamt, *COSMO-RS: From Quantum Chemistry to Fluid Phase Thermodynamics and Drug Design*, Elsevier Science, 2005.
- 2 A. Klamt, F. Eckert and W. Arlt, *Annu. Rev. Chem. Biomol. Eng.*, 2010, **1**, 101-122.
- 3 A. P. Abbott, D. Boothby, G. Capper, D. L. Davies and R. K. Rasheed, *JACS*, 2004, **126**, 9142-9147.
- 4 A. P. Abbott, G. Capper, D. L. Davies, R. K. Rasheed and V. Tambyrajah, *Chem. Commun.*, 2003, 70-71.
- 5 Q. Zhang, K. De Oliveira Vigier, S. Royer and F. Jerome, *Chem. Soc. Rev.*, 2012, **41**, 7108-7146.

3. Eco-Friendly Synthesis of Caffeic Acid Phenethyl Ester Using Deep Eutectic Solvents

3.1 Abstract

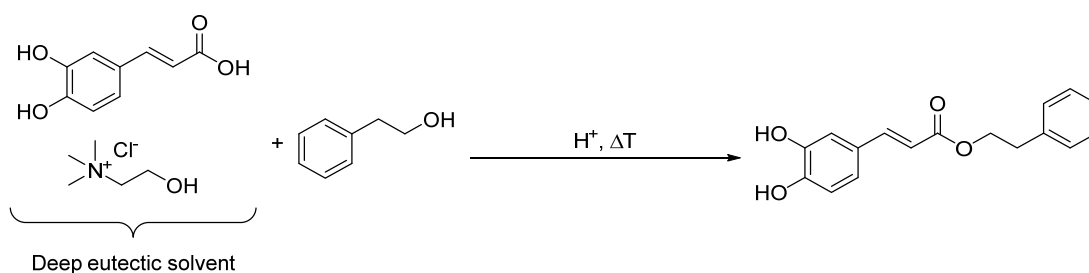
In this chapter a new strategy towards the synthesis of caffeic acid phenethyl ester is introduced. The reaction is carried out in a deep eutectic solvent which consists of caffeic acid and choline chloride. Caffeic acid is used as part of the solvent and as reactant. Phenethyl alcohol is soluble in this mixture in every molar ratio, and as a consequence no additional solvent is necessary. At first, enzymes were incorporated in the reaction mixture. However, the enzymatic reaction was not efficient. Therefore, an acid-catalyzed esterification was performed in the deep eutectic solvent. Reaction conditions were optimised with respect to the molar ratio of phenethyl alcohol and caffeic acid, and by varying the amount and nature of the acid catalyst as well as the reaction time. The obtained caffeic acid phenethyl ester could easily be separated from the reaction mixture by simply adding water to destroy the deep eutectic by solubilisation of choline chloride in the aqueous phase.

3.2 Introduction

Caffeic acid phenethyl ester (CAPE) has become an interesting molecule since it shows favourable pharmacological and biological properties, such as antimicrobial effects, anti-inflammatory or anticancer and immune modulatory activities.¹⁻⁶ Further, CAPE is an active flavonoid which plays an important role in the antioxidant activity of propolis.¹ However, the isolation of CAPE from honeybee propolis is time-consuming and suffers from impurities.⁷ Moreover, there are some disadvantages concerning the synthesis of CAPE since hazardous and deleterious chemical reagents are being used.^{4, 5, 8-11} To overcome these drawbacks, new synthetic approaches have to be investigated. For example, Ho Ha *et al.* prepared CAPE via an enzyme catalysed reaction which was carried out in an ionic liquid (IL).^{12, 13} ILs are salts which show melting points below 100 °C and are used in a wide range of applications. In organic synthesis they are employed as reaction media as an alternative to classic organic solvents.¹⁴

However, a lot of ILs are toxic and harmful to the environment. Further, their synthesis and purification is often expensive and time-consuming.^{15, 16} A good alternative to ILs are deep eutectic solvents (DESS). Recently, Durand *et al.* performed lipase-catalysed reactions in

DESs.¹⁷⁻²⁰ So it is tempting to combine the enzymatic reaction of CAPE with a DESs. For that reason, an enzymatic approach and an acid-catalysed esterification were chosen for the synthesis of CAPE. The reaction of the acid-catalysed esterification is shown in Scheme IV-1. A DES, comprising choline chloride (ChCl) and caffeic acid (CA), which was first reported by Maugeri *et al.*, was employed as the reaction medium.²¹ Additionally, mixtures comprising ethylammonium chloride (EAC) and CA were tested for lipase-catalysed reactions. It is advantageous that CA can be used as part of the solvent and as reactant. The formation of a DES is mandatory, because CA is nearly insoluble in the second reactant phenethyl alcohol (PA). However, by generating a DES in advance the solubility properties of CA are changed and the ChCl-CA (molar ratio 2-1) mixture becomes miscible with PA in every composition. For comparison, solubility tests showed that no CA is soluble in PA at room temperature and only 2.6 wt% of CA are soluble in PA at 50 °C. By using a DES the utilization of an additional solvent is avoided. The non-toxic and biodegradable medium guarantees a procedure which follows the 12 principles of green chemistry.²²



Scheme IV-1. Reaction scheme of the esterification to synthesise caffeic acid phenethyl ester.

3.3 Preparation of the Deep Eutectic Solvents and Reaction Mixtures

In order to form a DES, ChCl and CA were mixed in a molar ratio of 2-1 under a nitrogen atmosphere and sealed to protect the samples from moisture. EAC-CA was used in various compositions. The vials were heated to 90 °C and stirred until a homogeneous liquid was formed. Subsequently, the temperature was reduced to 80 °C and PA was injected (Figure IV-9). To start the enzymatic reaction, the enzyme and small amounts of water were added and the reaction mixtures stirred for 2 days at 40 to 60 °C, depending on the nature of the enzyme. The esterification was started by adding the acid catalyst and stirring the samples at 80 °C. All samples were covered with aluminium foil to prevent degradation by light. The progress of the reaction was analysed by HPLC analysis.



Figure IV-9 Samples with different amounts of PA before the addition of enzyme or acid.

3.4 Results and Discussion

3.4.1 Rheological Behaviour of the Reaction Mixtures

The temperature dependant rheological behaviour was tested for different mass ratios of DES (ChCl-CA (2-1))-PA, since high viscosities can decrease the reaction rate in case of diffusion-controlled chemical reactions. The results are depicted in Figure IV-10. The measurements were carried out according to the procedure described in III 2.8.

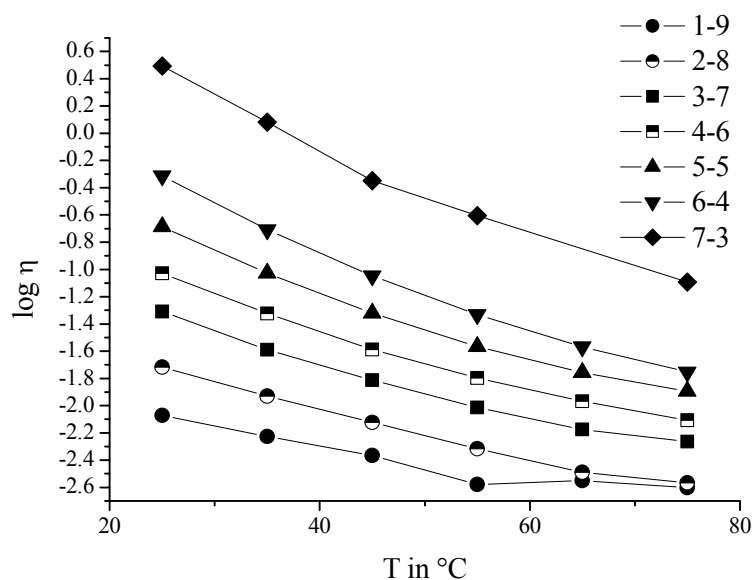


Figure IV-10. Logarithmic plot of different viscosities of different compositions of DES-PA as a function of temperature. Viscosities were measured in Pa·s.

The viscosities were measured in a temperature range from 25 °C to 75 °C. All mixtures behaved like Newtonian fluids. The viscosities decreased with increasing temperature. As expected, the viscosities decreased with increasing content of PA as can be seen in Table IV-10. For example, at 25 °C, the viscosity of a mass ratio of DES-PA 1-9 was determined to be 8.49 mPa·s whereas a mixture of DES-PA 7-3 showed a viscosity of 3105 mPa·s. The high viscosity of the mixtures is caused by the high content of DES. Its rheological behaviour may be attributed to electrostatic and van der Waals interactions or a small void volume.²³ However, it was not possible to measure the viscosity of the pure DES, as it is solid up to 67 °C.²¹

Table IV-10. Temperature-dependant viscosities of different compositions of DES-PA. Viscosities are given in mPa·s.

Mass ratio DES-PA	η at 25 °C	η at 35°C	η at 45°C	η at 55°C	η at 65°C	η at 75°C
1-9	8.49	5.94	4.31	2.64	2.82	2.49
2-8	19.1	11.7	7.54	4.82	3.24	2.71
3-7	49.1	25.7	15.4	9.69	6.69	5.43
4-6	93.6	47.5	26	16.0	10.8	7.83
5-5	206	98.8	47.6	27.2	17.5	12.7
6-4	443	168	85.3	49.3	31.3	23.5
7-3	3105	1204	448	248	-	80.7

3.4.2 *Lipase-Catalysed Reactions*

To synthesise CAPE, lipase-catalysed reactions were performed. Different eutectic and low-melting mixtures and various enzymes were tested. The reaction conditions were varied with respect to water content, amount and type of enzyme, and pH. As reaction media EAC-CA and ChCl-CA, respectively, were employed.

In Table IV-11, different compositions are listed for reaction mixtures containing EAC and CA catalysed by Novozym 435. In all mixtures, if not stated otherwise, the amount of DES or LMM was 1.9 g, the amount of PA 3 g and the amount of water 0.5 g. The experiments were performed at 60 °C with a reaction time of 2 d.

Table IV-11. Enzymatic reactions catalysed by Novozym 435 in EAC-CA.

Molar ratio EAC-CA	m (Novozym 435) in mg	Conversion rate in %	Remarks
2-1 ^a	100	0.63	
3-1 ^a	100	0.50	
4-1 ^a	104	0.29	
2-1 ^b	80	1.95	
1-1 ^b	82	2.84	
1-2 ^b	80	2.51	
3-1 ^b	80	1.45	
2-1 ^b	81	1.55	No water added
2-1 ^b	80	2.73	0.2 g glacial acetic acid added
2-1 ^b	80	1.56	0.2 g sodium hydroxide added
2-1 ^b	80	1.54	0.3 g water added
2-1 ^b	199	-	0.2 g glacial acetic acid added
2-1 ^b	200	-	
2-1 ^b	200	-	1g PA + 0.2 g acetic acid added
2-1 ^b	199	-	0.2 g sulphuric acid added
2-1 ^b	0	-	No enzyme added
2-1 ^b	80	-	No water added
2-1 ^b	80	-	No water added/molecular sieve
2-1 ^b	0	-	No water added
2-1 ^b	0	-	No water added/molecular sieve

^aungrinded Novozym 435, ^bgrinded Novozym 435

The conversion rate, ranging between 0 and 2.8%, turned out to be very poor. The variations have no significant influence on the outcome. Durand *et al.* suggested that the grinding of the immobilised enzyme increases the conversion rate.¹⁸ In the presented experiments, this effect could not be confirmed.

Further, mixtures comprising ChCl and CA were tested. The amount of DES was 2 g and had a molar ratio of ChCl-CA of 2-1. The reaction mixtures were stirred for two days at 60 °C. Additionally, the influence of a molecular sieve with a diameter of 3 Å and the addition of glacial acetic acid was examined. The different experiments are summarised in Table IV-12. No conversion was observed by HPLC measurements.

Table IV-12. Reaction mixtures with different amounts of PA, water and enzyme.

m (PA) in g	m (H ₂ O) in g	m (Novozym 435) in mg	Remarks
16	1.3	45	
12.1	1.4	41	
16.4	1.3	73	
11.9	0.5	80	
3.0	0.5	71	
3.0	0.5	0	
3.0	0.5	200	0.2 g glacial acetic acid added
3.0	0.5	200	
3.0	0.5	0	0.2 g glacial acetic acid added
0.67	0	80	molecular sieve added
0.67	0	79	
0.67	0	0	molecular sieve added
0.67	0	0	

In another set of experiments, different types of lipases were tested in a mixture of ChCl-CA (molar ratio 2-1). The experiments were carried out at 40 °C and the reaction time was 2 d. The type and amount of lipases as well as the added quantity of water are listed in Table IV-13. For all experiments, 2 g of DES and 3 g of PA were used. HPLC analysis showed that CAPE could not be obtained during the process.

3. Eco-Friendly Synthesis of Caffeic Acid Phenethyl Ester Using Deep Eutectic Solvents

Table IV-13. Various lipases tested for the enzyme catalysed reaction between CA and PA to CAPE.

Lipase	m (enzyme) in mg	m (H ₂ O) in g
<i>Rhizopus niveus</i>	100	0.50
<i>Rhizopus arrhizus</i>	99	0.50
<i>Mucor miehei</i>	52	0.50
<i>Hog pancreas</i>	99	0.66
<i>Pseudomonas cepacia</i>	71	0.50
<i>Aspergillus niger</i>	41	0.64
<i>Candida cylindracea</i>	199	0.65

3.4.3 Acid-Catalysed Esterification

Since a lipase-catalysed reaction was not successful, acid-catalysed reactions were carried out. The preparation of the reaction mixtures consisting of DES (ChCl-CA), PA, and an acid catalyst is described in section IV 3.3. The set of reaction conditions was optimised with respect to the content of PA and CA, and by varying the amount and nature of the acid catalyst, as well as the reaction time.

3.4.3.1 Variation of the Content of Phenethyl Alcohol

HPLC measurements revealed that no CAPE is formed by mixing the DES and PA under heating. Therefore, the idea occurred to add an acid catalyst. First, sulphuric acid and *p*-toluenesulfonic acid were tested.

Table IV-14. Content of PA in wt% in the reaction mixture with corresponding molar conversions from CA to CAPE. The reactions were carried out over night at 80 °C.

<i>p</i> -Toluenesulfonic acid as catalyst		Sulphuric acid as catalyst	
Content of PA in wt%	Molar conversion of CA to CAPE in %	Content of PA in wt%	Molar conversion of CA to CAPE in %
26.3	17.2	20.5	6.2
38.8	31.8	38.4	14.9
52.5	48.3	53.7	44.2
77.8	70.4	61.7	65.0
80.2	74.5	79.7	67.1
83.8	67.8	83.6	56.4

The reaction was carried out overnight at 80 °C. The results indicate a decent conversion rate, but seem to be dependent on the amount of PA used. For that reason, the amount of PA was varied. The results are summarised in Table IV-14. The highest conversion rate of CA to CAPE (74.5%) was accomplished for 80.2 wt% PA. *p*-Toluenesulfonic acid was used as catalyst. Experiments with sulphuric acid as catalyst showed similar results (conversion rate of 67.1% and a content of 79.1% of PA).

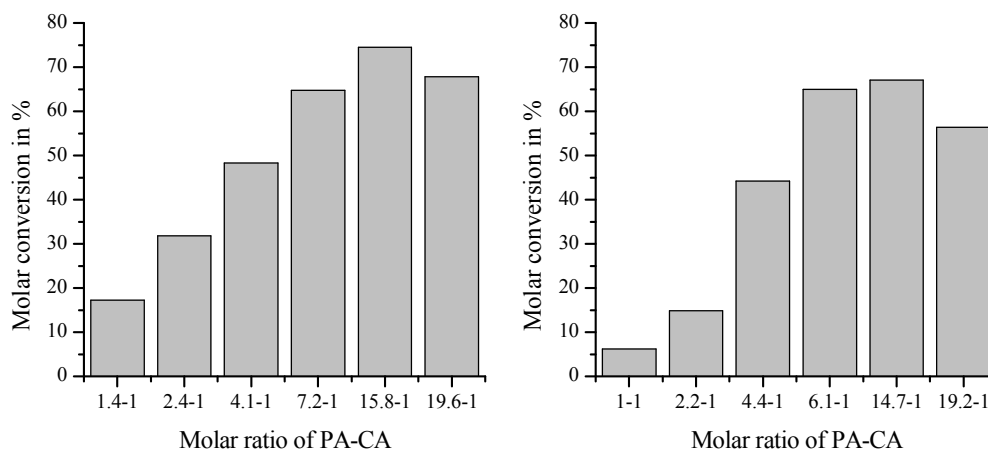


Figure IV-11. Molar conversion rate of CA to CAPE in % as a function of molar ratio of PA-CA. Right diagram: Reaction was catalysed by *p*-toluenesulfonic acid. Left diagram: Reaction was catalysed by sulphuric acid.

Additionally, in Figure IV-11 the conversion rate as a function of molar ratio of PA-CA is depicted. The highest conversion was obtained for a molar ratio of 15.8-1 PA-CA with *p*-toluenesulfonic acid as catalyst. For sulphuric acid as catalyst a molar ratio of 14.7-1 of PA-CA was most efficient. These results indicate that an excess of PA is required for a yielding conversion. The latter was also confirmed by other approaches.^{12, 24} Another reason for the better conversion with higher PA content might be the reduced viscosity which facilitates diffusion.

3.4.3.2 Variation of the Acid Catalyst

In a second set of experiments, other acid catalysts were tested. First, carboxylic acids such as oxalic acid, malonic acid, and acetic acid were introduced. However, the molar conversion rates were low. The highest conversion rate, 12.9%, was achieved for oxalic acid. Further, the catalytic power of two solid acids, Amberlyst 15 and Amberlite IR-120, was investigated

3. Eco-Friendly Synthesis of Caffeic Acid Phenethyl Ester Using Deep Eutectic Solvents

in order to perform the reaction in a more eco-friendly way. They have the great advantage of being environmentally benign and can be easily removed from the reaction mixture by filtration.^{25, 26} Both catalysts were tested with a molar ratio of 15.8-1 PA-CA. HPLC analysis showed a molar conversion rate of 72% for Amberlyst 15 and 65% for Amberlite IR-120. Due to these results, we decided to use Amberlyst 15 for further experiments (see Figure IV-12 for structure).

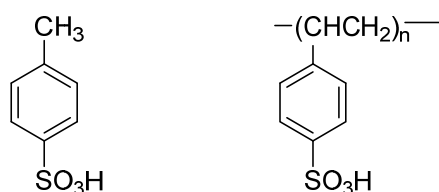


Figure IV-12. Chemical structures of *p*-toluenesulfonic acid (left) and Amberlyst 15 (right).

Amberlyst 15 is a macro reticular polystyrene based ion exchange resin with acidic sulfonic groups which can be used for several acidic catalysed reactions.²⁵ Its easy removal from the reaction mixture, the uncomplicated use and regeneration afterwards are further advantages.^{25, 27}

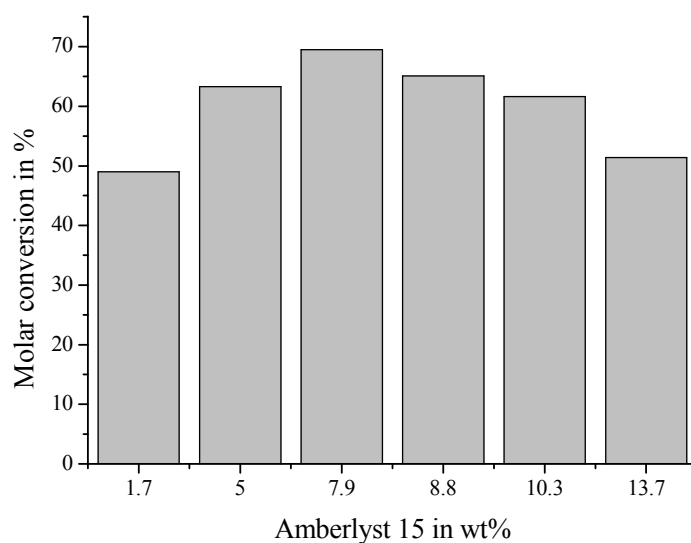


Figure IV-13. Molar conversion of CA to CAPE as a function of Amberlyst 15 in wt%. The molar ratio of CA, ChCl and PA was kept constant.

In another set of experiments, the amount of Amberlyst 15 was optimized. The results can be seen in Figure IV-13. The results elucidate that the conversion of CAPE is most efficient

using 7.9 wt% of Amberlyst 15. All reactions were performed overnight at 80 °C and the molar conversion was determined by HPLC according to III 2.5.

3.4.3.3 *Kinetic Study of the Reaction Time*

In order to further improve the reaction conditions, the kinetic behaviour of the reaction was studied. The amount of CAPE in the reaction mixture was quantified after 4, 8, 14, and 26 hours of reaction. One set of experiments was performed for 8 wt% of Amberlyst 15, the other with 13 wt% of Amberlyst 15.

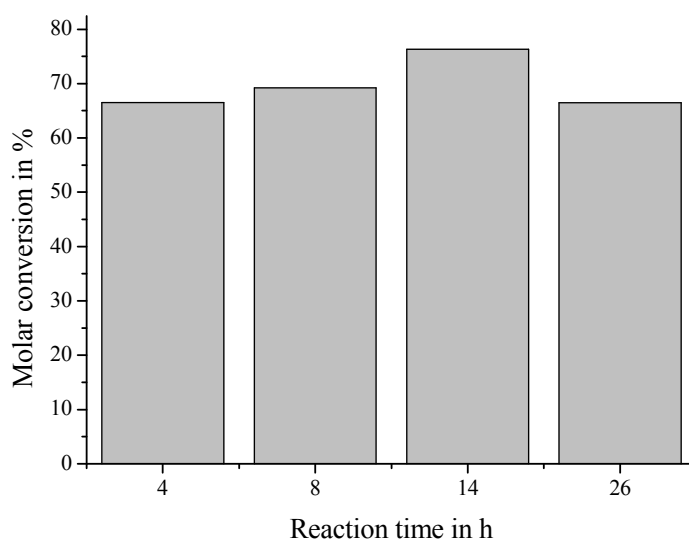


Figure IV-14. Molar conversion of CA to CAPE as a function of time. The ratio of CA, ChCl, PA was kept constant. The amount of Amberlyst 15 was 8 wt%.

A reaction time of 14 h turned out to be the most efficient with a molar conversion of 76.3% for mixtures containing 8 wt% Amberlyst 15. The reaction mixture comprising 13 wt% exhibits the highest molar conversion of 76.6% after 8h. The results are depicted in Figure IV-14 and Figure IV-15. In both cases, the conversion rate decreases as a function of time. A possible reason could be the degradation of CAPE by heat or acidity. The molar conversions were determined by HPLC analysis described in section III2.5.

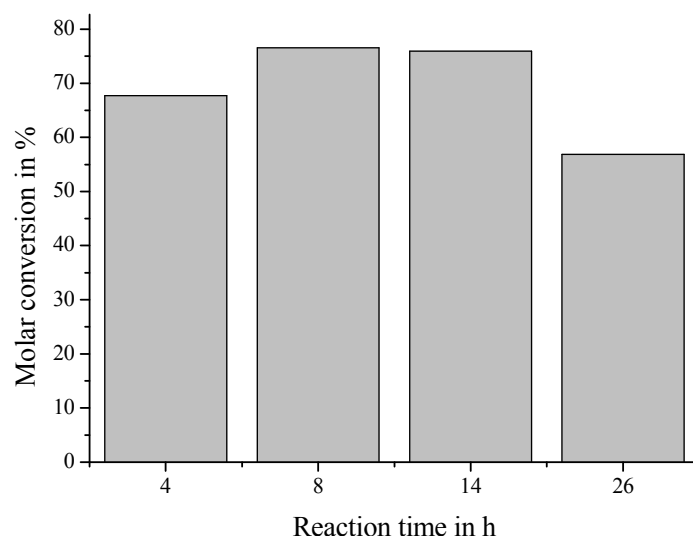


Figure IV-15. Molar conversion of CA to CAPE as a function of time. The ratio of CA, ChCl, PA was kept constant. The amount of Amberlyst 15 was 13 wt%.

3.4.4 Isolation of Caffeic Acid Phenethyl Ester

Another important point is the isolation of the product. Usually, toxic and volatile solvents are required.⁸⁻¹¹ However, in this case, after the elimination of the catalyst by filtration, CAPE was isolated using only water. Since PA is only slightly soluble in water at 20°C, the reaction mixture was poured into hot water. In this step, ChCl was removed from the reaction mixture, since it is highly soluble in water. Upon cooling to room temperature, CAPE precipitated and was collected by filtration. The product was identified via ¹H NMR spectroscopy.

3.5 Concluding Remarks

Rheological measurements of the reaction mixtures showed that the viscosity is dependent on the ratio of DES-PA and the temperature. As a consequence, the viscosity can be tuned for the application.

Further, the enzymatic esterification of CA and PA catalysed by different lipases, but mainly by Novozym 435, was investigated. As reaction media, mixtures of EAC-CA and ChCl-CA, respectively, were tested. A reaction between CA and PA catalysed by Novozym 435 was already reported to work in ILs.¹² HPLC analysis of the performed reactions revealed that almost no CAPE was formed. Reasons for this observation might be the denaturation of the

enzymes by the salty and acidic DES or a low reactivity of CA due to a strong hydrogen bond network.²⁸ Also consecutive reactions of CAPE could be responsible for the low yield.

However, a new, eco-friendly approach towards the synthesis of CAPE was demonstrated by the acid-catalysed esterification. The insolubility of CA in PA was overcome by the formation of a DES. Therefore, no additional solvent was required. The DES consisted of CA and ChCl. Thereby, CA acts as part of the DES as well as reactant. ChCl is a biodegradable and non-toxic substance. Furthermore, Amberlyst 15 was employed as an acidic catalyst, since this resin can be recycled and easily removed from the reaction mixture. The reaction conditions were optimised and a molar conversion up to 76.6 % was achieved. The product was isolated by using hot water. These properties are in good accordance with the 12 principles of green chemistry.²² Moreover, a new spectrum of application is disclosed for DESs, since a significant number of DESs can be imagined enabling various synthetic approaches without solvents.^{21, 29-31}

3.6 References

- 1 A. Russo, R. Longo and A. Vanella, *Fitoterapia*, 2002, **73**, Supplement 1, 21-29.
- 2 F. Shahidi, P. K. Janitha and P. D. Wanasundara, *Crit. Rev. Food Sci. Nutr.*, 1992, **32**, 67-103.
- 3 W.-K. Jung, D.-Y. Lee, J.-H. Kim, I. Choi, S.-G. Park, S.-K. Seo, S.-W. Lee, C.-M. Lee, Y.-M. Park, Y.-J. Jeon, C. H. Lee, B.-T. Jeon, Z.-J. Qian, S.-K. Kim and I.-W. Choi, *Process Biochem.*, 2008, **43**, 783-787.
- 4 Y.-J. Lee, P.-H. Liao, W.-K. Chen and C.-C. Yang, *Cancer Lett.*, 2000, **153**, 51-56.
- 5 J.-H. Chen, Y. Shao, M.-T. Huang, C.-K. Chin and C.-T. Ho, *Cancer Lett.*, 1996, **108**, 211-214.
- 6 G. Murtaza, S. Karim, M. R. Akram, S. A. Khan, S. Azhar, A. Mumtaz and M. H. H. Bin Asad, *Biomed Res. Int.*, 2014, **2014**, 9.
- 7 M. Marcucci, C., *Apidologie*, 1995, **26**, 83-99.
- 8 T. Hashimoto, M. Tori, Y. Asakawa and E. Wollenweber, *Z. Naturforsch., C: Biosci.*, 1987, **43**, 470-472.
- 9 M. Touaibia and M. Guay, *J. Chem. Educ.*, 2011, **88**, 473-475.
- 10 K. Nakamura, T. Nakajima, T. Aoyama, S. Okitsu and M. Koyama, *Tetrahedron*, 2014.

- 11 T. R. Burke, Jr., M. Fesen, A. Mazumder, J. Yung, J. Wang, A. M. Carothers, D. Grunberger, J. Driscoll, Y. Pommier and K. Kohn, *J. Med. Chem.*, 1995, **38**, 4171-4178.
- 12 S. Ha, T. Anh, S. Lee and Y.-M. Koo, *Bioprocess Biosystems Eng.*, 2012, **35**, 235-240.
- 13 S. Ha, T. Anh and Y.-M. Koo, *Bioprocess Biosystems Eng.*, 2013, **36**, 799-807.
- 14 T. Welton, *Chem. Rev.*, 1999, **99**, 2071-2084.
- 15 M. Deetlefs and K. R. Seddon, *Green Chem.*, 2010, **12**, 17-30.
- 16 J. H. Clark and S. J. Tavener, *Org. Process Res. Dev.*, 2006, **11**, 149-155.
- 17 E. Durand, J. Lecomte, B. Barea, E. Dubreucq, R. Lortie and P. Villeneuve, *Green Chem.*, 2013, **15**, 2275-2282.
- 18 E. Durand, J. Lecomte, B. Baréa, G. Piombo, E. Dubreucq and P. Villeneuve, *Process Biochem.*, 2012, **47**, 2081-2089.
- 19 E. Durand, J. Lecomte, B. Baréa and P. Villeneuve, *Eur. J. Lipid Sci. Technol.*, 2014, **116**, 16-23.
- 20 E. Durand, J. Lecomte and P. Villeneuve, *Eur. J. Lipid Sci. Technol.*, 2013, **115**, 379-385.
- 21 Z. Maugeri and P. Dominguez de Maria, *RSC Advances*, 2012, **2**, 421-425.
- 22 P. T. Anastas and M. M. Kirchhoff, *Acc. Chem. Res.*, 2002, **35**, 686-694.
- 23 Q. Zhang, K. De Oliveira Vigier, S. Royer and F. Jerome, *Chem. Soc. Rev.*, 2012, **41**, 7108-7146.
- 24 D. Grunberger, R. Banerjee, K. Eisinger, E. Oltz, L. Efros, M. Caldwell, V. Estevez and K. Nakanishi, *Experientia*, 1988, **44**, 230-232.
- 25 R. Pal, T. Sarka and S. Khasnobis, *Arkivoc*, 2012, **2012**, 570-609.
- 26 J. Otera and J. Nishikido, *Esterification: Methods, Reactions, and Applications*, Wiley, 2009.
- 27 M. Petrini, R. Ballini, E. Marcantoni and G. Rosini, *Synth. Commun.*, 1988, **18**, 847-853.
- 28 M. B. Turner, S. K. Spear, J. G. Huddleston, J. D. Holbrey and R. D. Rogers, *Green Chem.*, 2003, **5**, 443-447.
- 29 L. LeBlanc, A. Paré, J. Jean-François, M. Hébert, M. Surette and M. Touaibia, *Molecules*, 2012, **17**, 14637-14650.
- 30 V. De Santi, F. Cardellini, L. Brinchi and R. Germani, *Tetrahedron Lett.*, 2012, **53**, 5151-5155.

- 31 L. H. Boudreau, J. Maillet, L. M. LeBlanc, J. Jean-François, M. Touaibia, N. Flamand and M. E. Surette, *PloS one*, 2012, **7**, e31833.

4. Towards Surfactantless and Waterless Microemulsions

4.1 Abstract

Recently, the presence of nano-clusters was shown in the monophasic region of ternary liquid mixtures without surfactants. The nano-cluster containing mixtures had similarities to classical microemulsions. Well-defined time-correlation functions were observed even far away from the demixion boundary for the systems water/ethanol/oil, where the oil was 1-octanol, fragrance molecules, or mosquito repellents. In this work, we show that the same structural description was obtained for surfactantless and waterless green microemulsions, using deep eutectic solvents instead of water. These results were deduced from dynamic light scattering as well as small-angle x-ray scattering for various compositions.

4.2 Introduction

Microemulsions are macroscopically homogeneous liquids comprising a polar and a non-polar constituent. A surfactant and, usually, a cosurfactant are necessary to obtain these translucent and thermodynamically stable solutions.¹⁻³ According to Winsor, microemulsions can be either a one-phase system (Winsor IV) or part of a multi-phase system as Winsor I, II, or III when it is in equilibrium with the oil phase, the aqueous phase or both phases, respectively.⁴ The type of the microemulsion is dependent on the composition. A microemulsion can be of three different types: water-in-oil, bicontinuous, or oil-in-water. The surfactant and cosurfactant form an interfacial film between the aqueous and oil phases.⁵ Microemulsions have been proven useful, particularly in the field of enhanced oil recovery,⁶ but also in cosmetic,⁷⁻¹⁰ food,^{11, 12} and pharmaceutical industry¹³⁻¹⁵ as well as cleaning agents.^{7, 16}

Mostly, the polar phase in microemulsions is an aqueous phase. However, this is not essential for the formulation of microemulsions. In literature, many publications deal with waterless microemulsions and their interesting properties. The pioneers in this field were Lattes *et al.* They replaced water by formamide in a system containing cyclohexane as oil and butanol as cosurfactant and studied the influence of two different surfactants.¹⁷ They published several papers using formamide as a highly structured solvent and utilised the resulting non-aqueous microemulsion, for example, as reaction medium to perform Diels-Alder reactions.¹⁸⁻²⁰ Another approach was made by Harrar *et al.* They studied non-aqueous

microemulsions containing an ionic liquid (IL), [Emim][EtSO₄], the oil limonene and Triton X-114 as surfactant.²¹ It was observed that a large thermal stability down to -35 °C can be achieved using high amounts of the IL. This phenomenon paves the way for applications such as extraction processes or reaction media for water-sensible reactions. Concerning perfumes, the effect of humidity on evaporation from aqueous and non-aqueous microemulsions containing perfume was investigated by Hamdan *et al.* They discovered that the weight loss is greater at lower humidity for both systems, but is higher for the aqueous system.²² Further, other waterless microemulsions were studied like the system ethylene glycol/sodium dodecyl sulfate (SDS)/decanol/toluene by Friberg *et al.*, who found a critical point²³. Also a system comprising dimethylacetamide (DMA)/sodium di-(2-ethylhexyl) sulfosuccinate (AOT)/octane was examined by Cai *et al.* In this study, the critical behaviour of the non-aqueous microemulsion was investigated.²⁴ Peyrelasse *et al.* did also a quantitative determination of the percolation threshold in waterless microemulsions.²⁵ They showed that a model for microemulsion could be successfully applied for non-aqueous microemulsions. The self-assembly of amphiphiles in the absence of water, the capability of reverse micelles to encapsulate non-aqueous polar organic solvents, the use of ILs or, the possibility to employ non-aqueous reverse micelles as nano-reactors are examples of current research topics on waterless microemulsions.²⁶

Recently, new approaches towards waterless and surfactantless microemulsions were performed. A good starting point is the Ouzo effect. As it is well known, the necessary condition for the Ouzo effect is the rapid addition of water, or any other solvent, to a highly or entirely miscible second solvent (e.g. ethanol) and a third component that is highly soluble in the second solvent, but not in the first one (e.g. anethole or octanol). While studying the Ouzo effect, it was discovered that nano-structures were present in the single-phase region, near the demixion boundary. This phenomenon was called “pre-Ouzo effect” and was discovered by Klossek *et al.*²⁶ The presence of these nano-structures was also observed using dynamic and static light scattering in surfactantless microemulsions containing various types of hydrophobic liquids, i.e. in the ternary mixtures water/benzyl alcohol/ethanol, or with ethyl lactate or γ -valerolactone.²⁷ To gain more knowledge about the molecular-level shape and the structure of these aggregates, molecular dynamics simulations were carried out with the system water/ethanol/octanol.²⁸ Swollen micelles-like aggregates were observed in the pre-Ouzo region. Diat *et al.* discovered that the single-phase in the pre-Ouzo region consists of two distinct nanoscopic pseudo-phases, one octanol-rich and one water-rich. These results

were obtained by combining small-angle neutron scattering with small- and wide-angle x-ray scattering.²⁹ The ethanol molecules were distributed between octanol-rich nano-domains and a water pseudo-phase with a slight accumulation at the interface and an exponential decay concentration on the water side. The distribution coefficient of ethanol between the two pseudo-phases was calculated. Thereby, the existence of fatty alcohol-rich domains of well-defined size in the order of 2 nm was proven.

Numerous surfactantless microemulsion formulations on the market present this nano-clustering. For example, such a nano-structuring may have an impact on the behaviour of mosquito repellents on the skin, or their diffusion into the upper skin layers.³⁰ In perfume or tinctures, Marcus *et al.* observed a nano-structuration in the pre-Ouzo region with four different perfumery molecules. From model formulations nano-droplets can be predicted in Eau de Toilette and Eau de Parfum. They can possibly appear in perfumes in presence of very hydrophobic fragrance molecules.³¹ Tchakalova *et al.* showed that the evaporation rate was following the volatility in such ternary solutions. They observed a strong evaporation of ethanol in the pre-Ouzo region, used in fresheners, while there is a noticeable auto-encapsulation of the fragrance when spontaneous emulsification is produced and the bulk water evaporates. Hence, pre-Ouzo formation with aggregates must be distinguished from critical fluctuations. In the case of pre-Ouzo long living aggregates, evaporation follows a non-linear path with a turn-over as an embedded eutectic occurs.³² Surfactantless microemulsions also showed the possibility to dissolve hydrophobic compounds, such as ibuprofen, in the presence of large amounts of water in the pressurized system water/acetone/CO₂.³³

Concerning the possible existence of surfactantless and waterless microemulsions, we can mention organic blends of biodiesel and diesel with ethanol and various additives, used as fuel. Biodiesel, a blend of fatty acid alkyl esters, is industrially produced by transesterification. The latter is a reaction of vegetable oils or a fat with an alcohol and yields fatty acid esters and glycerol. The exact knowledge of the phase equilibrium is essential for the optimization of the biodiesel production and purification. Liquid-liquid equilibria for the glycerol/ethanol/biodiesels systems were therefore studied, where biodiesels came from canola oil, cottonseed oil, soybean oil, coconut oil and sunflower oil.³⁴⁻³⁸ The term “microemulsion” is never used in the related papers, as no connection between these solutions and surfactantless waterless microemulsions was made. Recently, Arpornpong *et al.* reported the possible existence of nano-droplets in such blends by investigating the

effects of co-solvent saturation and unsaturation on the phase behaviour and on the viscosity of a biofuel.³⁹ The question of the existence of nano-droplets in waterless and surfactantless microemulsion is set. It can be noted that Silva *et al.* also observed nanostructures in mixtures of ethanol and diesel oil (or synthetic diesel) in presence of additives, also inferred from dynamic light scattering data.⁴⁰ However, the technique used in these two last studies is not enough to postulate the presence of a microemulsion, as critical molecular fluctuations may occur and give a signal in dynamic light scattering similar to those arising from fluctuating nano-droplets.

In this chapter, green surfactantless and waterless microemulsions are formulated and characterised. Water was replaced with two different deep eutectic solvents (DESs), i.e. choline chloride-ethylene glycol (1-4) (DES1) and choline chloride-urea (1-2) (DES2). At first, a phase diagram comprising DES1, a mixture of tetrahydro furfuryl alcohol (THFA)-Brij 30 ($\zeta = 2-1$), and diethyl adipate (DEA) as non-polar phase was performed. Further, surfactantless and waterless systems containing DES/THFA/DEA were investigated. DESs have considerable advantages compared to classical ILs. They are easy to produce, non-volatile, biodegradable and have low cost.⁴¹⁻⁴³ Further, THFA stems from wood chemistry and is also biodegradable⁴⁴. Diethyl adipate is also of very low toxicity.⁴⁵

The domains of existence of the single clear and homogeneous phase were established for each system using ternary phase diagrams. Dynamic light scattering (DLS), as well as small-angle X-ray scattering (SAXS) were carried out to characterize the nano-domains.

4.3 Results and Discussion

4.3.1 Ternary Phase Diagrams

At first, a waterless phase diagram comprising DES1/THFA-Brij 30 ($\zeta = 2-1$)/DEA was recorded. It is presented in Figure IV-16.

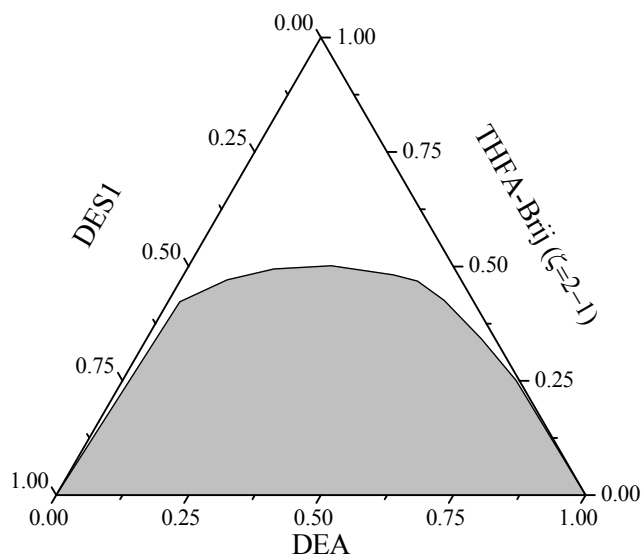


Figure IV-16. Pseudo-ternary phase diagram of a waterless DES1/THFA-Brij 30 ($\zeta = 2-1$)/DEA system at 25°C. The white area marks the single phase domain and the grey the multiphasic region.

The phase diagram shows a monophasic, clear domain. To find out if also a single-phase region is present in a surfactantless system, a phase diagram without Brij 30 was performed.

Figure IV-17 presents the phase diagrams obtained for the two waterless and surfactantless systems. A common trend can be observed, as a single, clear and homogeneous phase and a multiphasic domain is obtained in each case.

The larger single translucent is found for the system DES1/THFA/DEA (Figure IV-17 a)). It can be noted that these systems fulfil the conditions needed to observe the Ouzo effect: a solvent A (DES) is added to a second solvent B (THFA), which is highly soluble or entirely miscible with solvent A, and a third component (DEA), which is highly soluble in solvent B, but not in solvent A. Dynamic and static light scattering measurements were carried out to

investigate the presence of possible nano-clustering in these surfactantless and waterless systems in analogy to the water containing solutions.

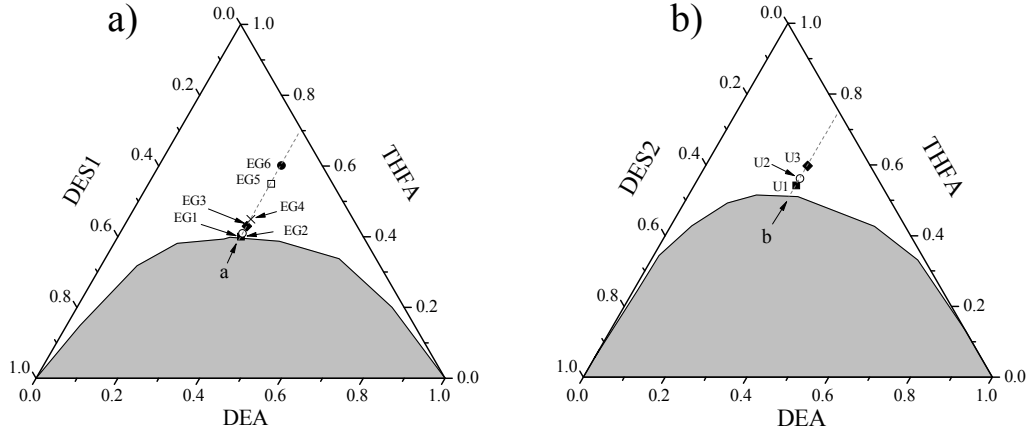


Figure IV-17. Pseudo-ternary phase diagrams of surfactantless and waterless systems a) DES1/THFA/DEA and b) DES2/THFA/DEA at 25 °C. The white area marks the single phase domain and the grey the multiphase region.

4.3.2 Dynamic Light Scattering

Dynamic light scattering (DLS) measurements were carried out following path a for the system DES1/THFA/DEA and path b for the system DES2/THFA/DEA. Path a and b are denoted in Figure IV-17.

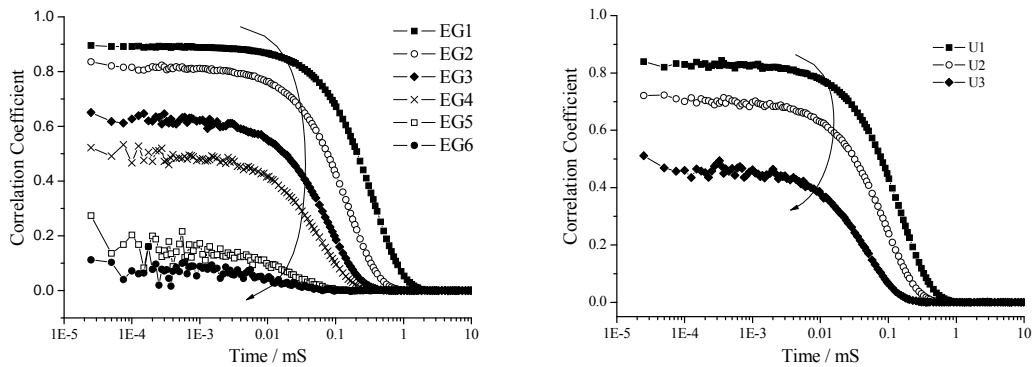


Figure IV-18. Time-dependent self-correlation functions as obtained from DLS measurement for the systems DES1/THFA/DEA (left) along path a and DES2/THFA/DEA (right) along path b at 25 °C.

The amount of DEA was kept constant on both paths and the amount of THFA was progressively increased. The correlation functions are well-defined near the demixion boundary and decreased gradually with an increasing amount of THFA (Figure IV-18). It can be observed that we cannot measure a time-correlation function at the end of path a, as the correlation coefficient for points EG5 and EG6 is almost equal to zero.

4.3.3 *Small Angle X-Ray Scattering*

SAXS measurements were carried out along path a for the system involving DES1 and path b for the system with DES2. The absolute intensity of the sample is directly proportional to the square of the electron density difference between both pseudo-phases (the DES-rich and the oil-rich ones), called the scattering contrast. The latter can be assessed when structures composed of two phases with different electron densities are present in the solution. Logically, the scattering contrast cannot be characterized if there are no structures in the solution.

As can be seen in Figure IV-19, the behavior in the variation of excess of scattering at low q -value in the SAXS spectra are in good accordance with those observed using DLS.

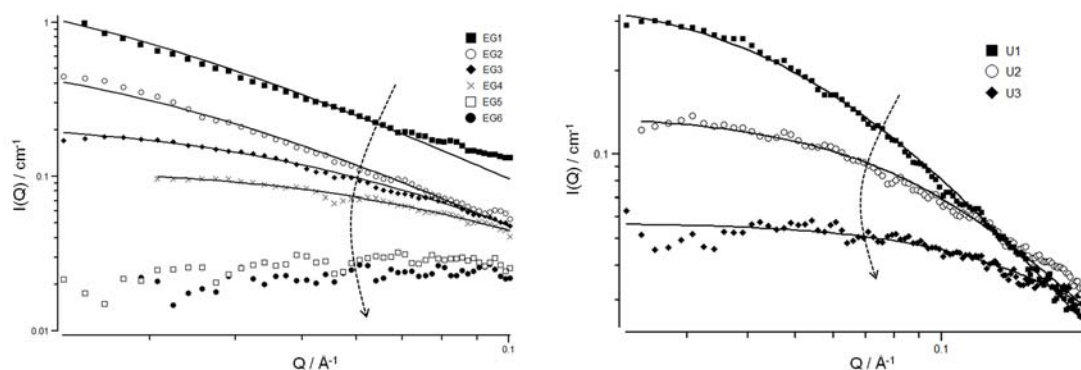


Figure IV-19. SAXS measurements on a log log scale and in absolute units for the system DES2/THFA/DEA (left) and DES2/THFA/DEA (right).

High intensities were also observed for samples EG1 and U1 which indicates that nano-structures are present at the beginning of path a and b, near the demixion boundary. With increasing distances from the demixion boundary, these nano-droplets became smaller and finally disappeared in favour of true molecular solutions.

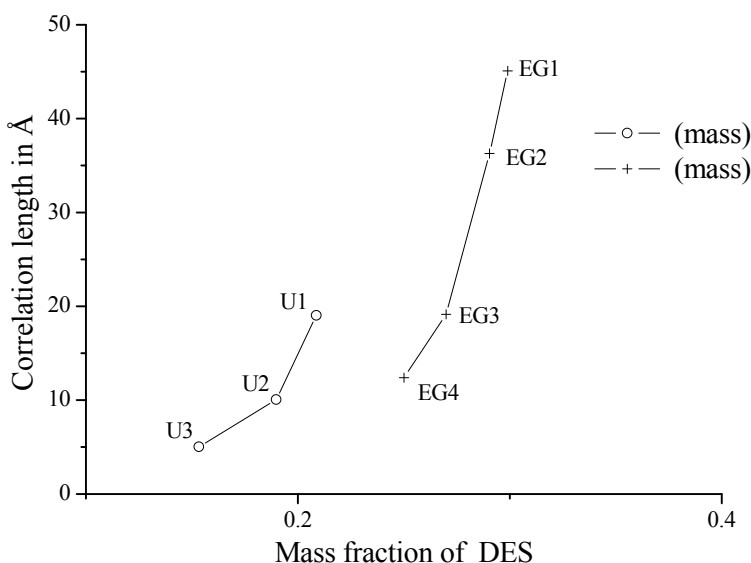


Figure IV-20. Correlation lengths in Å obtained from the Ornstein-Zernike fits versus the mass fraction of the DESs.

The characteristic length decreased from 45 Å for EG1 to 12 Å for EG4, and from 19 Å for U1 to 5 Å for U3 (see Figure IV-20, respectively the curves with crosses and open circles). Along path a and b for the systems containing DES1 and DES2, the characteristic length is more important for DES1 near the demixion boundary. This may be explained by the size of the EG molecule which is larger than urea molecules. EG may form larger clusters.

SAXS experiments proof and confirm the existence of a nano-clustering near the demixion boundary for these types of system, in the pre-Ouzo zone. This nano-structuration is less and less pronounced when the composition is farther away from the demixion boundary.

4.4 Concluding Remarks

In this chapter, the presence of nano-structuration in the pre-Ouzo region for waterless and surfactantless green microemulsions was investigated. The two investigated systems containing DES/THFA/DEA meet the requirements of the Ouzo effect in the biphasic zone and present similar phase diagrams. DLS as well as SAXS experiments were carried out in the pre-Ouzo region. Well-defined time-correlation functions appeared in the pre-Ouzo region and even far from the demixion boundary. These results combined with the SAXS measurements show the presence of spatial fluctuations. These fluctuations are independent

of molecular critical fluctuations which can appear near a critical point. By the way, this is also the first time that microemulsions were formulated using DES instead of water.

The obtained results confirm previous studies where such fluctuations were observed in aqueous systems also fulfilling all the required conditions for the Ouzo effect.^{26, 30, 31} The results aim at proofing that the pre-Ouzo effect is general and independent of the presence of water. However, it cannot be excluded that this general behavior, i.e. the presence of a nano-clustering in the pre-Ouzo region, may depend on the presence of hydrogen bonds between the molecules. These bonds were present in all the investigated systems and hence, further studies are now necessary to check this point.

4.5 References

- 1 B. Lindman and H. Wennerström, *Top. Curr. Chem.*, 1980, **87**, 1-83.
- 2 G. Kogan A., N., *Adv. Colloid Interface Sci.*, **2006**, **123**, 369–385.
- 3 M. L. Klossek, D. Touraud and W. Kunz, *Green Chem.*, 2012, **14**, 2017-2023.
- 4 P. A. Winsor, *Trans. Faraday Soc.*, 1948, **44**, 376-398.
- 5 D. F. Evans and H. Wennerström, *The Colloidal Domain: Where Physics, Chemistry, Biology, and Technology Meet*, Wiley, 1999.
- 6 M. F. Nazar, S. S. Shah and M. A. Khosa, *Pet. Sci. Technol.*, 2011, **29**, 1353-1365.
- 7 W. von Rybinski, M. Hloucha and I. Johansson, *Microemulsions in cosmetics and detergents, from Microemulsions*, Blackwell Publishing Ltd., 2009.
- 8 M. Hloucha, H.-M. Haake and G. Pellon, *Cosmet. Toiletries*, 2009, **124**, 58-69.
- 9 C. Solans and H. Kunieda, *Industrial Applications of Microemulsions*, Taylor & Francis, 1996.
- 10 F. Comelles, *J. Dispersion Sci. Technol.*, 1999, **20**, 491-511.
- 11 N. Garti, *Curr. Opin. Colloid Interface Sci.*, 2003, **8**, 197-211.
- 12 J. Flanagan and H. Singh, *Crit. Rev. Food Sci. Nutr.*, 2006, **46**, 221-237.
- 13 M. J. Lawrence and G. D. Rees, *Adv. Drug Del. Rev.*, 2000, **45**, 89-121.
- 14 B. K. Paul and S. P. Moulik, *Curr. Sci.*, 2001, **80**, 990-1001.
- 15 M. Fanun, *Curr. Opin. Colloid Interface Sci.*, 2012, **17**, 306-313.
- 16 H. D. Doerfler, A. Grosse and H. Kruessmann, *Tenside, Surfactants, Deterg.*, 1996, **33**, 432-440.
- 17 I. Rico and A. Lattes, *Nouv. J. Chim.*, 1984, **8**, 429-431.
- 18 I. Rico and A. Lattes, *J. Colloid Interface Sci.*, 1984, **102**, 285-287.

-
- 19 A. A.-Z. Samii, A. de Savignac, I. Rico and A. Lattes, *Tetrahedron*, 1985, **41**, 3683-3688.
- 20 M. Gautier, I. Rico, A. Ahmad-Zadeh Samii, A. de Savignac and A. Lattes, *J Colloid Interface Sci*, 1986, **112**, 484-487.
- 21 A. Harrar, O. Zech, R. Hartl, P. Bauduin, T. Zemb and W. Kunz, *Langmuir*, 2011, **27**, 1635-1642.
- 22 S. Hamdan, F. B. H. Ahmad, Y. Y. Dai, K. Dzulkefly and K. H. Ku Bulat, *J. Dispersion Sci. Technol.*, 1999, **20**, 415-423.
- 23 S. E. Friberg and W. M. Sun, *Colloid. Polym. Sci.*, 1990, **268**, 755-759.
- 24 H.-L. Cai, X.-Q. An, B. Liu, Q.-A. Qiao and W.-G. Shen, *J. Solution Chem.*, 2010, **39**, 718-726.
- 25 J. Peyrelasse, C. Boned and Z. Saidi, *Phys. Rev. E: Stat. Phys., Plasmas, Fluids, Relat. Interdiscip. Top.*, 1993, **47**, 3412-3417.
- 26 M. L. Klossek, D. Touraud, T. Zemb and W. Kunz, *ChemPhysChem*, 2012, **13**, 4116-4119.
- 27 M. L. Klossek, D. Touraud and W. Kunz, *PCCP*, 2013, **15**, 10971-10977.
- 28 S. Schöttl, J. Marcus, O. Diat, D. Touraud, W. Kunz, T. Zemb and D. Horinek, *Chem. Sci.*, 2014.
- 29 O. Diat, M. L. Klossek, D. Touraud, B. Deme, I. Grillo, W. Kunz and T. Zemb, *J. Appl. Crystallogr.*, 2013, **46**, 1665-1669.
- 30 J. Marcus, M. Mueller, J. Nistler, D. Touraud and W. Kunz, *Colloids Surf., A*, 2014, **458**, 3-9.
- 31 J. Marcus, M. L. Klossek, D. Touraud and W. Kunz, *Flavour Fragrance J.*, 2013, **28**, 294-299.
- 32 V. Tchakalova, F. Testard, K. Wong, A. Parker, D. Benczedi and T. Zemb, *Colloids Surf., A*, 2008, **331**, 40-47.
- 33 R. F. Hankel, P. E. Rojas, M. Cano-Sarabia, S. Sala, J. Veciana, A. Braeuer and N. Ventosa, *Chem Commun (Camb)*, 2014, **50**, 8215-8218.
- 34 M. B. Oliveira, S. Barbedo, J. I. Soletti, S. H. V. Carvalho, A. J. Queimada and J. A. P. Coutinho, *Fuel*, 2011, **90**, 2738-2745.
- 35 F. M. R. Mesquita, A. M. M. Bessa, D. D. de Lima, H. B. de Sant'Ana and R. S. de Santiago-Aguiar, *Fluid Phase Equilib.*, 2012, **318**, 51-55.
- 36 A. B. Machado, Y. C. Ardila, L. Hadlich de Oliveira, M. Aznar and M. R. Wolf Maciel, *J. Chem. Eng. Data*, 2012, **57**, 1417-1422.

- 37 F. M. R. Mesquita, N. S. Evangelista, H. B. de Sant'Ana and R. S. de Santiago-Aguiar, *J. Chem. Eng. Data*, 2012, **57**, 3557-3562.
- 38 F. M. R. Mesquita, F. X. Feitosa, N. E. Sombra, R. S. de Santiago-Aguiar and H. B. de Sant'Ana, *J. Chem. Eng. Data*, 2011, **56**, 4061-4067.
- 39 N. Arpornpong, C. Attaphong, A. Charoensaeng, D. A. Sabatini and S. Khaodhiar, *Fuel*, 2014, **132**, 101-106.
- 40 E. J. Silva, M. E. D. Zaniquelli and W. Loh, *Energy Fuels*, 2006, **21**, 222-226.
- 41 A. P. Abbott, G. Capper, D. L. Davies, R. K. Rasheed and V. Tambyrajah, *Chem. Commun.*, 2003, 70-71.
- 42 A. P. Abbott, D. Boothby, G. Capper, D. L. Davies and R. K. Rasheed, *JACS*, 2004, **126**, 9142-9147.
- 43 International Programme on Chemical Safety's INCHEM service, <http://www.inchem.org/>, Accessed 30.10.2013.
- 44 P. S. Chemicals, *Technical Bulletin*, 2005.
- 45 Toxicology data network, <http://toxnet.nlm.nih.gov/>, Accessed 9.01.2015.

V Summary

This thesis focuses on the properties, development and application of deep eutectic solvents (DESs) and low-melting mixtures (LMMs). The work is divided into four chapters.

- New low-melting mixtures
- COSMO-RS calculations of deep eutectic solvents
- Eco-friendly synthesis of caffeic acid phenethyl ester using deep eutectic solvents
- Towards surfactantless and waterless microemulsions

In the first chapter, new low-melting mixtures, novel binary and ternary DESs and LMMs are introduced. Mainly carnitine and betaine compounds were used amongst others. These ammonium compounds serve as alternative to choline, which is mostly used in DESs. The state of matter of the mixtures was determined at 80 °C, room temperature and 0 °C. It was discovered that mixtures containing glycolic acid have a time-dependent increase in water content. This leads to the assumption that glycolic acid might react with the ammonium compound. L-Carnitine showed good results, since mixtures with urea and malonic acid, respectively, were liquid at 0 °C. L-Carnitine is naturally produced by the human body, biodegradable and non-toxic. Therefore, it is a promising substance for the utilisation in DESs and LMMs.

Furthermore, sugar-based LMMs comprising choline chloride (ChCl), urea as well as glucose (Glu) and sorbitol (Sor), respectively, with varying molar ratios are presented. Decomposition temperatures, glass transition temperatures as well as refractive indices, densities, viscosities and the influence of the water content on the viscosity of the DES were investigated. It was revealed that the glass transition temperature can be reduced to -36.6 °C. This is a large decrease, since the binary mixture consisting of ChCl and urea with a molar ratio of 1-2 has a melting point of 12 °C.¹ However, the water free sugar-based mixtures have a rather high viscosity at room temperature, which limits their applicability. With a water content of 7.8 wt% the viscosity of ChCl-urea-Glu (1-1-1) drops by a factor of 50.

To conclude, it was shown that DESs and LMMs can be tuned by varying the hydrogen bond donor (HBD) and hydrogen bond acceptor (HBA). Also the addition of a third component can reduce the melting point. Thereby, the choice of the additional substance and the

composition is an important issue. Further, the properties are dependent on the water content. With this knowledge, a whole new class of LMMs can be created and tailored for the desired application. Another important advantage of sugar-based LMMs is their biodegradability and non-toxicity. For that reason, eco-friendly chemistry can be carried out.

In the second chapter, different DESs were calculated with the conductor-like screening model for realistic solvation (COSMO-RS). COSMO-RS is capable to predict HBD and HBA abilities of molecules. Since DESs are partly formed by hydrogen bonding, COSMO-RS is an important tool for their evaluation. The HBD and HBA abilities of a molecule are visualised in so-called σ -surfaces and plotted in the corresponding σ -profiles. From these profiles, a first hint towards the formation of a DESs can be deduced. In a set of experiments, DESs consisting of urea and different choline halides (CHX) were tested. The σ -profiles of the different molecules and ions show that urea is a HBD, whereas fluoride, chloride, bromide and iodide are HBAs. The strength of the HBA decreases in the order $F^- > Cl^- > Br^- > I^-$. Concerning DESs, it was discovered that the stronger the hydrogen bond, the stronger the depression of the melting point.^{1,2} Therefore, according to the σ -profiles and with respect to the halide ions, the depression of the melting point must increase in the order $I^- < Br^- < Cl^- < F^-$. To corroborate this hypothesis, phase diagrams of the melting temperature as a function of molar ratio were calculated for the ChX-urea mixtures. The calculations were performed with the solid-liquid equilibrium (SLE) option. It computes a range of mixtures between the components and searches for possible concentrations of solidification. The obtained phase diagrams confirm the prediction of the σ -profiles. The melting points of the mixtures decrease in the order ChI-urea > ChBr-urea > ChCl-urea. All mixtures showed a eutectic molar ratio of 2-1. Since the predictions for CHF-urea were not very accurate, the phase diagram was not taken into account. The fluoride anion is a very small highly charged anion. This might be a reason for the less precise calculation.³ Moreover, differential scanning calorimetry (DSC) was performed to compare the computed values to experimental results. Although the measured results differ from the predictions, the trend could be confirmed.

COSMO-RS is a useful tool for the prediction of DESs. By evaluating the σ -profiles, a first qualitative conclusion can be made. They give insight into the interactions between the HBD and the HBA. Nevertheless, the results of the SLE calculations indicate only a trend. A reason for that might be the small ion size of some halide ions as well as the fact that DESs are not only dependent on hydrogen bonds.⁴

Among other applications, DESs serve as media for chemical reactions. Chapter IV 3 focuses on the utilisation of a DESs for the synthesis of caffeic acid phenethyl ester (CAPE). CAPE is one of the most active compounds in honey bee propolis and exhibits some interesting pharmacological and biological properties. The isolation of CAPE from honey bee propolis is often challenging, since it is time-consuming and suffers from impurities. Also the chemical synthesis has some drawbacks, since it includes harmful chemicals. Therefore, it is important to find alternatives. A DES comprising caffeic acid (CA) and ChCl fulfils the requirements for an environmental friendly reaction medium. Moreover, CA can be used directly for the synthesis. In a first set of experiments, the DES ChCl-CA with a molar ratio of 2-1 was mixed with different ratios of phenethyl alcohol. In general, CA is not soluble in PA. However, when a DES with ChCl is formed before, ChCl-CA mixes with PA in every ratio. A homogeneous fluid can be formed and no further solvent is needed. Since a lipase-catalysed synthesis towards CAPE did not succeed, an acid-catalysed esterification was carried out. First experiments were performed with sulphuric acid and *p*-toluenesulfonic acid as catalyst. The results indicated a decent conversion rate. However, the conversion seems to be dependent on the amount of PA. Therefore, the content of PA was optimised. To further improve the reaction conditions, sulphuric and *p*-toluenesulfonic acid were substituted by the solid acid catalyst Amberlyst 15. Amberlyst 15 has the advantage of being environmentally benign and can be easily removed from the reaction mixture. After optimising the amount of Amberlyst 15 with regards to the conversion rates and the reaction time, the most effective conditions were found. All in all, a molar conversion rate of 76.3 % was achieved. In order to isolate CAPE, only hot water was used.

These properties are in good accordance with the 12 principles of green chemistry.⁵ Further, a new spectrum of application is disclosed for DESs, since a significant number of DESs can be imagined enabling a large amount of possible syntheses without solvents.

In the last chapter, waterless and surfactantless microemulsions containing DESs as polar phase were investigated. Recently, Klossek *et al.* discovered the “pre-Ouzo effect” in ternary mixtures, for instance, water/benzyl alcohol/ethanol.⁶ Further, Diat *et al.* found that in a water/octanol/ethanol system the single-phase in the pre-Ouzo region consists of two distinct nanoscopic pseudo-phases, one octanol-rich and one water-rich. The ethanol molecules were distributed between octanol-rich nano-domains and a water pseudo-phase with slight accumulation at the interface and an exponential decay concentration on the water side.⁷ The

shape on a molecular level and the structure of these aggregates were also calculated by molecular dynamics simulations.⁸

With this knowledge, the question of the existence of nano-droplets in waterless and surfactantless microemulsion is set. Therefore, water was replaced with two different DESs to formulate and characterise surfactantless and waterless microemulsions ChCl-ethylene glycol (1-4) and ChCl-urea (1-2) were used as polar phase, tetrahydrofurfuryl alcohol (THFA) as cosurfactant and diethyl adipate as non-polar phase. THFA stems from wood chemistry and, like the DESs, is biodegradable. Diethyl adipate is also of very low toxicity. Ternary phase diagrams were carried out and the domains of the single clear and homogeneous phase were determined. To characterise the nano-domains, dynamic light scattering (DLS), as well as small angle X-ray scattering (SAXS) was performed. In both phase diagrams, a monophasic single phase domain appears. DLS and SAXS measurements were performed for mixtures near the demixion boundary. The content of THFA was then gradually increased. DLS measurements revealed well-defined correlation functions near the demixion boundary. With increasing amount of THFA, the correlation function decreased. This leads to the assumption that nano-clustering is present in mixtures near the border. For the same mixtures used for the DLS measurements, SAXS measurements were performed. The experiments proof and confirm the existence of a nano-clustering near the demixion boundary, i.e. in the pre-Ouzo region. This nano-clustering is less and less pronounced when the composition is farther from the demixion boundary. The results also corroborate previous studies where such fluctuations were observed in aqueous systems also fulfilling all the requirements for the Ouzo effect. The present study also shows that the pre-Ouzo effect is general and independent from the presence of water. However, it cannot be excluded that the nano-clustering is dependent on hydrogen bonds, since in all systems hydrogen bonding is present. Therefore, further studies are necessary to check this point.

1.1 References

- 1 A. P. Abbott, G. Capper, D. L. Davies, R. K. Rasheed and V. Tambyrajah, *Chem. Commun.*, 2003, 70-71.
- 2 Q. Zhang, K. De Oliveira Vigier, S. Royer and F. Jerome, *Chem. Soc. Rev.*, 2012, **41**, 7108-7146.
- 3 A. Klamt, F. Eckert and W. Arlt, *Annu. Rev. Chem. Biomol. Eng.*, 2010, **1**, 101-122.

- 4 A. P. Abbott, D. Boothby, G. Capper, D. L. Davies and R. K. Rasheed, *JACS*, 2004, **126**, 9142-9147.
- 5 P. T. Anastas and M. M. Kirchhoff, *Acc. Chem. Res.*, 2002, **35**, 686-694.
- 6 M. L. Klossek, D. Touraud and W. Kunz, *PCCP*, 2013, **15**, 10971-10977.
- 7 O. Diat, M. L. Klossek, D. Touraud, B. Deme, I. Grillo, W. Kunz and T. Zemb, *J. Appl. Crystallogr.*, 2013, **46**, 1665-1669.
- 8 S. Schöttl, J. Marcus, O. Diat, D. Touraud, W. Kunz, T. Zemb and D. Horinek, *Chem. Sci.*, 2014.

VI Appendix

1. New low melting mixtures

1.1 Density

Table VI-1. Densities of the carbohydrate-urea-choline chloride mixtures in a temperature range of 15 °C to 65 °C.

T in °C	ρ in g cm ⁻³			
	Glu-U-ChCl1	Glu-U-ChCl2	Sor-U-ChCl1	Sor-U-ChCl2
15	1.315	1.314	1.291	1.289
25	1.310	1.309	1.285	1.283
35	1.305	1.303	1.279	1.278
45	1.299	1.298	1.274	1.272
55	1.294	1.293	1.268	1.266
65	1.289	1.287	1.262	1.261

1.2 Viscosity

Table VI-2. Viscosities of the carbohydrate-urea-choline chloride mixtures in a temperature range of 15 °C to 75 °C.

T in °C	η in Pa s			
	Glu-U-ChCl1	Glu-U-ChCl2	Sor-U-ChCl1	Sor-U-ChCl2
15	1580 ± 115	560 ± 33.6	67.7 ± 3.6	42.5 ± 1.4
25	154 ± 5.1	56.9 ± 2.1	11.4 ± 0.32	7.42 ± 0.20
35	23.2 ± 0.82	8.92 ± 0.33	2.54 ± 0.073	1.71 ± 0.053
45	4.92 ± 0.16	1.98 ± 0.065	0.730 ± 0.020	0.507 ± 0.013
55	1.34 ± 0.024	0.559 ± 0.008	0.260 ± 0.005	0.174 ± 0.002
65	0.468 ± 0.020	0.213 ± 0.032	0.113 ± 0.003	0.080 ± 0.001
75	0.193 ± 0.004	0.091 ± 0.002	0.056 ± 0.001	0.043 ± 0.000

Table VI-3. Water contents with corresponding viscosities of Glu-U-ChCl1. The measurements were carried out at 25 °C.

Water content (weight %)	η in Pa s
0.39	154 ± 5.1
1.28	101 ± 5.1
2.84	31.3 ± 1.2
7.74	4.6 ± 0.1

1.3 Thermogravimetric Analysis

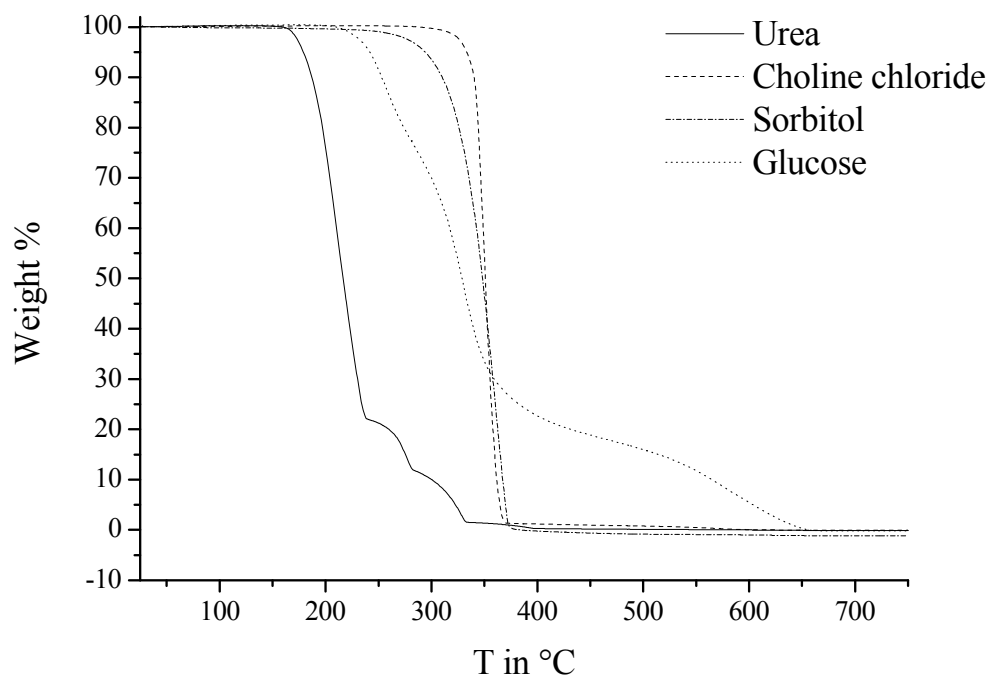


Figure VI-1. Thermograms for urea, choline chloride, sorbitol and glucose.

1.4 Differential Scanning Calorimetry

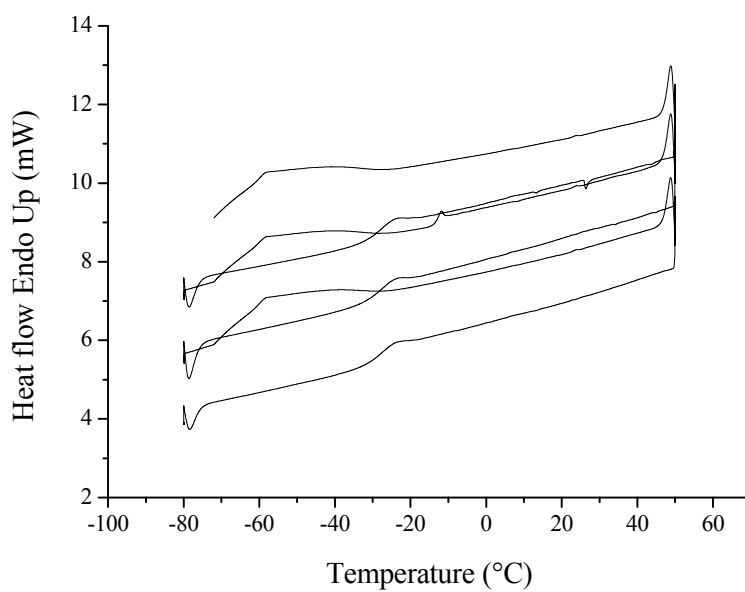


Figure VI-2. DSC curve of Glu-U-ChCl1 from -80 °C to 50 °C and with a heating/cooling rate of 15 °C min⁻¹.

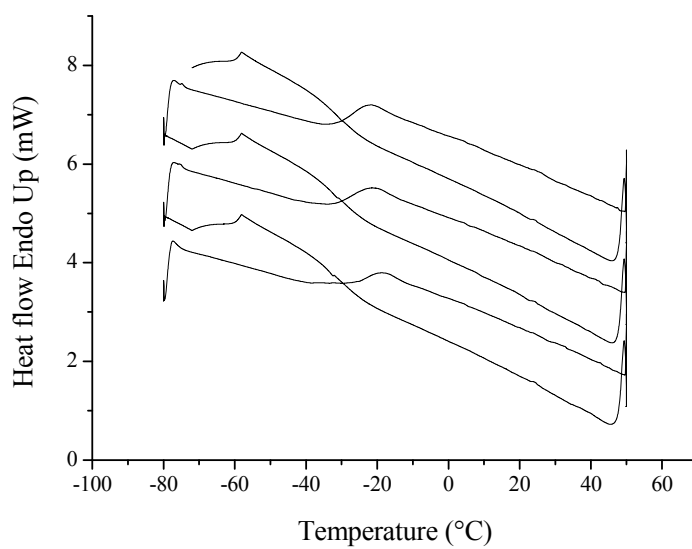


Figure VI-3. DSC curve of Glu-U-ChCl2 from -80 °C to 50 °C and with a heating/cooling rate of 15 °C min⁻¹.

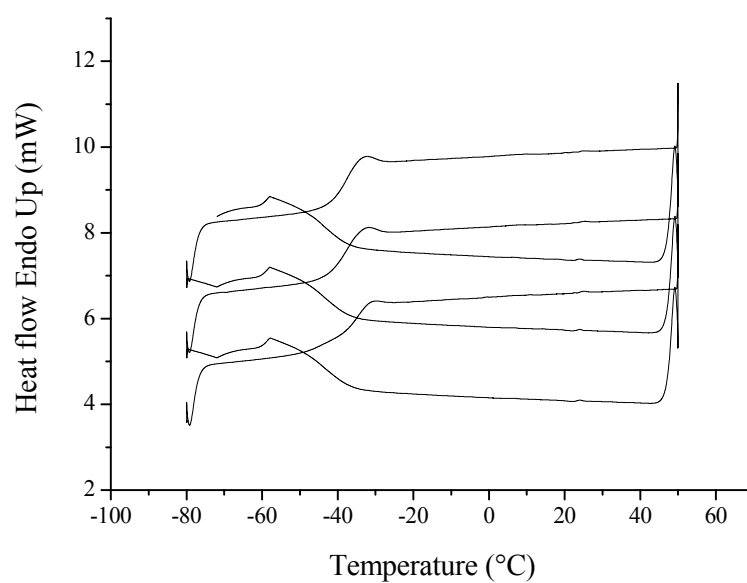


Figure VI-4. DSC curve of Sor-U-ChCl1 from -80 °C to 50 °C and with a heating/cooling rate of 15 °C min⁻¹.

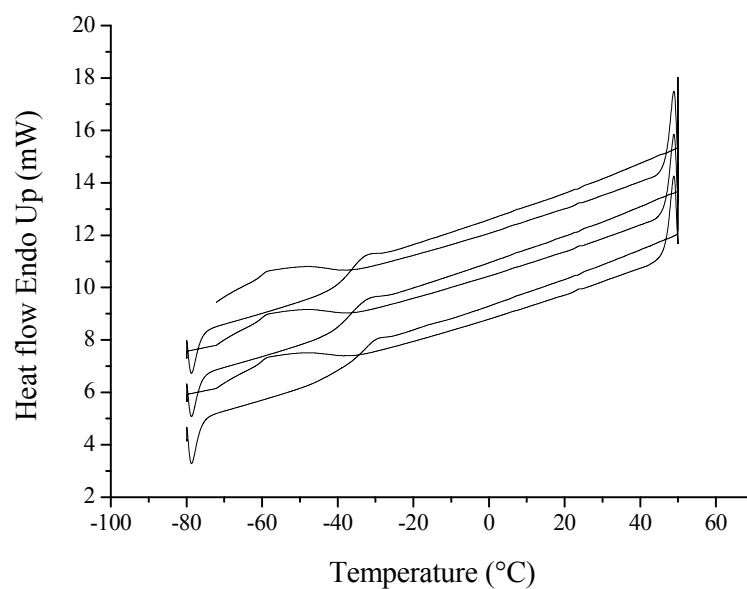


Figure VI-5. DSC curve of Sor-U-ChCl2 from -80 °C to 50 °C and with a heating/cooling rate of 15 °C min⁻¹.

2. COSMO-RS Calculations of Deep Eutectic Solvents

2.1 Differential Scanning Calorimetry

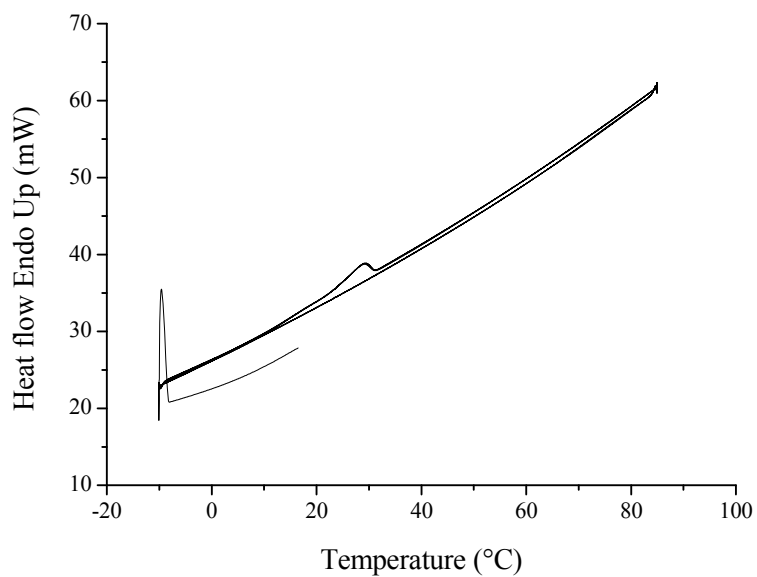


Figure VI-6. DSC curve of Urea-ChCl from -10 °C to 85 °C and with a heating/cooling rate of 5 °C min⁻¹.

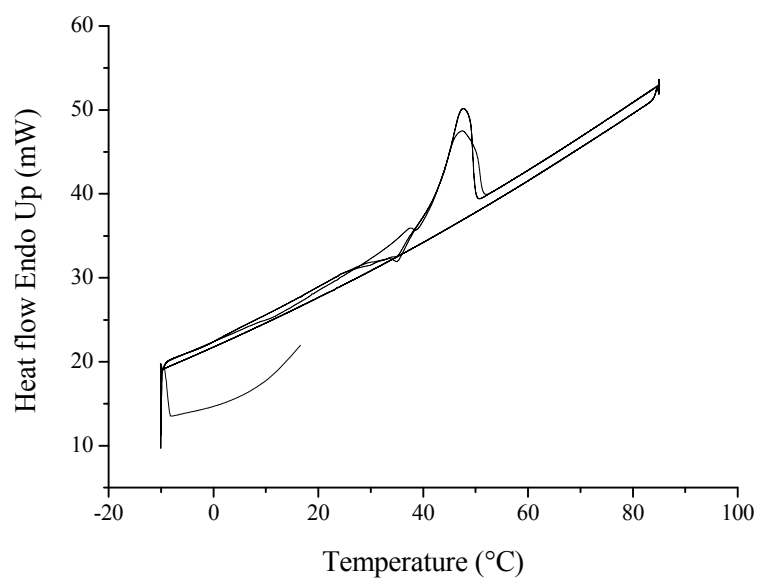


Figure VI-7. DSC curve of Urea-ChBr from -10 °C to 85 °C and with a heating/cooling rate of 5 °C min⁻¹.

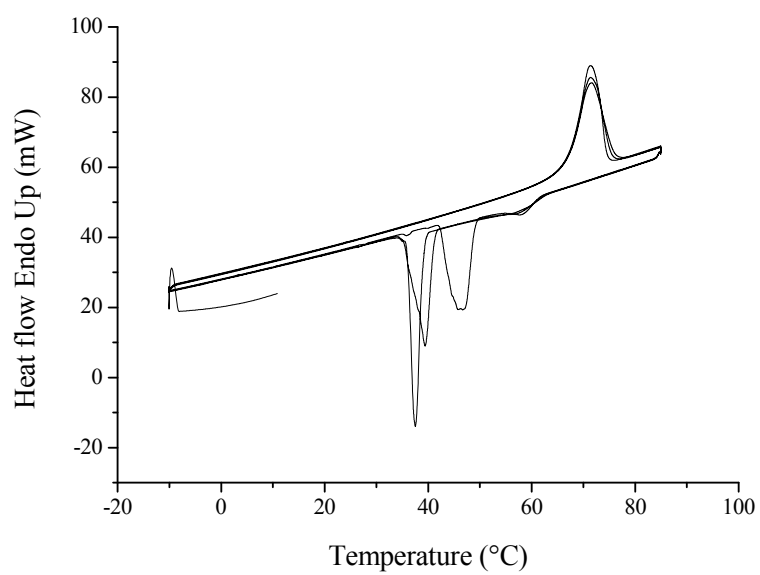


Figure VI-8. . DSC curve of Urea-ChBr from -10 °C to 85 °C and with a heating/cooling rate of 5 °C min⁻¹

3. Eco-Friendly Synthesis of Caffeic Acid Phenethyl Ester Using Deep Eutectic Solvents

3.1 Viscosity

Table VI-4. Viscosities of mixtures with different mass ratios of DES-PA in a temperature range of 15 °C to 75°C.

T in °C	η in mPa s						
	1-9	2-8	3-7	4-6	5-5	6-4	7-3
25	8.49 ± 0.22	19.1 ± 0.50	49.1 ± 0.70	93.6 ± 1.6	206 ± 3.6	486 ± 5.4	3105 ± 61.6
35	5.94 ± 0.27	11.7 ± 0.35	25.7 ± 0.82	47.5 ± 0.77	93.8 ± 1.8	196 ± 3.7	1204 ± 23.0
45	4.31 ± 0.24	7.54 ± 0.18	15.4 ± 0.24	25.8 ± 0.67	47.6 ± 0.67	89.9 ± 1.7	447 ± 8.6
55	2.64 ± 0.93	4.82 ± 0.78	9.69 ± 0.62	16.0 ± 0.23	27.2 ± 0.78	46.5 ± 0.60	247 ± 215
65	2.82 ± 0.98	3.24 ± 0.24	6.69 ± 1.36	10.8 ± 0.18	17.5 ± 0.55	27.0 ± 0.76	-
75	2.49 ± 0.27	2.71 ± 0.26	5.43 ± 1.02	7.83 ± 0.16	12.7 ± 0.16	17.7 ± 0.12	80.7 ± 71.7

3.2 Composition, Reaction Time and Molar Conversion

Table VI-5. Composition of the reaction mixtures given in g, reaction time (RT) , concentration c(dilution) of the dilution of the reaction mixture in methanol used for HPLC measurements given in mg/mL, the determined peak area with corresponding standard deviation (SD) and the resulting molar conversion rate of CA to CAPE in %.

Catalyst	m(CA)	m(ChCl)	m(PA)	m(acid)	Reaction time	c(dilution)	Peak area	SD	Molar conversion
Sulphuric acid	0.445	0.702	0.296	0.088	1 d	7.6	6.786E+06	3.90E+05	6.2
	0.464	0.680	0.713	0.115	1 d	11.8	2.043E+07	9.41E+05	14.9
	0.439	0.667	1.282	0.068	1 d	5.0	1.953E+07	1.02E+06	44.2
	0.451	0.702	1.857	0.063	1 d	4.0	1.886E+07	2.32E+05	65.0
	0.896	1.395	9	0.207	1 d	11.4	2.840E+07	8.15E+05	67.1
	0.443	0.696	4.654	0.112	1 d	10	2.478E+07	9.53E+05	66.8
	0.45	0.701	5.853	0.202	1 d	7.0	1.219E+07	4.42E+05	56.4
<i>p</i> -Toluenesulfonic acid	0.457	0.705	0.415	0.07	1 d	8.6	2.034E+07	8.92E+05	17.2
	0.447	0.713	0.736	0.74	1 d	4.6	1.641E+07	6.87E+05	31.8
	0.459	0.682	1.263	0.071	1 d	4.6	2.036E+07	7.31E+05	48.3

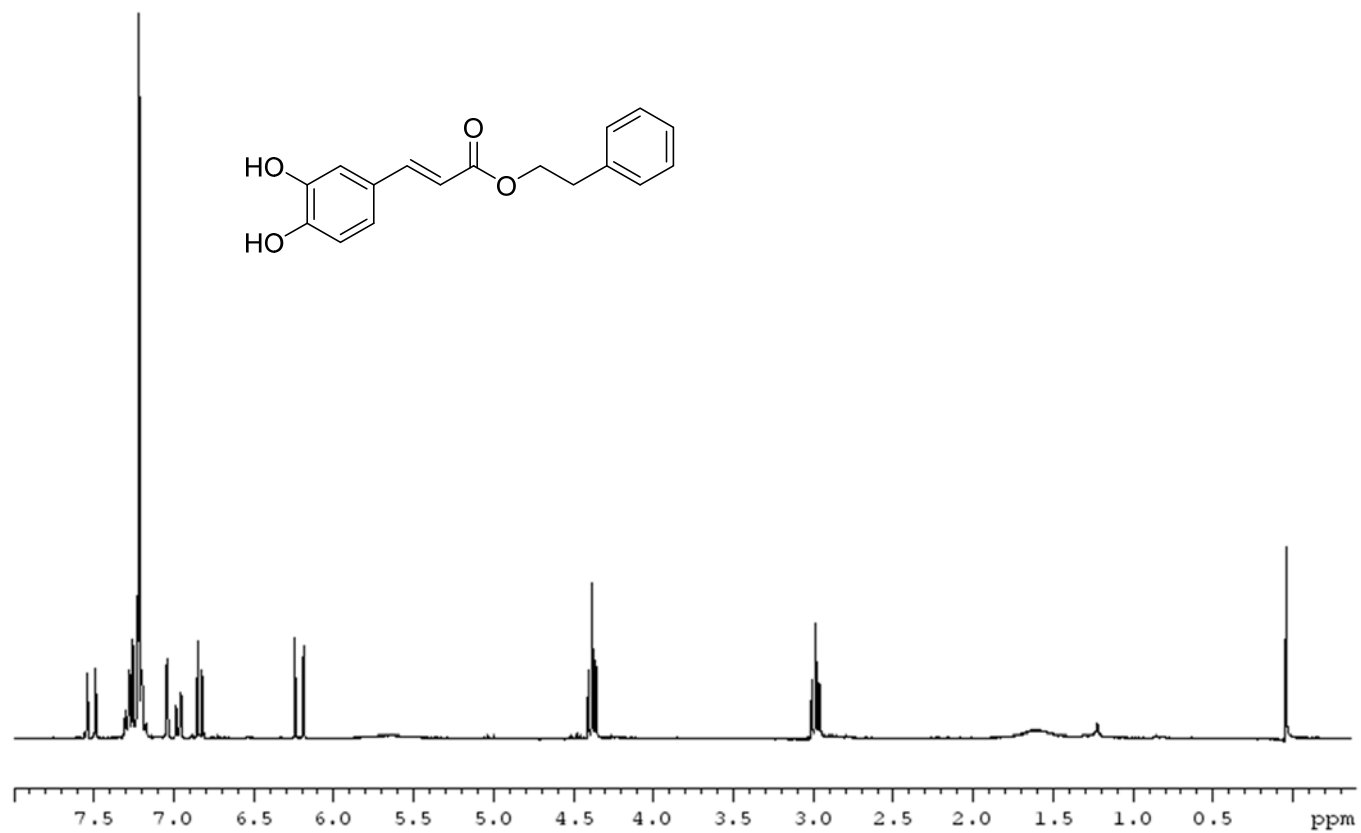
VI Appendix

Catalyst	m(CA)	m(ChCl)	m(PA)	m(acid)	Reaction time	c(dilution)	Peak area	SD	Molar conversion
<i>p</i> -Toluenesulfonic acid	0.463	0.702	2.252	0.045	1 d	9.4	2.704E+07	7.34E+05	43.5
	0.469	0.701	4.099	0.067	1 d	11.0	3.098E+07	2.60E+06	64.8
	0.450	0.704	4.677	0.075	1 d	7.8	2.188E+07	1.32E+06	74.5
	0.443	0.7	5.894	0.088	1 d	7.8	1.625E+07	7.06E+05	67.8
Acetic acid	0.481	0.707	1.857	0.177	1 d	9.8	3.572E+05	1.03E+03	0.5
	0.459	0.696	4.05	0.15	1 d	7.2	1.245E+05	3.64E+03	0.4
Oxalic acid	0.467	0.695	1.905	0.1	1 d	9.6	3.934E+06	1.13E+05	5.6
	0.45	0.696	4.208	0.1	1 d	12.4	3.242E+06	2.13E+05	6.4
	0.457	0.716	2.031	0.205	1 d	3.8	2.368E+06	9.41E+04	9.4
	0.445	0.702	2.149	0.405	1 d	4.6	3.538E+06	1.39E+05	12.9
Malonic acid	0.472	0.687	1.749	0.103	1 d	3.8	2.214E+05	5.66E+04	0.8
	0.473	0.696	4.066	0.103	1 d	6.0	3.923E+05	1.65E+04	1.5

Catalyst	m(CA)	m(ChCl)	m(PA)	m(acid)	Reaction time	c(dilution)	Peak area	SD	Molar conversion
Amberlite IR120	0.446	0.699	4.639	0.622	1 d	5.6	1.414E+07	3.26E+05	64.7
	0.446	0.705	4.566	0.495	1 d	1.3	2.502E+07	7.54E+05	72.1
Amberlyst 15	0.455	0.752	4.606	1.322	1 d	6.6	1.261E+07	3.98E+05	54.4
	0.455	0.752	4.600	0.501	1 d	6.2	1.670E+07	4.88E+05	69.5
	0.453	0.689	4.489	0.297	1 d	8.6	2.166E+07	4.48E+05	63.3
	0.442	0.688	4.620	0.097	1 d	17.8	3.315E+07	9.12E+05	49.0
	0.458	0.687	6.010	0.502	1 d	8.0	1.758E+07	1.04E+06	69.4
	0.458	0.700	2.018	0.501	1 d	8.0	2.986E+07	1.17E+06	52.3
	0.455	0.694	4.492	0.544	1 d	9.0	2.337E+07	7.08E+05	65.1
	0.458	0.709	4.525	0.652	1 d	6.4	1.569E+07	3.39E+05	61.6
	0.448	0.692	4.595	0.908	1 d	14.8	2.939E+07	8.27E+05	51.4
	0.439	0.700	4.482	0.499	4h	11.4	2.928E+07	6.95E+05	66.5

VI Appendix

Catalyst	m(CA)	m(ChCl)	m(PA)	m(acid)	Reaction time	c(dilution)	Peak area	SD	Molar conversion
Amberlyst 15	0.442	0.685	4.420	0.806	4h	14.0	3.736E+07	5.82E+05	67.7
	0.439	0.700	4.482	0.499	8h	11.6	3.102E+07	5.33E+05	69.2
	0.442	0.685	4.420	0.806	8h	11.0	3.319E+07	1.27E+06	76.6
	0.447	0.688	4.518	0.498	14h	7.8	2.328E+07	8.73E+05	76.3
	0.465	0.710	4.465	0.814	14h	7.0	2.167E+07	5.09E+05	75.9
	0.439	0.700	4.482	0.499	26h	11.2	2.876E+07	8.20E+05	66.5
	0.442	0.685	4.420	0.806	26h	7.6	1.703E+07	6.40E+05	56.9

3.3 NMRCaffeic acid phenethyl ester in CDCl₃:

4. Towards Surfactantless and Waterless Microemulsions

4.1 Composition of the Samples

Table VI-6. Compositions of the mixtures used for DLS and SAXS measurements. The fraction of DEA, THFA and DES are given in weight %.

Sample	Type of DES	DEA	THFA	DES
E1	DES1	30	40	30
E2	DES1	30	41	29
E3	DES1	30	43	27
E4	DES1	30	45	25
E5	DES1	30	47	23
E6	DES1	30	55	15
U1	DES2	25	54	21
U2	DES2	25	56	19
U3	DES2	25	60	15

4.2 Density, Viscosity and Refractive Index

Table VI-7. Densities, viscosities and refractive indices of the mixtures used for DLS and SAXS measurements at 25 °C.

Sample	ρ in g cm ⁻³	η in mPa s	Refractive Index
E1	1.0567	9.87	1.4466
E2	1.0560	9.29	1.4450
E3	1.0543	8.80	1.4449
E4	1.0532	8.33	1.4441
E5	1.0519	7.50	1.4439
E6	1.0467	6.44	1.4436
U1	1.0730	16.18	1.4571
U2	1.0690	13.95	1.4559
U3	1.0631	10.62	1.4536

5. List of Figures

<i>Figure I-1. The goal a solvent should attain is the agreement of its performance in the chemical and engineering process, the minimisation of energy use as well as the avoidance of adverse influence on environment, health and safety.²</i>	2
<i>Figure II-1. Exemplary phase diagram of a binary mixture.</i>	8
<i>Figure II-2. σ-surface (left) and σ-profile (right) of water. The blue areas mark a HBD, the red areas a HBA, and the green areas a non-polar region.</i>	27
<i>Figure II-3. σ-Profile for a mixture of chloroform and acetone.</i>	28
<i>Figure II-4. Three different types of microemulsion a) oil-in-water, b) water-in-oil or c) bicontinuous.</i>	32
<i>Figure II-5. Scheme of a phase diagram of water, oil and surfactant showing 1, 2, and 3 phase domains. The phase diagram is typical for a system with a nonionic surfactant</i>	33
<i>Figure II-6. Ternary phase diagram which shows the optimal region to solubilise a hydrophobic molecule with the minimum of eco-solvent.⁴³</i>	36
<i>Figure II-7. Scheme of coherent laser light hitting a particle resulting in scattered light and definition of the scattering vector q.</i>	37
<i>Figure II-8. Small angle scattering of radiation by a sample. Angles normally used are shown.⁵⁶</i>	39
<i>Figure II-9. Molecular structures of caffeic acid (CA) and caffeic acid phenethyl ester (CAPE).</i>	44
<i>Figure III-1. Chromatogram of a mixture of CA and CAPE.</i>	56
<i>Figure III-2. Standard curve for CAPE in methanol.</i>	57
<i>Figure IV-1. Mixture of Glucose-Urea-ChCl (1-1-1) at room temperature.</i>	71
<i>Figure IV-2. Densities of the mixtures as a function of temperature.</i>	72
<i>Figure IV-3. Logarithmic plots of the different viscosities of the low melting mixtures as a function of temperature. The viscosities are given in Pa·s.</i>	73
<i>Figure IV-4. Logarithmic plot of the viscosity of a Glu-U-ChCl mixture as a function of water content. The viscosities are given in Pa·s.</i>	73
<i>Figure IV-5. Weight losses of the mixtures in % as a function of temperature.</i>	74
<i>Figure IV-6. σ-surface (left) and σ-profile (right) of urea. The blue areas mark a HBD, the red areas a HBA and the green areas a non-polar region.</i>	80
<i>Figure IV-7. σ-profiles of urea, the choline cation and halide anions from fluoride to iodide.</i>	82

<i>Figure IV-8. Calculated phase diagrams by COSMO-RS of diverse urea-choline halide mixtures.</i>	84
<i>Figure IV-9 Samples with different amounts of PA before the addition of enzyme or acid.</i> ..	89
<i>Figure IV-10. Logarithmic plot of different viscosities of different compositions of DES-PA as a function of temperature. Viscosities were measured in Pa·s.</i>	89
<i>Figure IV-11. Molar conversion rate of CA to CAPE in % as a function of molar ratio of PA-CA. Right diagram: Reaction was catalysed by p-toluenesulfonic acid. Left diagram: Reaction was catalysed by sulphuric acid.</i>	94
<i>Figure IV-12. Chemical structures of p-toluenesulfonic acid (left) and Amberlyt 15 (right).</i>	95
<i>Figure IV-13. Molar conversion of CA to CAPE as a function of Amberlyst 15 in wt%. The molar ratio of CA, ChCl and PA was kept constant.</i>	95
<i>Figure IV-14. Molar conversion of CA to CAPE as a function of time. The ratio of CA, ChCl, PA was kept constant. The amount of Amberlyst 15 was 8 wt%.</i>	96
<i>Figure IV-15. Molar conversion of CA to CAPE as a function of time. The ratio of CA, ChCl, PA was kept constant. The amount of Amberlyst 15 was 13 wt%.</i>	97
<i>Figure IV-16. Pseudo-ternary phase diagram of a waterless DES1/THFA-Brij 30 ($\zeta = 2-1$)/DEA system at 25°C. The white area marks the single phase domain and the grey the multiphasic region.</i>	105
<i>Figure IV-17. Pseudo-ternary phase diagrams of surfactantless and waterless systems a) DES1/THFA/DEA and b) DES2/THFA/DEA at 25 °C. The white area marks the single phase domain and the grey the multiphasic region.</i>	106
<i>Figure IV-18. Time-dependent self-correlation functions as obtained from DLS measurement for the systems DES1/THFA/DEA (left) along path a and DES2/THFA/DEA (right) along path b at 25 °C.</i>	106
<i>Figure IV-19. SAXS measurements on a log log scale and in absolute units for the system DES2/THFA/DEA (left) and DES2/THFA/DEA (right).</i>	107
<i>Figure IV-20. Correlation lengths in Å obtained from the Ornstein-Zernike fits versus the mass fraction of the DESs.</i>	108
<i>Figure VI-1. Thermograms for urea, choline chloride, sorbitol and glucose.</i>	121
<i>Figure VI-2. DSC curve of Glu-U-ChCl1 from -80 °C to 50 °C and with a heating/cooling rate of 15 °C min⁻¹.</i>	122
<i>Figure VI-3. DSC curve of Glu-U-ChCl2 from -80 °C to 50 °C and with a heating/cooling rate of 15 °C min⁻¹.</i>	122

<i>Figure VI-4. DSC curve of Sor-U-ChCl1 from -80 °C to 50 °C and with a heating/cooling rate of 15 °C min⁻¹.....</i>	<i>123</i>
<i>Figure VI-5. DSC curve of Sor-U-ChCl2 from -80 °C to 50 °C and with a heating/cooling rate of 15 °C min⁻¹.....</i>	<i>123</i>
<i>Figure VI-6. DSC curve of Urea-ChCl from -10 °C to 85 °C and with a heating/cooling rate of 5 °C min⁻¹.....</i>	<i>124</i>
<i>Figure VI-7. DSC curve of Urea-ChBr from -10 °C to 85 °C and with a heating/cooling rate of 5 °C min⁻¹.....</i>	<i>125</i>
<i>Figure VI-8. . DSC curve of Urea-ChBr from -10 °C to 85 °C and with a heating/cooling rate of 5 °C min⁻¹.....</i>	<i>125</i>

6. List of Schemes

<i>Scheme II-1. Reaction of lipase-catalysed alcoholysis of phenolic esters with 1-octanol in a DES.⁴¹</i>	18
<i>Scheme II-2. Scheme of acid-catalyzed reaction of CA and phenethyl alcohol to CAPE.¹⁷</i>	45
<i>Scheme II-3. Reaction scheme of the base-catalyzed alkylation of CA and β-bromoethylbenzene.⁴⁵</i>	46
<i>Scheme II-4. Reaction scheme of the esterification of CA and phenethyl alcohol using DCC as condensing agent.¹⁸</i>	46
<i>Scheme II-5. Three-step synthesis to CAPE according to Touaibia and Guay.⁴⁹</i>	47
<i>Scheme II-6. Reaction scheme of the hydrolysis of 5-chlorogenic acid and the synthesis of CAPE catalysed by chlorogenate hydrolase.⁵⁰</i>	47
<i>Scheme II-7. Reaction scheme of the lipase-catalysed esterification of CA and phenethyl alcohol in an IL.⁵⁷</i>	48
<i>Scheme IV-1. Reaction scheme of the esterification to synthesise caffeic acid phenethyl ester.</i>	88

7. List of Tables

<i>Table II-1. Typical structures of organic salts and HBD used for DESs.³</i>	9
<i>Table II-2. Freezing points (T_f) of various ChCl-HBD DESs with corresponding melting temperatures of the pure HBD (T_m^*).</i>	10
<i>Table II-3. Compositions and melting points (T_m) of different sugar-based LMMs.</i>	10
<i>Table II-4. Structures, compositions and freezing points (T_f) of different DES with corresponding melting points (T_m^*) of the pure HBD. The temperatures are given in °C.</i>	12
<i>Table II-5. Densities of different DESs and glycerol systems at 25 °C.</i>	14
<i>Table II-6. Viscosities of different DESs and glycerol systems at 25 °C.</i>	14
<i>Table II-7. Examples of organic reactions in ChCl-urea (1-2).</i>	16
<i>Table II-8. Examples of organic reactions in sugar-based LMMs.</i>	17
<i>Table II-9. Reaction scheme, activity and selectivity of the transesterification of ethyl sorbate with 1-propanol.⁴⁰</i>	18
<i>Table III-1. Gradient table for HPLC analysis.</i>	56
<i>Table III-2. Results of the linear fit of the standard curve.</i>	57
<i>Table IV-1. Melting points of mixtures of carbohydrates, urea and inorganic salts in different compositions.</i>	66
<i>Table IV-2. Used ammonium compounds with their corresponding abbreviation and molecular structure.</i>	67
<i>Table IV-3. List of performed LMMs comprising an ammonium compound and HBDs. The state of matter was determined at 80 °C, room temperature and 0 °C.</i>	68
<i>Table IV-4. Time-dependent water contents of ACH-GA mixtures.</i>	70
<i>Table IV-5. Molar ratios and refractive indices as well as the water content of the four prepared low-melting mixtures</i>	71
<i>Table IV-6. Glass transition temperature (T_g), heat capacity (ΔC_p) and molar heat capacity changes at T_g (ΔC_{pm}).</i>	76
<i>Table IV-7. Freezing temperatures T_f in °C of some choline-derived DESs with different anions and urea as HBD. All molar ratios of the salt and HBD are 1-2.</i>	81
<i>Table IV-8. SLE temperatures of mixtures comprising urea and a choline halide with corresponding molar fractions of urea.</i>	83
<i>Table IV-9. Melting temperatures (T_m) of the different choline halide-urea mixtures (molar ratio 1-2) obtained from DSC with corresponding melting temperatures of the pure choline halide salts (T_m^*) and the calculated SLE temperatures (T_{SLE}).</i>	85

<i>Table IV-10. Temperature-dependant viscosities of different compositions of DES-PA. Viscosities are given in mPa·s.....</i>	<i>90</i>
<i>Table IV-11. Enzymatic reactions catalysed by Novozym 435 in EAC-CA.....</i>	<i>91</i>
<i>Table IV-12. Reaction mixtures with different amounts of PA, water and enzyme.....</i>	<i>92</i>
<i>Table IV-13. Various lipases tested for the enzyme catalysed reaction between CA and PA to CAPE.....</i>	<i>93</i>
<i>Table IV-14. Content of PA in wt% in the reaction mixture with corresponding molar conversions from CA to CAPE. The reactions were carried out over night at 80 °C.</i>	<i>93</i>
<i>Table VI-1. Densities of the carbohydrate-urea-choline chloride mixtures in a temperature range of 15 °C to 65 °C.....</i>	<i>120</i>
<i>Table VI-2. Viscosities of the carbohydrate-urea-choline chloride mixtures in a temperature range of 15 °C to 75 °C.....</i>	<i>120</i>
<i>Table VI-3. Water contents with corresponding viscosities of Glu-U-ChCl1. The measurements were carried out at 25 °C.....</i>	<i>121</i>
<i>Table VI-4. Viscosities of mixtures with different mass ratios of DES-PA in a temperature range of 15 °C to 75°C.....</i>	<i>126</i>
<i>Table VI-5. Composition of the reaction mixtures given in g, reaction time (RT) , concentration c(dilution) of the dilution of the reaction mixture in methanol used for HPLC measurements given in mg/mL, the determined peak area with corresponding standard deviation (SD) and the resulting molar conversion rate of CA to CAPE in %.</i>	<i>127</i>
<i>Table VI-6. Compositions of the mixtures used for DLS and SAXS measurements. The fraction of DEA, THFA and DES are given in weight %.</i>	<i>132</i>
<i>Table VI-7. Densities, viscosities and refractive indices of the mixtures used for DLS and SAXS measurements at 25 °C.....</i>	<i>132</i>

8. List of Publications

Veronika Fischer and Werner Kunz

Properties of sugar-based low-melting mixtures

Mol. Phys., 2014, **122**,1241-1245

Doris Rengstl, Veronika Fischer and Werner Kunz

Low-melting mixtures based on choline Ionic Liquids

PCCP, 2014, **16**, 22815-22822

Veronika Fischer, Didier Touraud and Werner Kunz

One pot synthesis of caffeic acid phenethyl ester (CAPE) via deep eutectic solvents

Submitted to ChemEurJ.

Veronika Fischer, Julien Marcus, Didier Touraud, Olivier Diat and Werner Kunz

Towards surfactantless and waterless microemulsions

Submitted to JCIS

9. List of Abbreviations

%	Percentage
[Emim][EtSO ₄]	1-Ethyl-3-methylimidazolium ethylsulfate
[Emim][Tf ₂ N]	1-Ethyl-3- methylimidazolium bis[(trifluoromethyl)sulfonyl]imide
[EtNH ₃][NO ₃]	Ethylammonium nitrate
°C	Degree Celsius
μ	Micro
3D	Three dimensions
5-CQA	5-Chlorogenic acid
A	Peak area
Å	Ångström
a ₀	Constant baseline value
a ₁	Dynamic part of the amplitude
ACH	Acetyl-α-carnitine hydrochloride
AOT	Sodium di-(2-ethylhexyl) sulfsuccinate
APS	Ammonium persulfate
B	Betaine
BCl	Betaine hydrochloride
bs	Broad singlet
c	Centi
C	L-Carnitine
CA	Caffeic acid
CALB	<i>Candida Antarctica</i> lipase B
CAPE	Caffeic acid phenethyl ester
CCl	DL-Carnitine hydrochloride
CDCl ₃	Chloroform-d ₁
CFC	Chlorofluorocarbon
ChBr	Choline bromide
ChCl	Choline chloride
ChF	Choline fluoride
ChI	Choline iodide
ChX	Choline halide
cm	Centimetre
cm ³	Cubic centimeter
COSMO	Conductor-like screening model
COSMO-RS	Conductor-like screening model for realistic solvation

COSMO <i>therm</i>	Program for COSMO-RS calculations
cP	Centipoise
CT	L-Carnitine- α -tartrate
d	Days
d	Doublet
D ₀	Diffusion coefficient
DCC	N,N'-Dicyclohexylcarbodiimide
dd	Doublet of doublets
DEA	Diethyl adipate
DES	Deep eutectic solvent
DLS	Dynamic light scattering
DMA	Dimethylacetamide
DMF	N,N-Dimethylformamide
DMU	1,3-Dimethyl urea
DNA	Deoxyribonucleic acid
DSC	Dynamic scanning calorimetry
e	Elementary electric charge
EAC	Ethylammonium chloride
EG	Ethylene glycol
F	Scattering amplitude
g	Gram
GA	Glycolic acid
Glu	Glucose
h	Hour
HBA	Hydrogen bond acceptor
HBD	Hydrogen bond donor
HIV	Human immunodeficiency virus
HMPA	Hexamethylphosphoramide
HOESY	Heteronuclear Overhauser effect spectroscopy
HPLC	High performance liquid chromatography
Hz	Hertz
I	Intensity
IL	Ionic liquid
J	Joule
K	Kelvin
k _B	Boltzmann constant
LMM	Low-melting mixture

m	Multiplet
m	Meter
M	Molar concentration
m	Milli
m	Mass
MA	Malonic acid
MeOH	Methanol
MHz	Megahertz
min	Minute
mol	Mole
mol%	Mole percentage
n	Nano
n	Refractive index
NF- κ B	Nuclear factor kappa-light-chain-enhancer of activated B cells
nm ²	Square nanometer
NMR	Nuclear magnetic resonance s
O/W	Oil-in-water
PA	Phenethyl alcohol
Pa	Pascal
Ph	Phenyl group
ppm	Parts per million
<i>p</i> -TSOH	<i>p</i> -Toluenesulfonic acid
q	Scattering vector
q	Quartet
r	Distance vector
Ref.	Reference
R _H	Hydrodynamic radius
RNA	Ribonucleic acid
RT	Room temperature
RTIL	Room-temperature ionic liquid
S	Siemens
s	Singlet
s	Seconds
SAXS	Small angle x-ray scattering
scCO ₂	Supercritical CO ₂
SD	Standard deviation
SDS	Sodium dodecyl sulfate

SLE	Solid-liquid equilibrium
SOCl ₂	Thionyl chloride
Sor	Sorbitol
t	Time
T	Temperature
t	Triplet
T _f	Freezing temperature
T _{fus}	Temperature of fusion
T _g	Glass transition temperature
TGA	Thermogravimetric analysis
THF	Tetrahydrofuran
THFA	Tetrahydro furfuryl alcohol
T _m	Melting temperature
T _m [*]	Melting temperature of the pure substance
T _{SLE}	Temperature at the solid-liquid equilibrium
UV-Vis	Ultraviolet-visible spectrophotometry
V	Volume
v:v	Volume to volume
VOC	Volatile organic compound
W	Watt
W/O	Water-in-oil
w/w-ratio	weight-to-weight ratio
wt%	weight percentage
x	Mole fraction
Γ	Decay rate
ΔC _p	Heat capacity change
ΔC _p _{fus}	Heat capacity of fusion change
ΔC _p _m	Molar heat capacity change
ΔG _{fus}	Gibbs free energy of fusion
ΔH _{fus}	Enthalpy of fusion
Δρ	Density contrast
ζ	weight ratio
η	Viscosity
θ	detection angle
λ	Wavelength
π	3.14159
ρ	Density

ρ_p	Density of the particle
ρ_s	Density of the solvent
ρ_{sample}	Density of the sample
ρ_{sb}	Density of the steel ball
σ	COSMO screening charge
τ	Delayed time
Φ	Phase

10. Eidesstattliche Erklärung

Ich erkläre hiermit an Eides statt, dass ich die vorliegende Arbeit ohne unzulässige Hilfe Dritter und ohne Benutzung anderer als der angegebenen Hilfsmittel angefertigt habe; die aus anderen Quellen direkt oder indirekt übernommenen Daten und Konzepte sind unter Angabe des Literaturzitats gekennzeichnet.

Weitere Personen waren an der inhaltlich-materiellen Herstellung der vorliegenden Arbeit nicht beteiligt. Insbesondere habe ich hierfür nicht die entgeltliche Hilfe eines Promotionsberaters oder anderer Personen in Anspruch genommen. Niemand hat von mir weder unmittelbar noch mittelbar geldwerte Leistungen für Arbeiten erhalten, die im Zusammenhang mit dem Inhalt der vorgelegten Dissertation stehen.

Die Arbeit wurde bisher weder im In- noch im Ausland in gleicher oder ähnlicher Form einer anderen Prüfungsbehörde vorgelegt.

Regensburg, _____

Veronika Fischer